THE PALEOMAGNETIC RECORD FROM ELK LAKE, MN, AND ITS IMPLICATIONS

A THESIS
SUBMITTED TO THE FACULTY OF THE GRADUATE SCHOOL
OF THE UNIVERSITY OF MINNESOTA

BY

DONALD RICHARD SPROWL

IN PARTIAL FULFILLMENT OF THE REQUIREMENTS
FOR THE DEGREE OF
DOCTOR OF PHILOSOPHY

JULY, 1985

ABSTRACT

The paleomagnetic record from Elk Lake, Minnesota is developed and its implications discussed. The magnetic record is set apart from previous records qualitatively and quantitatively by the high subsampling rate (2 cm, ≈15 yr) of four parallel sediment cores and by the time control provided by annual laminations in the sediment. Excellent stratigraphic control is provided by the annual laminations and by fine scale (2-5 cm) variations in magnetic susceptibility.

The magnetic record, with uncertainties, is a compilation of measurements made on samples taken from four major sediment cores. The cores were azimuthally oriented, allowing absolute declination to be estimated. The 18 m sediment section extends from the present back to about 12000 years ago. Age estimates with uncertainties are provided by counting the varves from the multiple cores. Radiocarbon dates available from the sediment, confirm the varve chronology.

Efforts to derive relative paleointensity from the sediments are complicated by a change in average magnetite grain size due to magnetite dissolution. Normalization by stirred resettling in known fields was inadaquate, apparently because of magnetic grains clumped with organic matter. ARM normalization of the NRM is shown to be insufficient for these sediments, but further normalization using MDF looks promising.

The magnetic record compares well with previous records from central North America, but does show differences in several of the directional features. The varve chronology provides improved time control for the central North American paleomagnetic record. While the average inclination and declination do not differ significantly from the expected axial dipole values, long term trends in the data suggest that, in general, averaging over significantly more than 12000 years may be necessary to average the magnetic signal to that of an axial dipole. Periodogram analysis of the directional data indicates the presence of periodic components in the record, but the periods are not easily related to physical phenomena. Comparison of the Elk Lake directional data with data from Europe indicate that a majority of the directional variation can be accounted for by westward drift of the field components at a rate of 0.2 °/yr.

TABLE OF CONTENTS

LIST OF FIGURES

List of Figures (cont)

List of Figures (continued)

Figure

ACKNOWLEDGEMENTS

It is a pleasure to pause here and thank the many people who have helped me along in the work of this book.

I have had many advisors as I have worked on this project, both formal and informal. Professor Subir K. Banerjee brought me to Minnesota, got me started, supported me financially and in every other way, waited patiently for me to get into gear, and has prepared me not only for research, but for all of the aspects of my future work. He is a worthy advisor indeed. Professor Herb Wright has been an ever willing help in the field and rich source of understanding of the Elk Lake historical picture and the sediment itself. Professor Christopher Bingham has been a vital source of statistical rigor and understanding for a student sorely lacking in both.

A special note of thanks is due to John King and Jim Marvin, without whom this five year project would have taken twenty. John's years of work in developing the field and laboratory methods used in this project as well as his paleomagnetic research, paved a smooth road for me to follow. A good portion of this project is simply following in John's footsteps. Jim's wizardry with the instruments in the lab was of incalculable worth to this project. This is most clearly demonstrated when Jim goes on vacation and the instruments quickly show their inability to tend themselves. He has also been a constant and patient source of ideas and common sense regarding research directions, for which I am very thankful.

Others who have helped me in many ways in the field and in the lab include Joe Hackenmueller, Bill Gruber, Ruth Harris, Seong Jae Doh, Xiang Yeun Zu, John Almendinger, Jim Almendinger, Horst Worm, and Ed Swain.

The Graduate School of the University of Minnesota has provided financial support in the form of a Stanwood Johnston Memorial Fellowship, a Doctoral Dissertation Fellowship, a Doctoral Dissertation Special Grant, and a Doctoral Dissertation Fellowship Travel Grant. The National Science Foundation provided financial support in the form of research grants EAR-7919986 and EAR-8219139. Obviously, completion of this project without this financial support would have been impossible.

Finally, I give my thanks to my wife, Donna, who has been my inspiration and help through all of these days. She has given her all to make this thesis possible.

CHAPTER 1: INTRODUCTION

A. Overview.

This dissertation records the results of five years of work on the paleomagnetic record from the sediments of Elk Lake in northern Minnesota. It is tempting to ask at the outset whether the sediments from Elk Lake are worthy of five years of work and a doctoral dissertation. I hope the following pages provide an affirmative answer.

In our study of the deep interior of the earth, we are naturally limited to the analysis of parameters that we can measure at the earth's surface. Most of these parameters tell us only of the statics of the interior, not the dynamics. Of the few that inform us about interior dynamics, only one, the earth's magnetic field, tells of the dynamics of the core. It is natural then to study the magnetic field as part of our study of the earth's interior. At present, we are not very close to realizing our goal of fully understanding the dynamics of the core, but progress is being made on at least two fronts. Workers in Magnetohydrodynamics are coming to understand how magnetic fields are generated in conducting fluids like the core. Other workers are striving to better describe the magnetic field itself. This is where the Elk Lake work fits in.

The first step towards understanding the magnetic field, is a careful observation of the field and its changes through time. Unfortunately, most of the changes in the field of high enough frequency to be studied historically originate outside of the earth. The major changes in the field of internal origin have periods greater than a few hundred years and require a prehistorical (paleo) magnetic record. Magnetic reversals, with frequencies of 10^6 years or so, are recorded in hard rocks and deep sea sediments, but these recording mechanisms cannot resolve the shorter period "secular variations". Variations with periods <10,000 years are recorded in archeological samples (Bucha et al, 1970, and many others) and recent lava flows (Champion, 1980), but both of these records are discontinuous and dating methods are sometimes uncertain.

Continuous records of field variation can be found in lake sediments, both wet and dry. The explanation for this is simple enough (Stacey, 1972; Verosub, 1977). As individual grains of a magnetic mineral settle through the water column, they are aligned by the earth's magnetic field, like little compass needles. When these aligned grains reach the bottom and are buried, they may continue to rotate in water filled voids for a time, but eventually they will be "locked in" and thus record the earth's magnetic field. If the earth's field changes subsequently, the locked-in grains will not be affected, while more recently deposited grains will be realigned by the new field. A sediment column will thus provide a

continuous record of the changes in the earth's field, with the fidelity of magnetic recording depending on the character of the sediment. In 1971, Mackereth exploited these ideas with the first wet lake paleomagnetic study. Since then, several groups have further studied depositional remanent magnetization (DRM) records, with continual improvement in methodology (Creer et al., 1972; Dodson et al., 1977; Shuey et al., 1977; Vitorello and Van der Voo, 1977; Banerjee et al., 1979; Turner and Thompson, 1981; King et al., 1983a; Creer et al., 1983; Lund and Banerjee, 1985).

With improvement in the quality of the magnetic records being obtained, the resolution limiting factor in many recent studies has been age control. Lake sediment paleomagnetic records are most often dated by radiocarbon. But radiocarbon dating is susceptible to systematic errors from extraneous carbon content (King, 1983) and the necessary extrapolation between dated points compromises the continuous nature of the magnetic record.

The Elk Lake paleomagnetic record improves on previous records in this respect. The sediment in Elk Lake contains annual laminations, which allow the magnetic record to be very carefully and continuously dated. The relatively high sedimentation rate ($\approx$ 2 mm/yr), coupled with the close subsampling interval, yields a high resolution, well dated magnetic record. The apparent fidelity of the Elk Lake magnetic recording mechanism completes our optimistic framework for the study. In the following chapters, I detail the procedures used in obtaining the sediment from the field, dating the sediment, and measuring the magnetic signal, and then, having developed the Elk Lake paleomagnetic record, I discuss the implications of this record for our understanding of lake sediment magnetic records, the earth's magnetic field, and the earth's fluid core.

B. Basic magnetic measurements.

This section defines a number of commonly used terms and describes the basic magnetic measurement techniques used in later chapters. The magnetic signal of the sediment is measured with a super-conducting magnetometer manufactured by Super Conducting Technologies, Inc. (SCT). Each of three cartesian axes is measured three times to obtain an averaged magnetic intensity for each axis. The resultant of the three axes is the sample magnetic vector, which may be translated into spherical coordinate scalars, inclination (I) (angle down from horizontal), declination (D) (angle clockwise from North in the horizontal plane), and intensity (J).

The total natural remanent magnetization (NRM) of a sample is the resultant of the

remanences of numerous microscopic magnetic grains. We assume, with good reason (Stacey and Banerjee, 1975), that the remanences of the majority of these grains are stable on the time scale of the study (~10,000 yr). However, it is clear that some of the grains are unstable even on the time scale of a few minutes or hours. The signals from these unstable grains are unlikely to represent the original paleofield signal. The standard technique for removing the unstable magnetic signal is alternating field (AF) demagnetization. The sample is placed in a zero field space and is then subjected to an alternating magnetic field whose peak strength is decreased every half cycle until it decays to zero (Schonstedt Instrument Company AF Sample Demagnetizer). Magnetic grains unstable enough to be affected by the initial peak field are divided into two fractions, one magnetized to the plus direction and the other to the minus direction. Because these two fractions effectively cancel one another, the signal remaining after AF treatment is that due to the stable grains, representing the original remanence. The peak AF field can be increased by steps to determine an appropriate "cleaning" field for all of the samples.

Similar to AF demagnetization is anhysteretic remanent magnetization (ARM) which is imparted by AF demagnetizing the sample with a non-symmetric or biased AF field. The resulting artificial remanence is useful for distiguishing sediment types and for normalizing NRM intensities.

Also useful for distinguishing sediment types is the initial magnetic susceptibility (X), measured on a Bartington Instruments susceptibility bridge. X is the signal induced in the sediment by a low-intensity, 1 KHz alternating magnetic field. Since X is a parameter of the bulk sediment, it is not dependent on the paleomagnetic field or on the original remanence of the sediment. Each of these basic magnetic techniques and measurements are put to good use in the following chapters.

CHAPTER 2: FIELD WORK

A. Elk Lake setting and history.

Elk Lake (Figure 1) is located in Itasca State Park, Clearwater County, in northwestern Minnesota (lat. 47.2° N, long. 95.2° W.). It is a hard-water lake, common in areas with gray calcareous till, and is mesotrophic biologically (Stark, 1976). An important physical characteristic of the mile-long lake is the 95 ft (28 m) deep hole in the southeastern end (Figure 2). The deep hole allows Elk Lake to preserve the annual laminations in the sediment. Lakes that freeze over in winter often have different depositional conditions in summer and winter, but in most cases the seasonal layers are mixed by currents or bottom dwelling organisms. The deep hole in Elk Lake is anoxic for part of the year (Stark, 1976), preventing bioturbation, and the depositional environment is quiet, so the seasonal layers are preserved.

Elk Lake dates from the last retreat of glaciers from the area. The primary land shaping agent was the Wadena lode of the Late Wisconsin ice sheet which brought Paleozoic limestone from southern Manitoba, forming the gray to buff sandy calcareous Itasca moraine some 20,000 years ago (Stark, 1976). Wright (1972) proposed that the bed of Elk Lake was part of an sub-glacial stream tunnel system. This tunnel was later filled by stagnant ice, probably buried, which may have been long lived, so that the age of the lake itself is uncertain.

B. Expedition histories.

The sediment analyzed in this study was collected on five separate expeditions to Elk Lake over a six year period. The insufficiency of the data from any one trip is due to the difficulty of access to the lake, the often violent weather conditions, the depth of water in the lake, the thickness of the sediment pile beneath the water, and the finite strength and endurance of the crew members. The quality of the combined data from the five trips is a tribute to the men and women who gave so much of themselves for the project.

In 1978, the United States Geological Survey undertook a project to study the paleoecology of Elk Lake. A single core, reaching to the bottom of the sediment pile, was obtained but was unsatisfactory in several regards. Because of an error in the field work, one core segment was doubled while one was missed. Additionally, because the core was unoriented and frozen, it was not adequate for paleomagnetic study. The core has been useful however for varve counting and correlation purposes, and for radiocarbon dating. Preliminary results of the USGS work have been published by Dean et al. (1984).

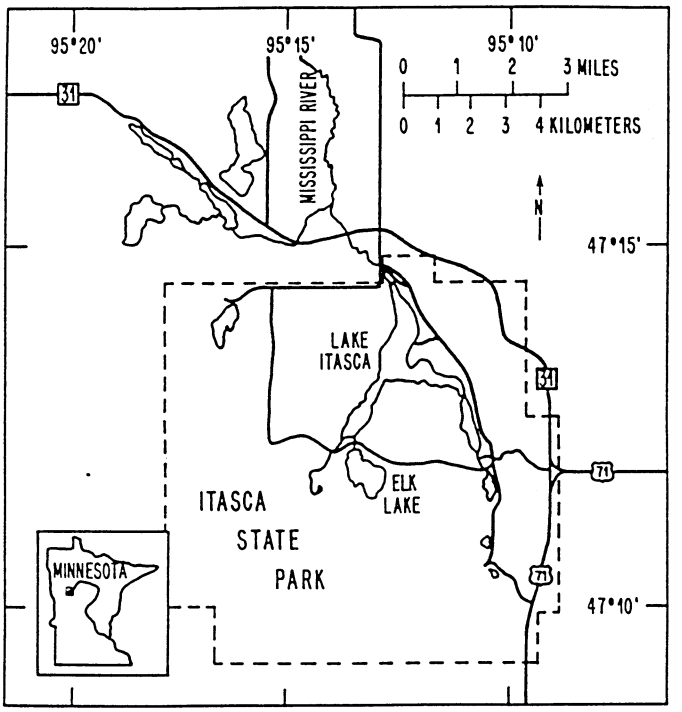

Figure 1: Itasca State Park and vicinity
(after Stark, 1976)

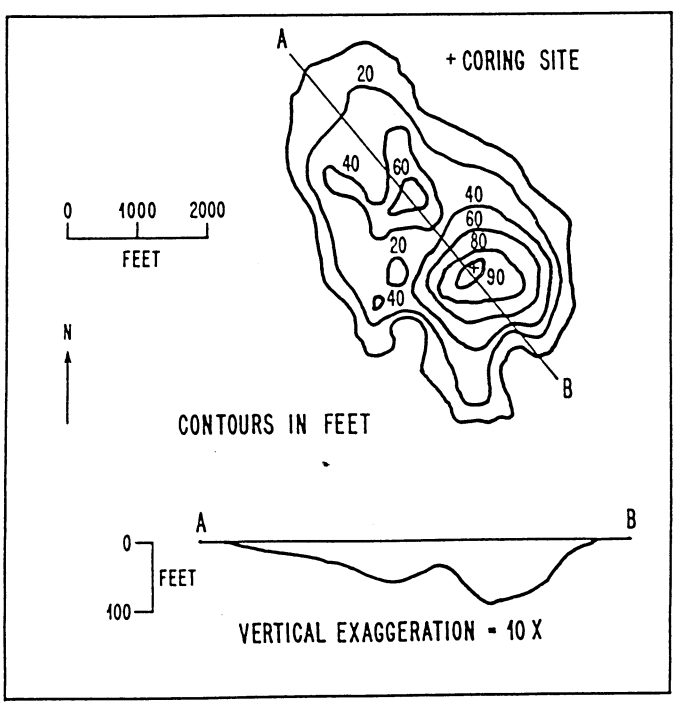

Figure 2: Elk Lake Bathymetry
(after Stark, 1976)

In the fall of 1980, we attempted to core the lake from a raft, rather than from the customary ice surface. Anchoring the vessel in high winds proved impossible, and the cores obtained were of uncertain orientation. In the winter of 1982, we were marginally successful, obtaining several short sections and two medium-length cores of good quality, before equipment failure sent us home. In the winter of 1983, we were blessed by perfect conditions and were finally successful in obtaining the difficult bottommost sediment, in two parallel long cores. All that remained for 1984 was a relatively simple trip to collect the remaining bits of the uppermost portion of the sediment section. The record of cores taken from 1980 to 1984 is plotted in Figure 3.

C. Field methods.

The Elk Lake sediment cores utilized in this study were taken in winter, using the ice as a working platform. Each core is made up of several drives or segments from a single hole (Figure 3). Each core segment is one or two meters in length and 5 or 8 cm in diameter, depending on which corer was used. The corers are modified Livingstone type piston corers (Figure 4), quite simple in design and operation: A hollow stainless steel tube (the corer) is fitted with an internal piston and then is lowered, with the piston at the bottom, to the starting point in the sediment, by means of a series of interconnecting extension rods. The piston is then secured by a cable fixed to the ice, while the tube is pushed down past it (Figure 4). At the end of the drive, the piston is at the top of the tube, which is full of sediment. The whole assembly can then be brought to the surface, with the piston holding the mud in the tube by vacuum. Successive drives down the same hole, made possible by the use of external casing from the ice to the sediment, make up a single sediment core. The extension rods are locked to one another with coupling sleeves, and to a frame at the surface, so that they may not rotate. This allows us to obtain absolute declination data from the sediment.

Each core segment was extruded in the field, marked with an orientation line, wrapped in plastic wrap and aluminum foil to prevent dehydration and oxydation, and transported to the lab. There, pairs of oriented samples were taken at 2-cm intervals from each core. The samples (2 cm x 2 cm x 1.8 cm) were taken with a non-magnetic mini-corer of square cross-section (Figure 5) and were placed in tightly fitting plastic boxes. The magnetic measurements detailed in Chapters 3, 5, and 6 were done on these boxed samples.

Because of the many cores and core segments used in the study, a short-hand

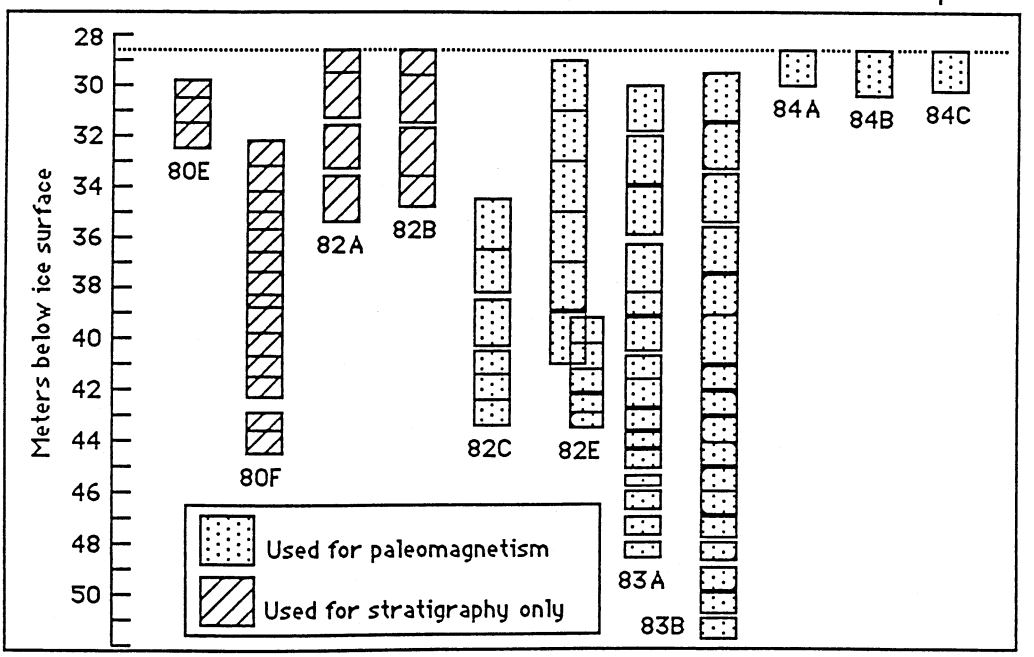

Figure 3 - Record of sediment recovered and uses for the various cores.

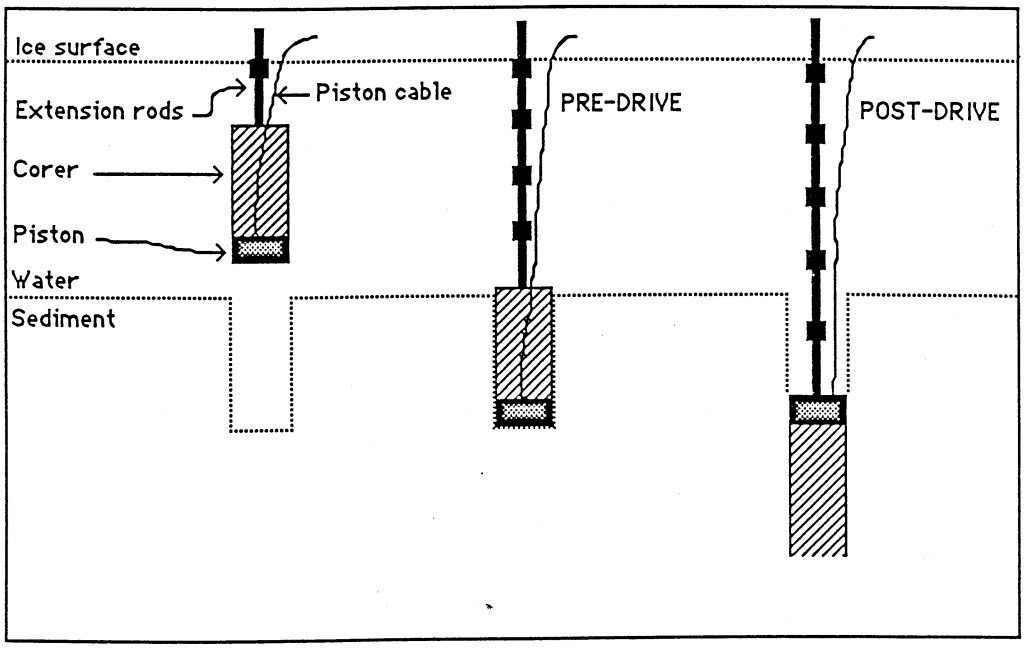

Figure 4 - The modified Livingston coring system. The hollow corer, with the piston at the bottom, is lowered to the start point (PRE-DRIVE). The piston is then fixed in space using the piston cable while the corer tube is pushed past it. The piston holds the sediment in the tube during recovery. External casing used is not shown.

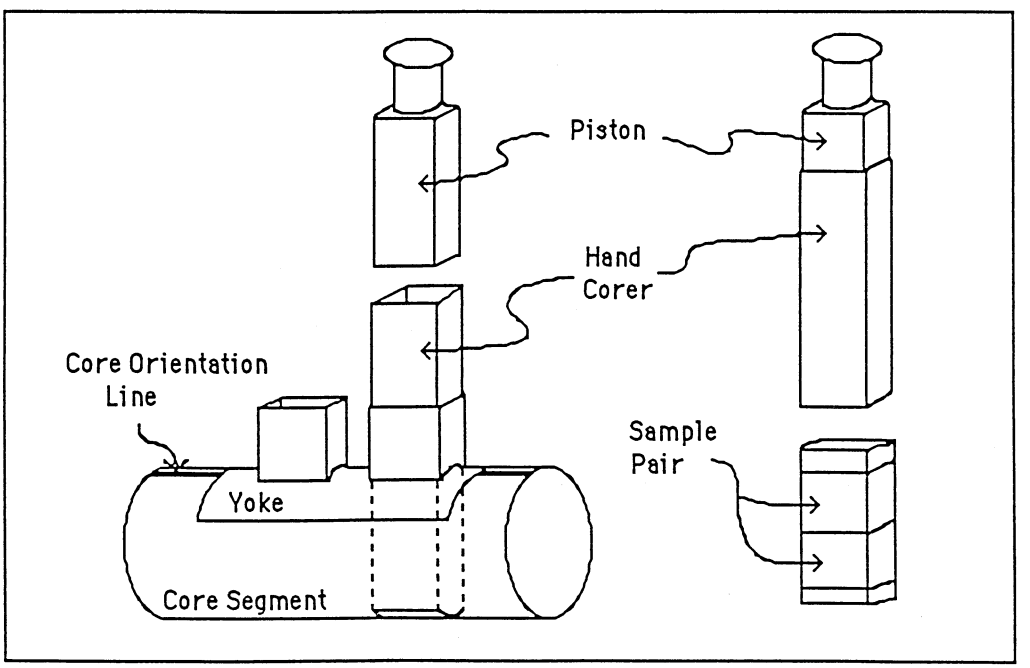

Figure 5 - Subsampling Apparatus (after Lund, 1981). The hollow, aluminum hand corer is used to obtain sample for measurement. The yolk maintains proper orientation of the hand corer relative to the core orientation line, which was scribed on the core during extrusion in the field.

nomenclature is used to identify them. A particular core, including all of the drives, is called by its year and letter (82c, 82e, 83a, etc.). Individual drives are given a number as well, beginning at the top and going down (83a01, 83a02, etc.).

D. Orientation uncertainties.

An important goal of the field work is to preserve the orientation of the sediment until it can be measured. The field methods described above, while state of the art, are not perfect in this regard, so a discussion of possible sources of error is appropriate. Once the samples are in plastic boxes, preservation of orientation is simple, but errors are possible previous to this step.

Important errors in the inclination record (< 10°) can result from non-vertical drives. The coring system is designed to take cores straight down (vertically), but since the corer is driven from the end of a long string of extension rods, verticality cannot be guaranteed. The basic check for inclination errors is to compare the records from three or more cores. We have two additional checks, 1) a bore hole monitoring device, which worked only intermittently, and 2) the apparent dip of the varves in the sediment. However, the assumption of horizontal varves may not be any more valid than the assumption of vertical drives. That we were able to descend as much as 23 m in the same hole, suggests that the drives were generally vertical. Additional errors in inclination (< 3°) can arise from the subsampling process. These errors are limited to individual sample pairs and are again checked for by comparison of multiple records.

Preserving the declination record is more difficult. While twisting of the core tube in the mud during a drive should be rare with the system used, each extension rod joint has an inherent looseness (<2°). Given ten rods, this could amount to 20° of difference between the true orientation and that measured at the top. Scribing the orientation on the sediment during extrusion is somewhat uncertain (<3°), as is the subsampling process, so we can account for as much as 25° of uncertainty in our measurement of declination. Our final estimate of these errors will come from the values obtained from the multiple cores.

CHAPTER 3 : STRATIGRAPHIC CONTROL

A. Susceptibility matching.

The first task in analyzing the paleomagnetic data from the multiple Elk Lake cores is to correlate the cores with regard to deposition time. Because the cores were all taken from the same location in the lake basin, an obvious course would be to match the cores by the depths recorded in the field notes. This is clearly shown to be inadaquate in Figure 6, which plots initial magnetic susceptibility (X) vs. recorded depth for the 1978, 1982, and 1983 cores. A number of unmistakable features are apparent in each of the cores in Figure 6, but these features do not occur at the same recorded depth in each core. This is due to changes in water level and exact coring location from year to year and uncertainty in the field record. It demonstrates that recorded depth is wholly inadaquate for core matching.

A common core matching method (King, 1983) involves assuming the depth of one core to be correct and using a linear or non-linear stretching algorithm to match the X logs of the remaining cores to that of the assumed core. The fine detail in the Elk Lake X record allows us to improve on this method by matching each core segment individually. This allows most of the gaps between drives to be uniquely determined. Figure 7 shows the same X logs as in Figure 6 with the depths adjusted as follows. The depth of core segment 83a01 was chosen as a beginning fixed reference. Correlation of overlapping sections (83b01, 82e01, 78j) with 83a01 was made easy by the presence of a conspicuous silt layer whose depth was fixed at 3018 cm. Because the gap between 83a01 and 83a02 is not well covered by other cores, the gap was assumed correct, giving 83a02 as a second fixed reference. Since 83a and 83b can be matched by shifting core segments without stretching them, the core segments from 83a02 and 83b02 on down were individually and alternately correlated using the X logs. This allowed the intra-core gaps to be uniquely determined down to 83a10, below which the 83a gaps were assumed correct. The depth corrected 83a and 83b X logs were then used as a reference for the remaining cores. The individual core segments of cores 78j, 78k, 82c, and 82e were matched to 83a and 83b using a linear stretching algorithm which chose as the best fit that which minimized the sum of squares of the differences in the X logs. A shift in depth of as little as 2 cm in the 82 and 83 cores is visually distinguishable in the curves, indicating that the matching of depths in these cores is accurate to 2 cm. Since this is the same as the subsampling interval, the depths of these cores are known without significant uncertainty, relative to the magnetic

Figure 6 (page 12) - Unmatched X. The magnetic susceptibility logs are plotted for cores 78j, 78k, 83a, 83b, 82c, and 82e. The depth scale is as recorded in the field notes. The X scale is with regard to core 78j, with the other cores shifted progressively 5 units to the right.

Figure 7 (page 13) - Matched X. The Figure 6 susceptibility logs are plotted identically, except that the depth scale has been adjusted as described in the text.

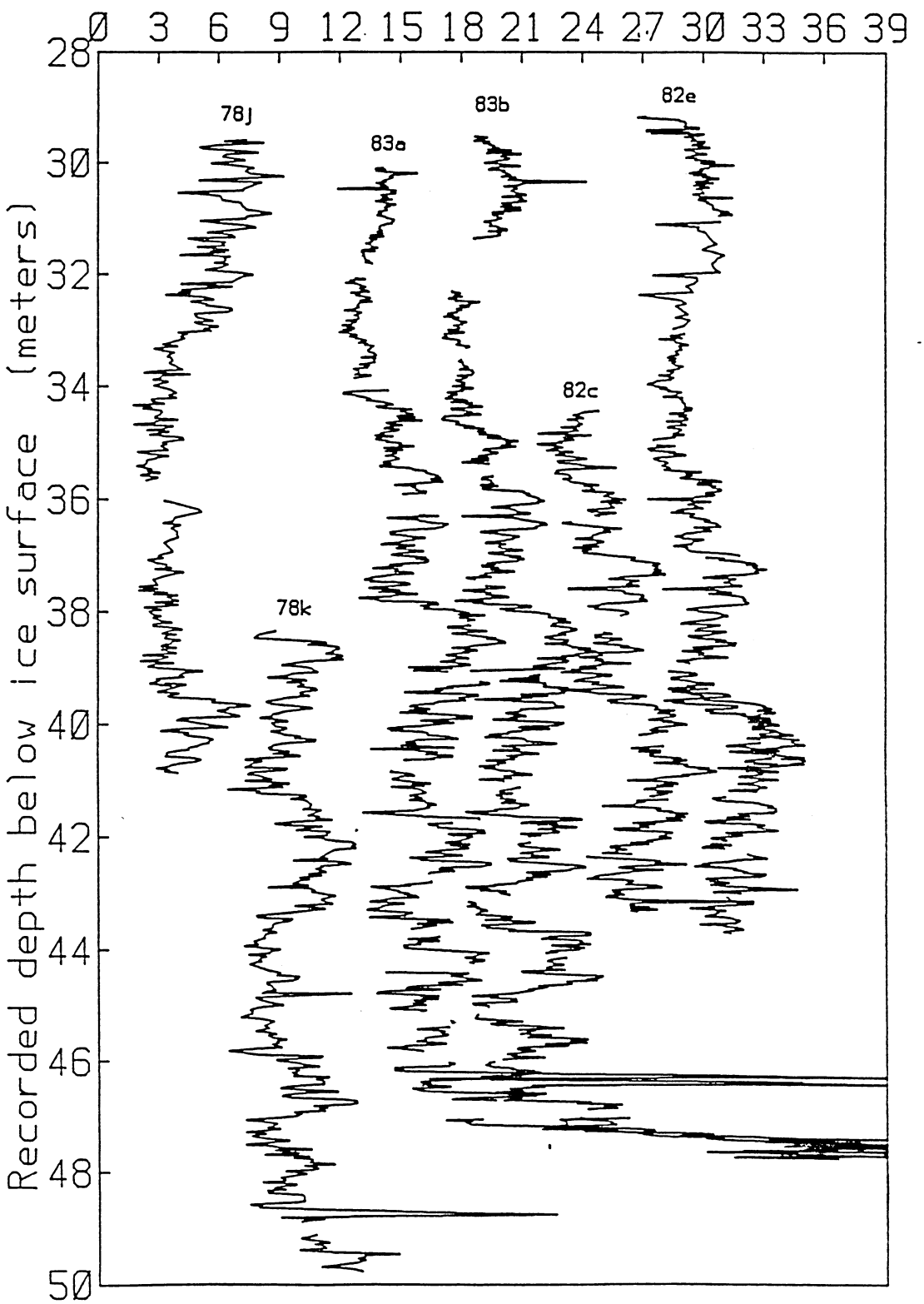
Elk Lake X (E-5 emu)
0 3 6 9 12 15 18 21 24 27 30 33 36 39
28 30 32 34 36 38 40 42 44 46 48 50
Recorded depth below ice surface (meters)
78J
78k
83a
83b
82c
82e

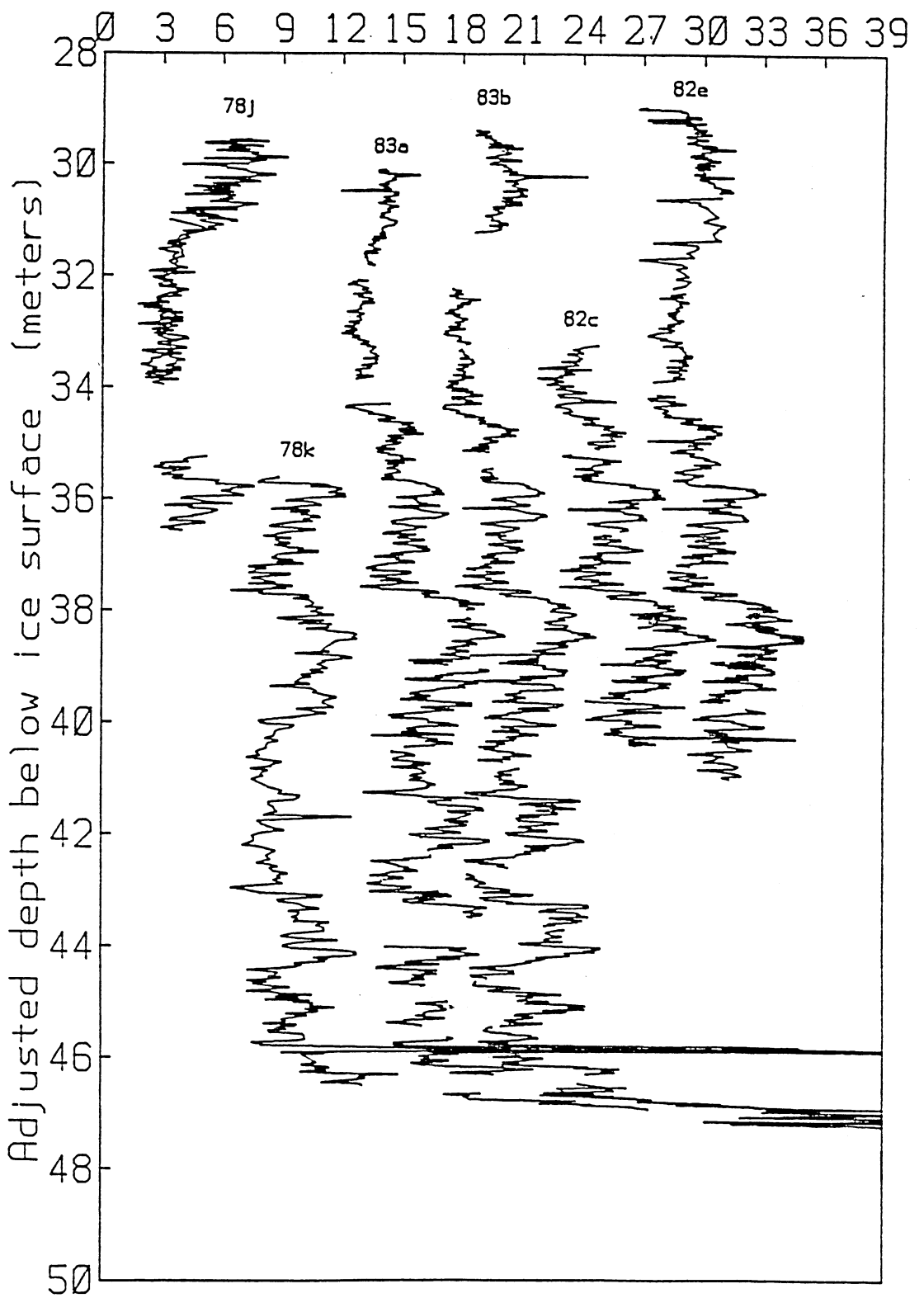
Elk Lake X (E-5 emu)
0 3 6 9 12 15 18 21 24 27 30 33 36 39
28 30 32 34 36 38 40 42 44 46 48 50
Adjusted depth below ice surface (meters)
78j
78k
83a
83b
82c
82e

record.

B. Elk Lake stratigraphy.

It is useful at this point to look in an overview sort of way at the sediment of Elk Lake and divide the sediment section into several distinguishable parts. Figure 8 divides the sediment into several zones based on rock magnetic parameters. "Rock magnetics" is a term encompassing most of the non-directional magnetic properties of the sediment. Plotted in Figure 8 are the X and ARM logs from core 83a. X and ARM are useful together, for while they both reflect changes in concentration of magnetite, ARM reflects the fine grained fraction while X relects the coarse grained fraction (King et al., 1982). Below 47 m (≈12000 years ago) in Figure 8, where both ARM and X are very high, the sediment is unvarved, inorganic, and of highly variable grain size, from silt to coarse sand. This represents late-glacial sedimentation rather than the deep lake sedimentation seen above 47 m. Since the late-glacial sediments are unvarved, the sedimentation rate is unknown, but it is variable and could well be quite high, so that little time is represented by these sediments. For these reasons, the magnetic signal from the late-glacial sediments will not be dealt with any further.

Above 47 m the sediment is a laminated marl, quite regular in magnetic character, until about 31 m (~1500 years ago) where ARM increases dramatically. This increase in ARM is due to a large increase in the amount of fine-grained magnetite, which will be discussed in detail in Chapter 6. The ARM plot conveniently divides the sediment into two parts, upper and lower. It is useful to divide the lower portion further into a middle section, from 31 to 41 m (~8000 ago), for which fourfold coverage is available, and a lower section, from 41 to 47 m, for which there is only twofold coverage.

The Elk Lake sediment can also be subdivided with regard to climatic history. Stark (1971,1976) and Dean et al. (1985) have detailed the limnologic and climatic history of Elk Lake, based on changes in chemistry, pollen, and diatoms in the sediment. The late-glacial sediments have a tundra type pollen assemblage, indicating a cold climate as might be expected. As the climate warmed, a spruce forest was established and then replaced by pine and then by prarie grasses (≈8500 ago), indicating a drier climate than at present. This climate persisted, with variations, until about 4000 years ago when the present day climate was established. This change in climate can also be seen in the varve record, varves from the recent period being more sharply defined than those from the drier period. The climatic divisions do not coincide with the magnetic divisions noted above, nor

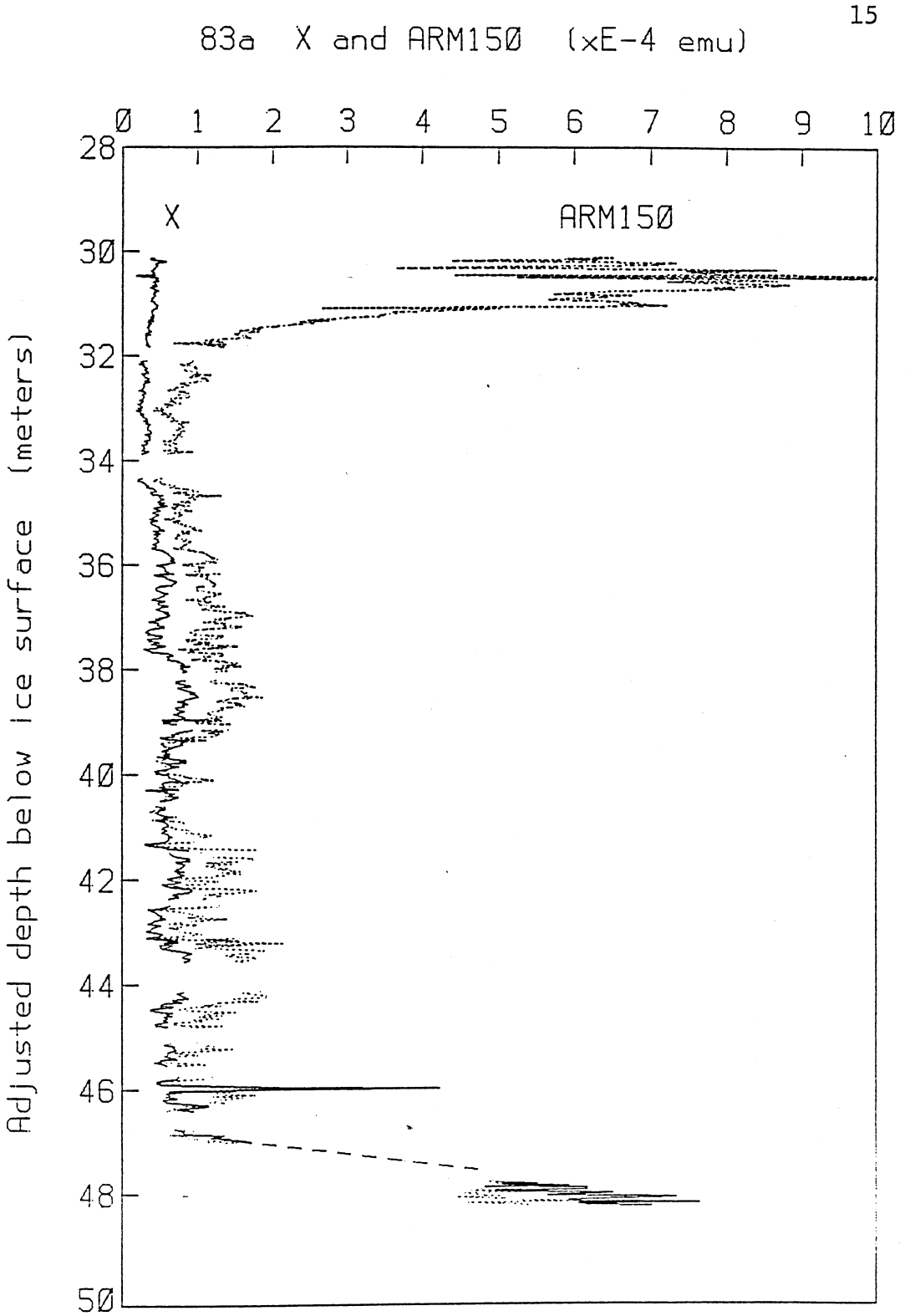

Figure 8 - X and Arm150. X from core 83a is plotted as a solid line. ARM is plotted as a dotted line.

should we necessarily expect them to.

CHAPTER 4: AGE CONTROL

A. Introduction.

With recent improvements in methods for obtaining paleomagnetic records from wet lake sediments, dating of the records is often the factor which limits resolution. Characteristically, sediments are dated by the radiocarbon method, which is inherently limited in resolution, and is susceptible to several systematic errors. Radiocarbon dates obtained from Elk Lake are discussed in section D of this chapter, but a major motivation in the study of Elk Lake is the availability of a better form of age control, annual laminations (varves). Varves provide excellent time control, making the magnetic record far more useful. Figure 9 is a photograph of a typical upper section of Elk Lake core, showing the varves. The varves are calcareous in nature, similar to those described by O'Sullivan (1983). In general, the varves consist of a dark organic layer deposited under the ice in winter and a light summer layer composed primarily of $CaCO_3$. The $CaCO_3$ is precipitated when the water temperature rises, or by phytoplankton photosynthesis. Dean et al. (1985)

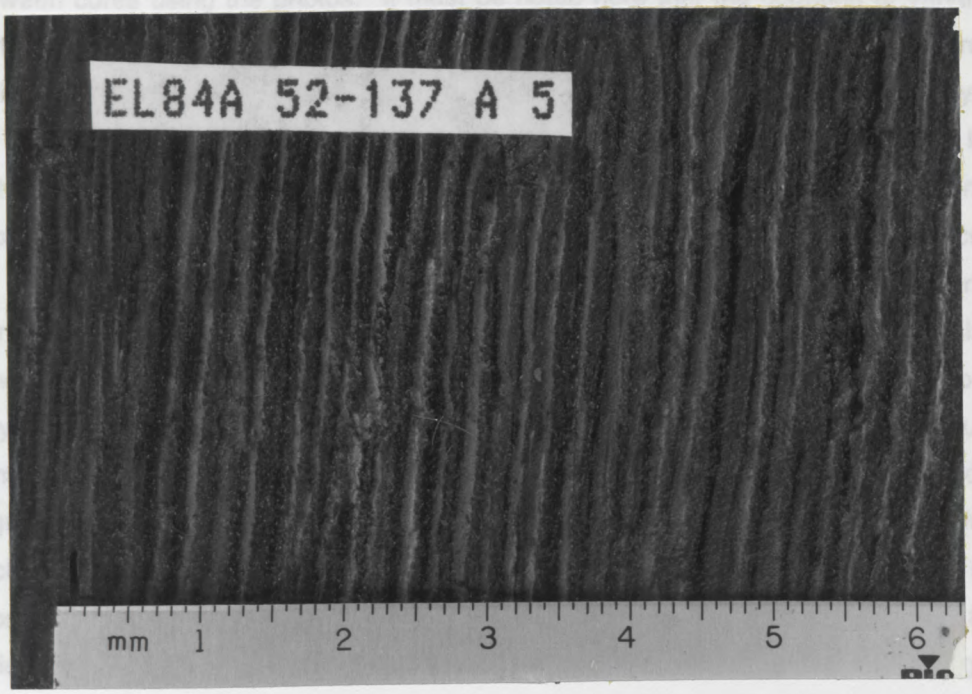

Figure 9 - Photograph of Elk Lake varves. Scale in cm.

note differences in the varves from the different climatic periods. In particular, during the warm period (8000-4000 years ago) the lowered water level allowed the influx of clastic material into the deep hole, modifying varve formation. The varves can be traced throughout the sediment section, but there is a definite change in varve quality during the warm period.

B. Varve Counting.

The time control provided by the annual laminations is of central importance to the paleomagnetic study. A couple of methods of counting the varves were attempted. Initially (cores 82c, 82e, and 83a), the core halves remaining after paleomagnetic subsampling were frozen and then the cores were polished and the varves were counted in a walk-in freezer. This method proved inadaquate because freezing caused ice wedges to form in the cores, making varve identification difficult. Therefore, the core halves from the remaining cores (83b, 82 a and b, all of 84, and some of 80) were left unfrozen. These halves were carefully scraped clean with a knife and photographed at 2:1 magnification (35 overlapping photos per meter). It was then very easy to count the varves and correlate between cores using the photos. It must be noted here that the counting of varves is partly science and partly art. The varves are distinguished visually as repeated patterns of various colors. There is often little doubt as to what constitutes an annual series of layers, but this is not always the case. Occasionally, there is a white or black layer which is less distinct or quite a bit thinner than its neighbors. Thus, the number of varves counted depends upon the judgment of the counter, which hopefully improves with experience.

For the purposes of obtaining multiple counts of equivalent sections, the varves were counted between prominent marker horizons. The record of counts obtained between 63 such marker horizons is contained in Appendix 1. The upper 3 m of section is very well covered by multiple cores from 82a,b,and e, 83b, and 84a,b,and c. The counts from the remaining 15 m of section are taken from 83b, with gaps between the 83b core segments covered by counts from 78k, 82c and e, and 83a. Given the best counts from each interval, the photos were used to assign best ages to every 2 cm of depth (the subsampling interval) in the sediment. Figures 10 through 13 represent these data in various ways. Figure 10 shows the number of varves per 2 cm sample vs. depth. Figure 11 is the reciprocal of Figure 10, showing the thickness of the varves vs. depth. Figure 12 is the same as Figure 11, except that varve thickness is plotted vs. cumulative varve years. Finally, Figure 13 is the integral of Figure 10, showing cumulative varve years vs. depth.

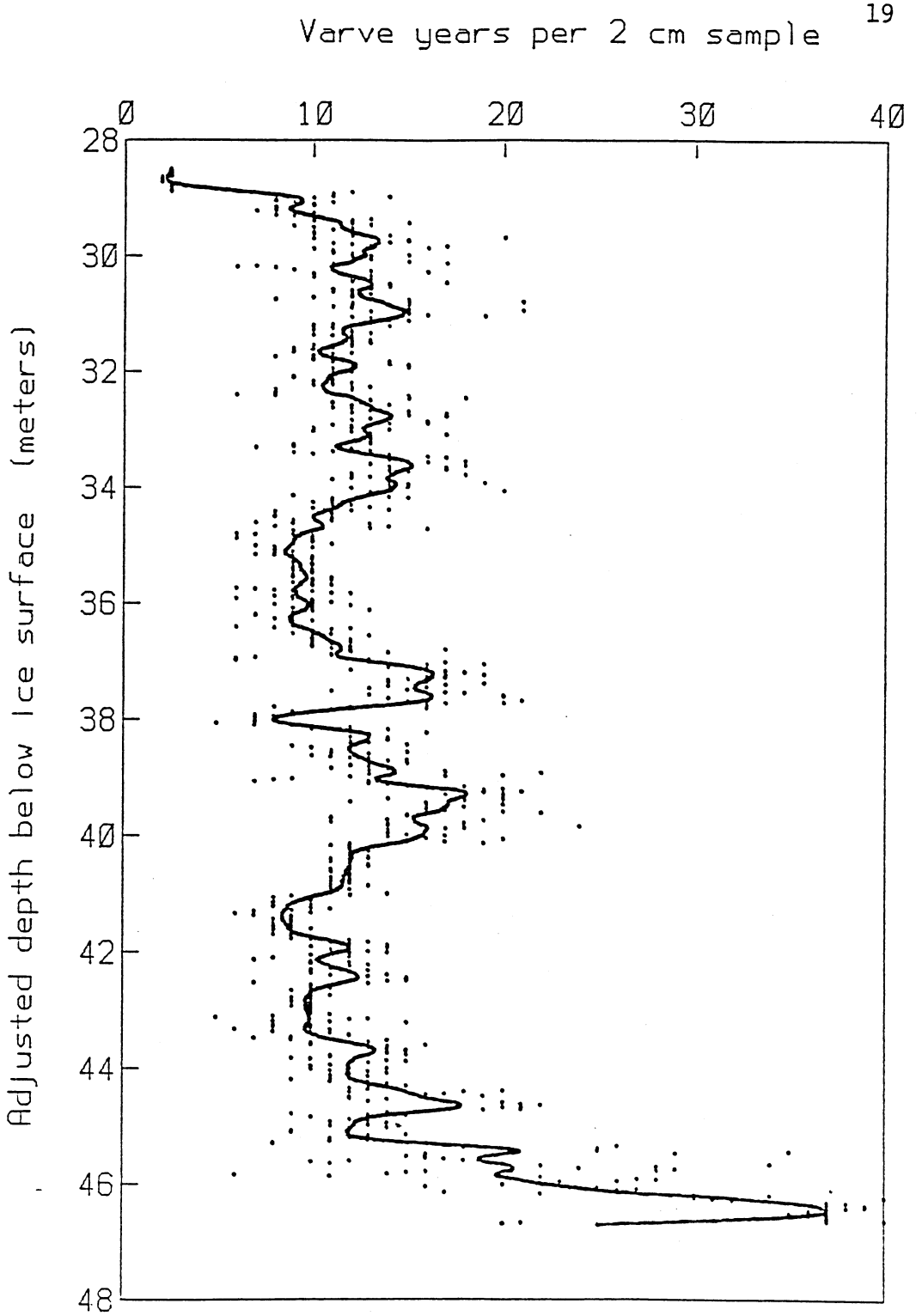

Figure 10 - Varve years per sample vs. depth. Varves have been counted or interpolated every 2 cm. from the sediment/water interface at 2848 cm to the late-glacial sediments at 4668 cm.

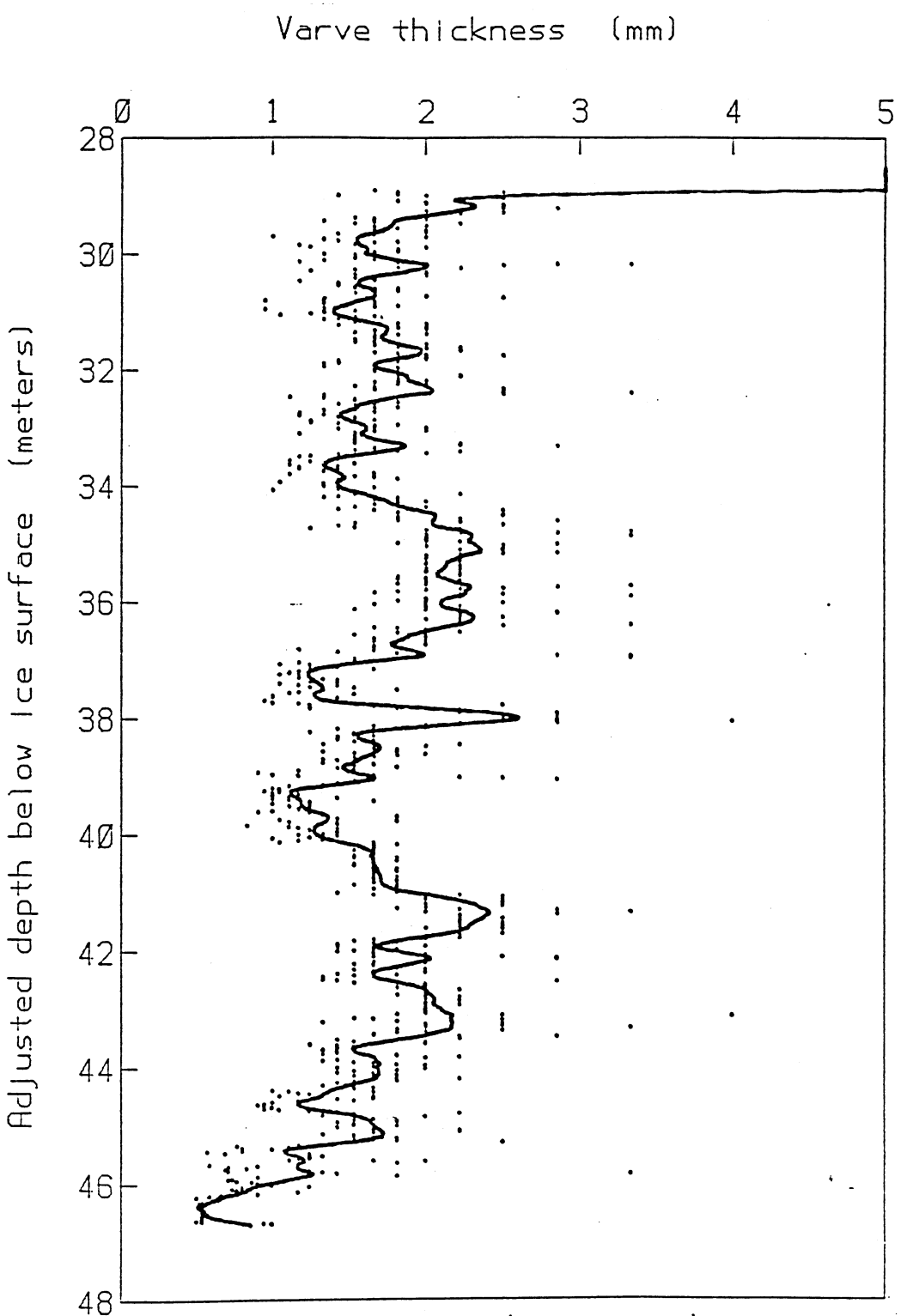

Figure 11 - Varve thickness (2 cm averages) vs. depth.

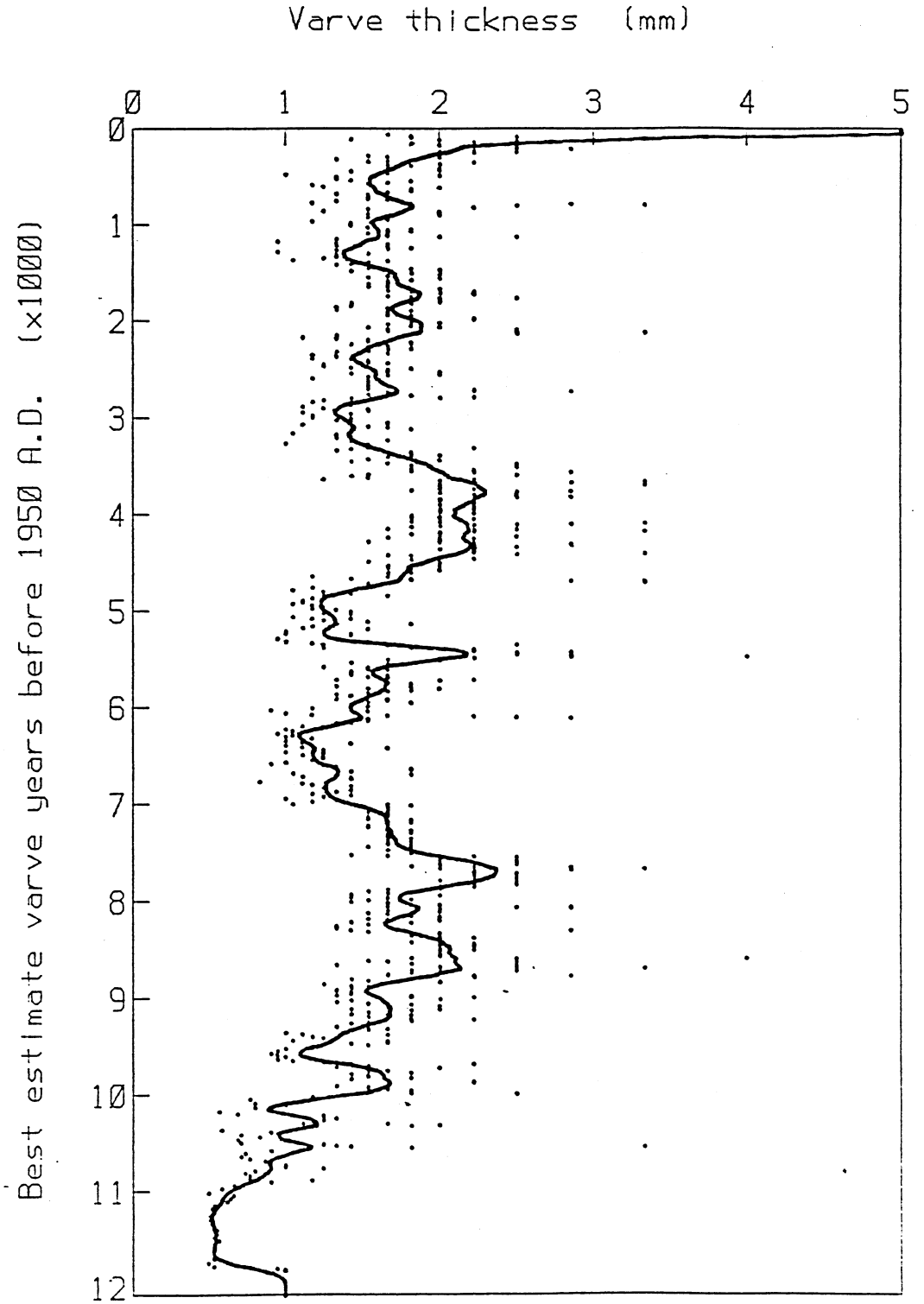

Figure 12 - Varve thickness vs. cumulative varve years.

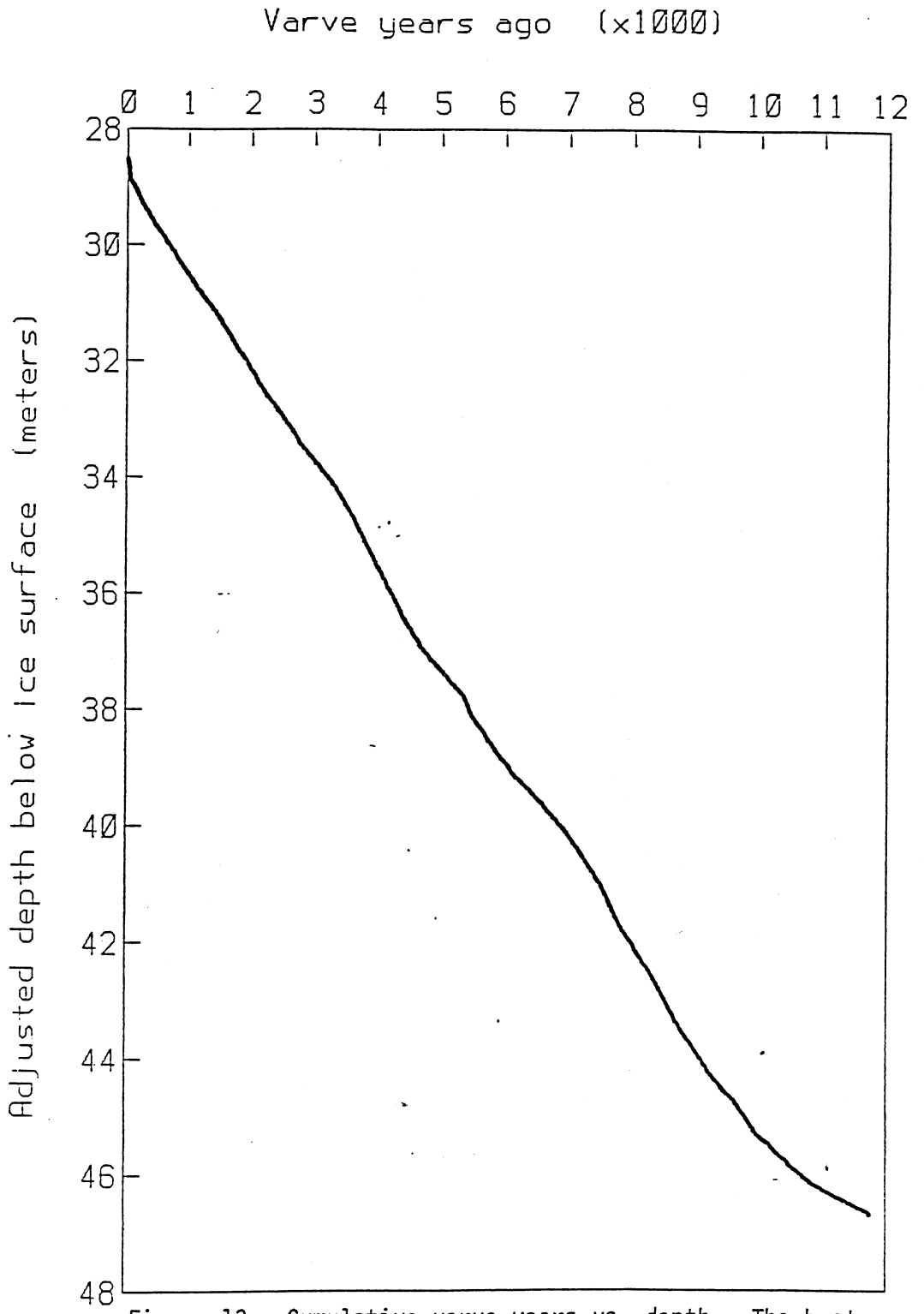

Figure 13 - Cumulative varve years vs. depth. The best estimate of the age for the transition to late-glacial sediments at 4668 cm. is 11744 years ago.

The bottom age, 11744 years ago, is the best estimate for the beginning date of the lake proper and the initiation of varve formation.

The best quantitative estimate of the uncertainty in the varve counts comes from multiple counts of the same section, from two faces of the same core, and from overlapping cores. If the counting errors are normally distributed with zero mean, the standard deviation of the counting errors is an estimate of the uncertainty in the counts. As an example, nine separate counts are available between marker horizons B and C: 148, 149, 151, 148, 151, 148, 147, 153, and 145. The mean of these is 148.9, and the standard deviation is 2.28. So with 95% confidence, the count would be 149 ± 4.6.

But the counting errors are almost certainly not normally distributed with zero mean. Because varves can be obscured or left undistinguished by whatever cleaning or polishing technique is used, counting too few varves is more likely than counting too many. It might be more appropriate then to think of varve counting as a binomial process where each of the varves (n) has a probability of being counted, p. The expected value of the count, k, is then np, and clearly $k \leq n$ for any $p < 1$. But estimating n from k when p is unknown is an unsolved problem.

For these reasons, the highest count from a given interval was used as an estimator of the actual number of varves present. This estimator is clearly biased to the high side to counter the natural bias toward missing varves. Since the varves were counted liberally rather than conservatively, the estimator may be overly biased. The counting uncertainties (described presently), on the other hand, are quite conservative, and the true age of the sediment almost certainly lies within the limits of 95% confidence. The final section of this chapter, dealing with the radiocarbon calibration curve, suggests that the best estimate varve counts are fairly accurate.

Relative uncertainties in the varve counts were assigned as follows. Each of the 63 counted intervals detailed in Appendix 1 was given a varve quality index, from poor to very good, based on the appearance of the varves. The record of varve quality vs. depth is given in Figure 14. The transition between drier climate sedimentation and recent sedimentation is easy to see at 34 m. Sections of sediment from each of the quality groups were carefully examined, and estimates of maximum possible counting errors due to varve quality were made. Additionally, estimates of counting uncertainties were made by treating the repeated counts of Appendix 1 as being normally distributed. The two sets of error estimates are compared in Table 1.

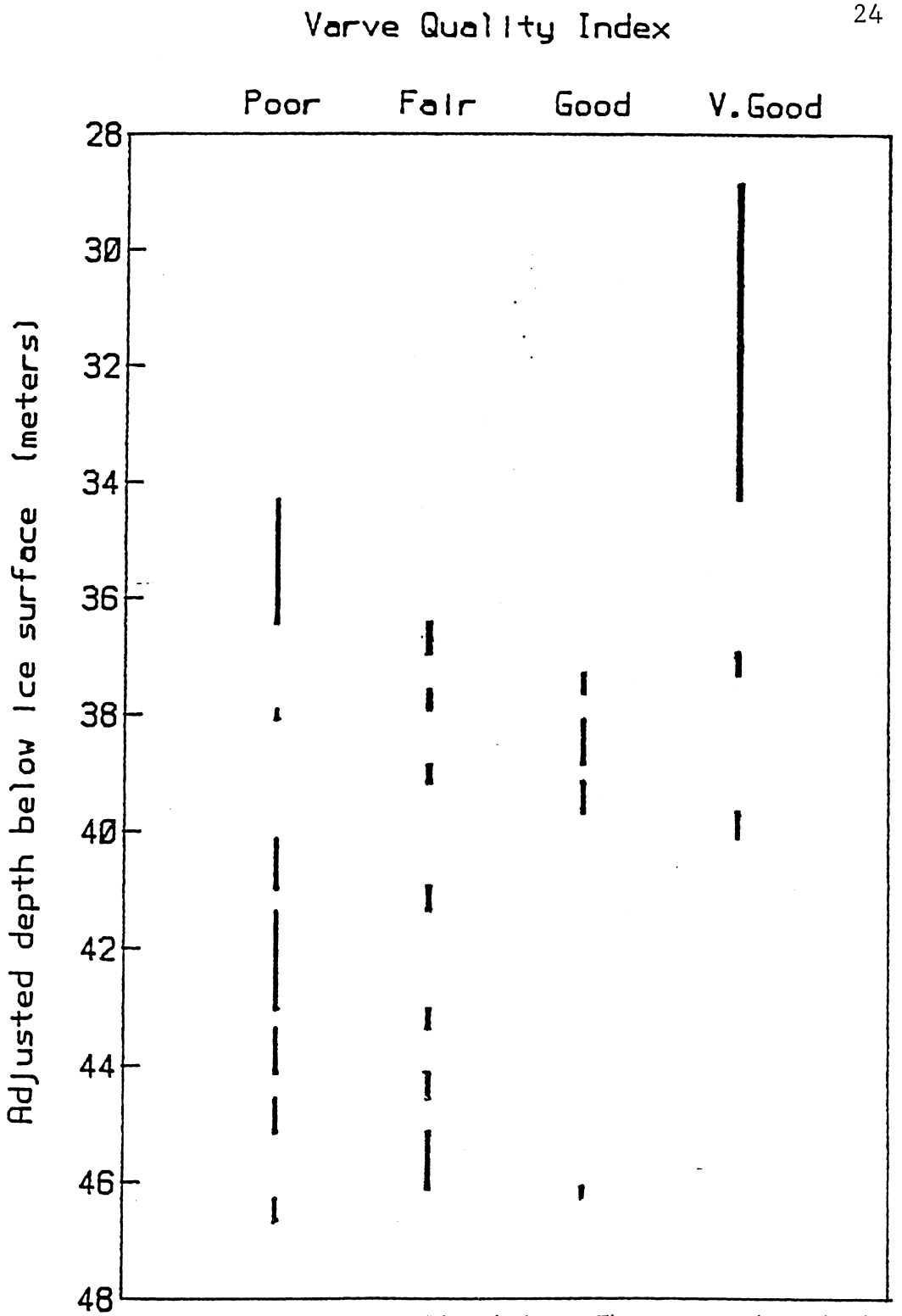

Figure 14 - Varve quality index. The varves through the various counting intervals are rated as to the uncertainty in distinguishing individual varves.

Quality index	Visual error estimate	Numerical error estimate	Average
Very good	10%	8%	9%
Good	20	10	15
Fair	30	8	19
Poor	40	12	26

Table 1. Error estimates for various quality indexes.

The numerical estimates are smaller than the visual ones because they reflect the variability in multiple best counts, while the visual estimates reflect the maximum possible uncertainty in the recognition of varves in a single core. The average of the two is taken as an estimate of the actual uncertainty in the varve counts. Figure 15 is a plot of cumulative varve years vs. depth, with the cumulative uncertainties plotted as the outer curves.

C. Dating the Uppermost Sediment.

The entire Holocene section of Elk Lake sediment contains varves of varying quality, except for the uppermost 30 cm or so of sediment. It is disappointing to lack varves in the uppermost sediment since this introduces an uncertainty into the dating of the whole section, but fortunately there is a reasonable explanation for the cessation of varve formation, and we have an independent means of dating this region.

The lack of varves in the upper 30 cm of sediment suggests a change in the depositional environment in Elk Lake. Stark (1971) interprets a darkening of the sediment and increased sedimentation rate as an increase in biologic productivity. She noted irregular and thick banding in the upper sediment, reflecting a change in sedimentation rather than a simple physical destruction of varves. The only reasonable cause for this change in sediment quality is the logging activity in the area around the turn of the century. Aaseng (1976) has detailed the history of logging in Itasca State Park. Logging began in the park in 1901 and continued through 1919, with major logging in the Elk Lake watershed in 1918. In the 1890's, logging was extensive to the north of the park in the Bemidgi area (Foster, 1976).

The effect of this logging activity can be clearly seen in the pollen diagram from an Elk Lake frozen surface core, as measured by John Almendinger (Figure 16). The Pinus total diagram plots the changes in the percent of pine pollen in the Elk Lake sediment. There is a clear decrease in pine pollen, from about 52% to about 35%, beginning at 25 cm depth, just where the change in sedimentation occurs. At the same point, there is a dramatic increase in the amount of Ambrosia pollen in the sediment. Ambrosia (ragweed)

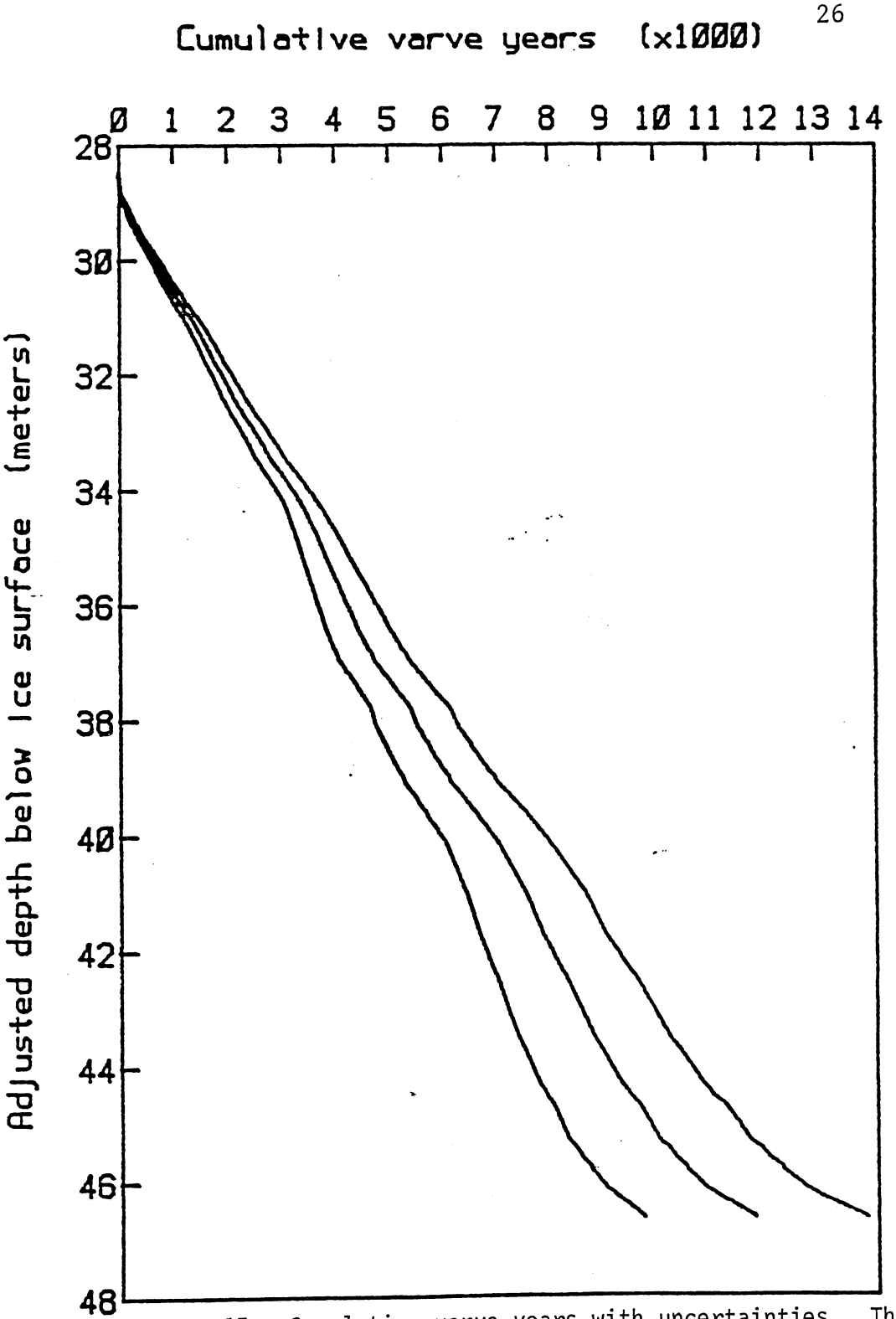

Figure 15 - Cumulative varve years with uncertainties. The best estimate of teh sediment age (center curve) is bounded by two limit of confidence curves.

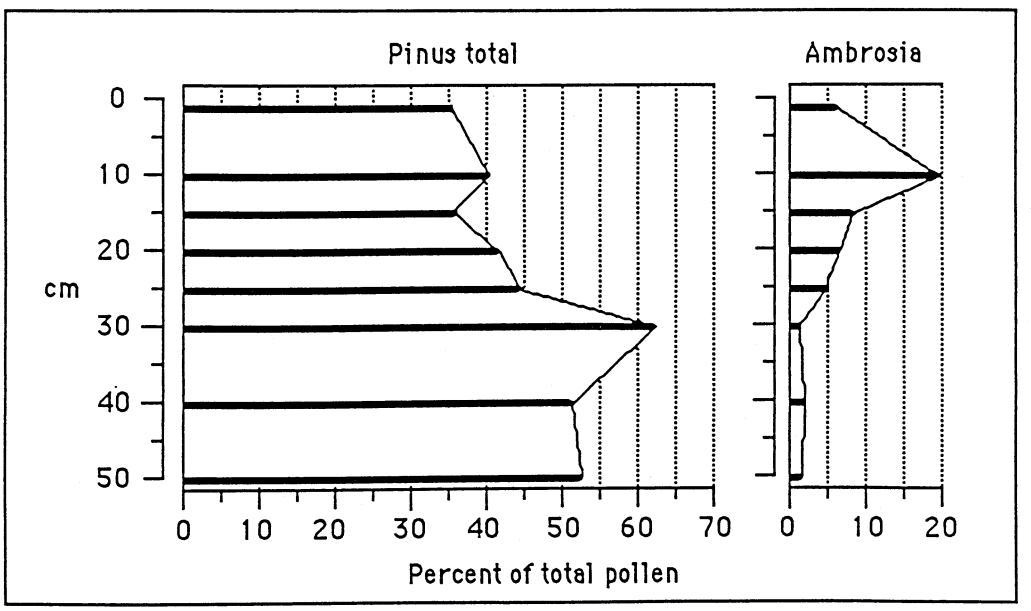

Figure 16. Elk Lake pollen diagram. Analysis performed by John C. Almendinger on frozen core #4, 1980.

is an efficient invader of open territory, and a rise in Ambrosia pollen is very commonly seen soon after the time of settlement. Thus, there are three events, the change in sedimentation, the pine decline, and the Ambrosia rise, which are recorded at the same point in the sediment of Elk Lake. All three are undoubtedly due to logging and settlement in the area.

Dating of this transition is made uncertain, however, by our lack of knowledge of the exact causes of the changes. In particular, it is not clear whether the changes in pollen are local or regional. Patterson (1978) studied the history of Squaw Lake, 4 km NW of Elk Lake, and concluded that the Ambrosia rise was a regional event, dating from about 1890. Important support for this conclusion is given by Foster (1976) who measured pollen changes in the sediment of Lower LaSalle Lake, 10 km to the north of Elk Lake. Lower LaSalle Lake is varved to the very top, which allowed Foster to carefully date both the pine decline and the Ambrosia rise. The Ambrosia rise begins between 1880 and 1890, while the pine decline begins between 1890 and 1900. It is suggested that this early rise in Ambrosia is due to settlement in the Red River valley to the west, which would make the Ambrosia marker quite regional. Logging around Lower LaSalle Lake did not commence until about 1898, so the pine decline may be somewhat regional as well. But neither regional logging nor regional settlement can account for the change in sedimentation and productivity recorded in Elk Lake. A more reasonable explanation for this change is the physical effect of logging in the Itasca area. Along with effects due to road construction and slash disposal, there were significant changes in water level. To allow logs to be driven down by Mississippi River, the water level was raised in Lake Itasca by the building of a dam at the north end outlet in 1902 (Brower, 1904; Dobie, 1959; Aaseng, 1976). Brower notes significant damage to the shoreline of Elk Lake by the flooding of 1903 and 1904, caused by the Itasca dam.

All of these evidences, taken together, suggest a date of about 1900 for the cessation of varve preservation in Elk Lake. Since there is quite a bit of uncertainty in this date, I have assigned the age 50 $\pm$ 20 years ago to the transition at 30 cm depth in the Elk Lake sediment, where the reference date is 1950 A.D., the convention used in radiocarbon studies. The sediment immediately below the transition is varved, providing good time control from there on down.

D. Radiocarbon dating.

In addition to the varve chronology, 14 radiocarbon dates are available for samples

from the 1978 cores. For these dates to be useful, a positive stratigraphic correlation must be made between the 78 cores and the 82 and 83 cores. This is complicated by an error in the 1978 field work, but a satisfactory correlation can be made with X (Figure 7, p. 13). A previously distributed brief dealing with the correlation is included as Appendix 2.

Table 2 lists the details of the radiocarbon samples from the 1978 cores. The corrected ^{14}C values are adjusted for the presence of old carbon. Because Elk Lake is situated on a calcareous till, and because of the hardness of the water, it is expected that the carbon in the sediment will be partly modern and partly old. The old fraction increases the apparent ^{14}C age of the sediments. While no method of fully correcting the ages is available, if a ^{14}C date is obtained from a horizon of known age, a correction factor can be calculated and applied to all of the dates. An obvious horizon to date would be the Ambrosia rise discussed in the last section. Unfortunately, the Ambrosia rise from Elk Lake has not been radiocarbon dated.

Two alternative correction methods have been tried. The first is to assume that the varve age of the youngest ^{14}C dated horizon is the true age. The youngest sample is QL1560 with a ^{14}C age of 1420 ± 80. The varve counts for the sediment section spanned by the ^{14}C sample run from 401-500 years ago. Assuming a correct age of 450 years ago, the correction factor would be 970 years with an uncertainty of at least 80 years. The 80 year uncertainty is the measuring precision of the ^{14}C date. An additional uncertainty, difficult to assess, arises from the variation in atmospheric carbon with time (Klein et al., 1982). The possible error in the carbonate correction from this source is as much as 200 yr.

Table 2 : Radiocarbon dates.

U.W. ref.	Core segment	Orig. depth	Adjust. depth	C14 Age	Corrected C14	Varve Age
QL1492	JF 90-100	3465-3475	3285-3295	3660 ± 130	2690 ± 210	2415-2485
QL1493	JI 33-43	3717-3727	3213-3223	3190 ± 100	2220 ± 180	1975-2035
QL1494	KC 93-104	4123-4134	3771-3779	5290 ± 100	4320 ± 180	5265-5330
QL1495	KI 69-79	4697-4707	4435-4443	8550 ± 140	7580 ± 220	9268-9335
QL1496	KK 29-35	4829-4835	4547-4552	9830 ± 150	8860 ± 230	10140-10180
QL1497	KL 80-88	4986-4994	4653-4658	11380 ± 180	10410 ±260	11500-11589
QL1498	KN 40-55	5101-5116	4801-4816	17000 ± 800	-	> 11800
QL1560	JA 78-88	3028-3038	2988-2993	1420 ± 80	450 ± 160	401-500
QL1561	JB 82-92	3122-3132	3034-3038	2270 ± 80	1300 ± 160	985-1050
QL1562	JE 86-96	3355-3365	3176-3185	3360 ± 70	2390 ± 150	1760-1810
QL1563	JF 79-90	3446-3457	3265-3276	3370 ± 70	2400 ± 150	2275-2365
QL1564	JI 90-100	3769-3779	3266-3276	3510 ± 90	2540 ± 170	2280-2358
QL1565	KC 11-21	4041-4051	3705-3713	5750 ± 120	4780 ± 200	4735-4830
QL1566	KF 81-96	4411-4426	4087-4103	7880 ± 50	6910 ± 130	7390-7500

The second method of correcting for old carbon is linear extrapolation to the Ambrosia rise. A straight line was fit to thirteen dates by the least squares method. Sample QL1498 was not included in the regression because it was taken from the late glacial sediments and is much older than the time of the glacial retreat from the area (Wright, 1972). It is presumably highly contaminated with glacial carbonate. The equation of the regression line through the thirteen points is :

^{14}C age = (depth in cm)(5.156 yr/cm) - (13490 yr). This yields a ^{14}C age of 1400 yr for the Ambrosia depth of 2888 cm, or a correction factor of 1350 yr. The 95 % confidence interval for the Ambrosia date (Larson and Marx, 1981, p. 420), assuming no uncertainty in the individual dates or depths, goes from 190 years to 2510 years. Figure 17 shows the radiocarbon dates and the two correction methods in graphical form. Also shown in Figure 17 is the best polynomial fit, not significantly different from the linear fit.

Because it appears to be less uncertain, the first correction method was used to produce the corrected dates of table 2 by adding (-970 $\pm$ 80 yr) to each date. The straight line fit to the corrected data is :

14C age = (depth in cm)(5.154 yr/cm)-(14452 yr). The corrected radiocarbon dates and the varve chronology are plotted together in Figure 18. While the uncertainies about the cumulative varve line are conservative, the error boxes on the radiocarbon dates represent the minimum possible uncertainty in the dates. The radiocarbon dates show a slightly higher average deposition rate, but the expected radiocarbon age at the sediment/water interface is 225 yr, indicating that the slope is probably too steep.

E. The radiocarbon calibration curve:

The above treatment of the radiocarbon dates assumed that ^{14}C production has remained constant throughout the last 12,000 years. But this known to be untrue. Variations in ^{14}C production through time require corrections to be made to the apparent ^{14}C ages. Radiocarbon dating of wood samples whose true ages are known through dendrochronology has produced an accurate calibration curve for the last 8000 years (Klein et al., 1982). Beyond 8000 years however, the curve is quite uncertain. Several varve chronologies are available back to ten or twelve thousand years ago, and the Elk Lake varve chronology can be added to these.

Figure 19 plots the Elk Lake data vs. the other calibration curves. The differences between the best varve ages and corrected ^{14}C ages for the Elk Lake samples represent the apparent variation in radiocarbon production through time. The solid curve is the

Figure 17 (p. 32) - Radiocarbon dates vs. adjusted depth. The boxes give the uncertainty in depth and the counting error of the dates. The counting error is the minimum uncertainty on the horizontal axis. Two best fitting regression lines are plotted, linear (left most at top and bottom) and polynomial. The two carbonate correction methods are shown at top left. The upper line segment shows the 95% confidence limits on the linear fit, extrapolated to the Ambrosia rise at 2888 cm. The second correction method, shifts the youngest radiocarbon date, 1420 ago at 2990 cm, to the varve age at this level, 450 ago (marked by the x).

Figure 18 (p. 33) - Comparison of varve chronology with radiocarbon dates. The two age scales are generally coincident, within the uncertainty limits, but they have somewhat different best-fitting slopes.

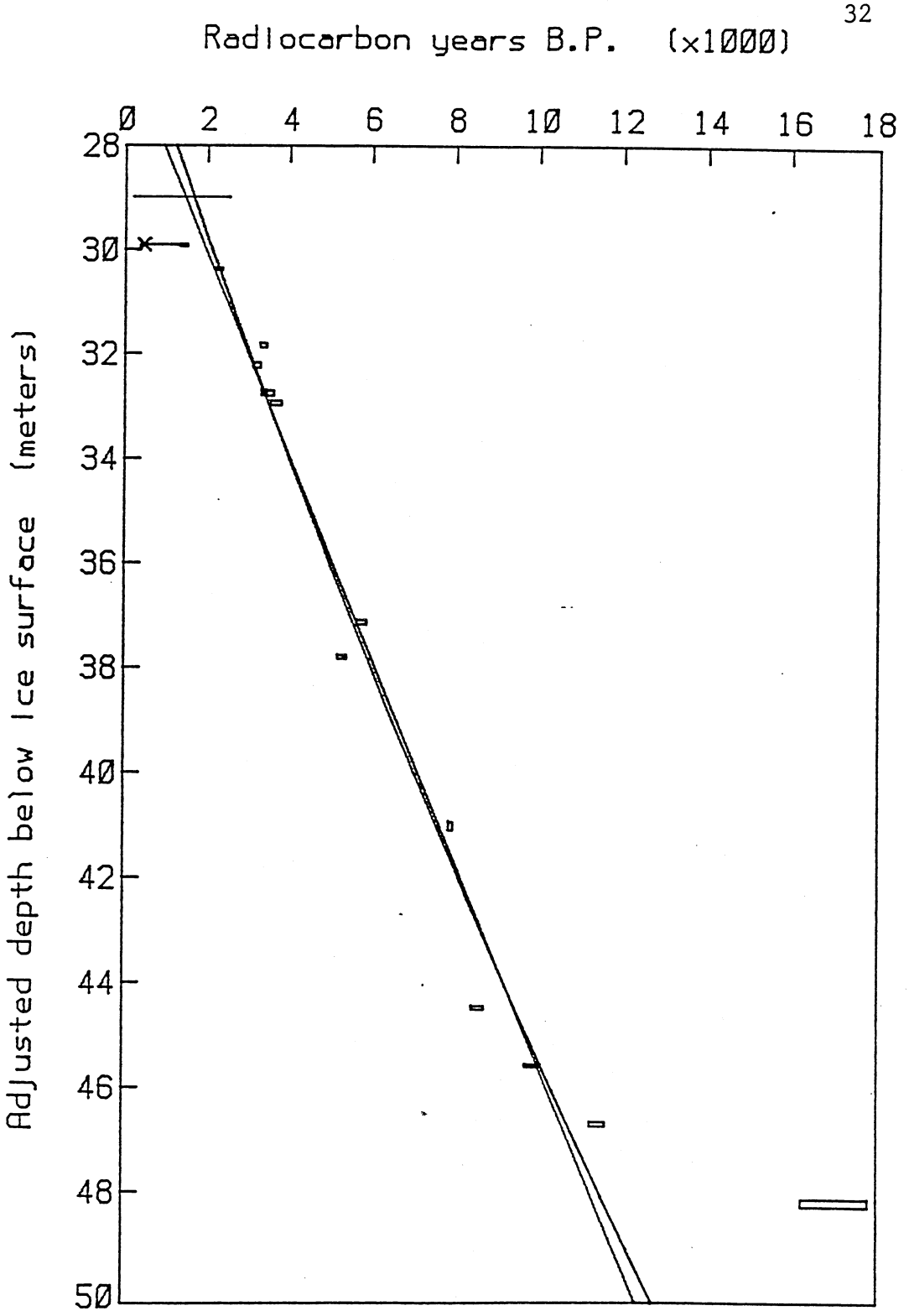
Radiocarbon years B.P. (x1000)
0
2
4
6
8
10
12
14
16
18
28
30
32
34
36
38
40
42
44
46
48
50
Adjusted depth below ice surface (meters)

Figure 17.

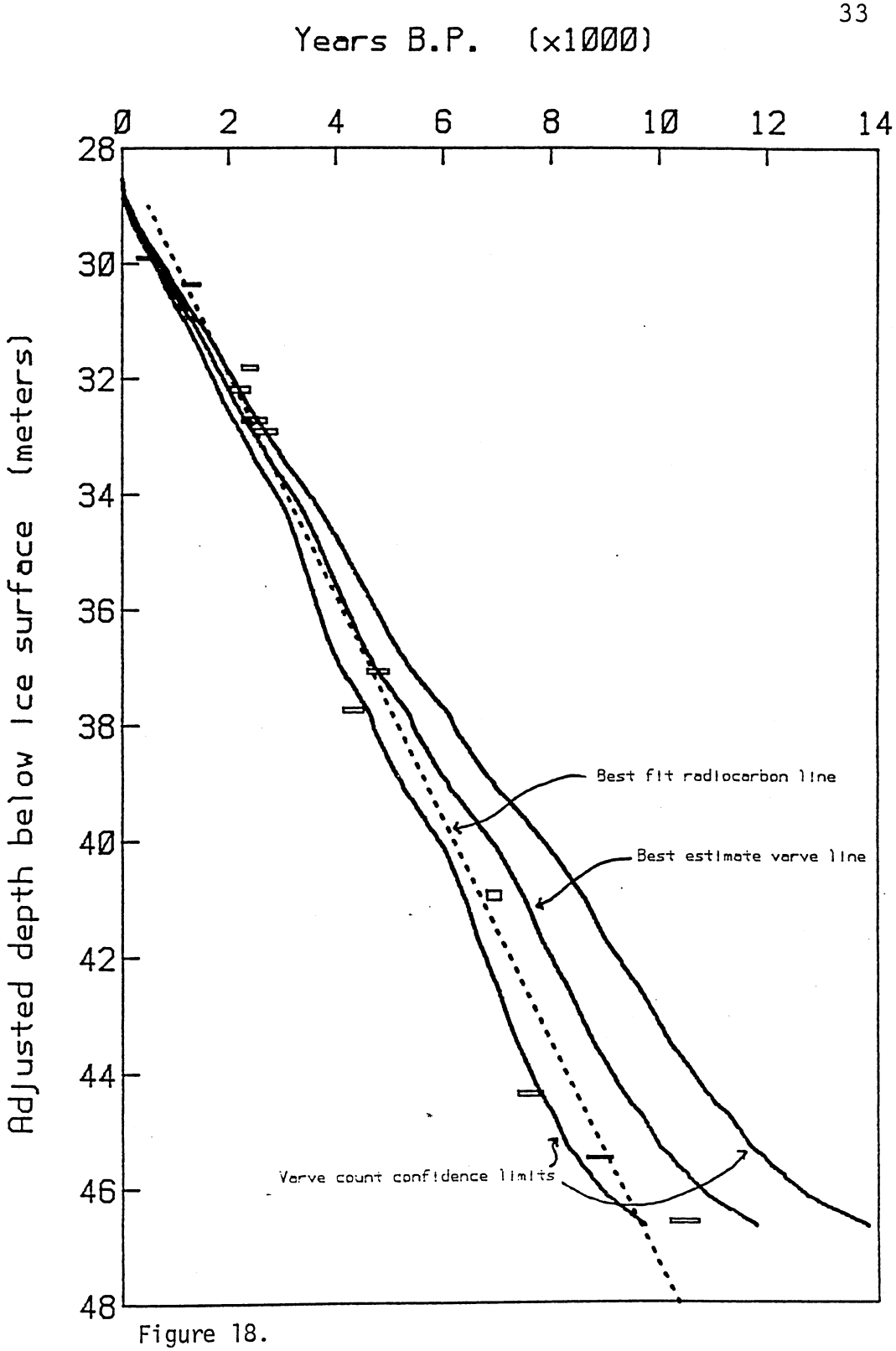
Years B.P. (x1000)
0
2
4
6
8
10
12
14
28
30
32
34
36
38
40
42
44
46
48
Adjusted depth below ice surface (meters)
Best fit radiocarbon line
Best estimate varve line
Varve count confidence limits

Figure 18.

dendrochronology correction curve (Klein et al., 1982) which is quite accurate. The dotted curve is Stuiver's (1970) curve from the varves of Lake of the Clouds in Minnesota. The dashed curve is from the Swedish varve chronology (Vogel, 1980 from Tauber, 1970). The divergence of the two varve calibration curves from each other and from the dendrochronology curve is an unresolved problem. The Elk Lake data are too few and too scattered to make a convincing curve, but several notes can be made. The seven points at less than 3000 years are all below the dendrochronology curve, indicating that the 970 year correction made to the radiocarbon dates is probably two or three hundred years too great. Given this, the remaining points follow the dendrochronlogy curve fairly well and lend support to Stuiver's calibration curve rather than Tauber's. The data from the last 3000 years imply that making a carbonate correction to the ^{14}C dates based on a single date from a known horizon (dating the Ambrosia rise is standard procedure in sediment studies) is not reliable. King (1983) has also noted this in his study of multiple ^{14}C dates from single horizons.

Figure 19, however, does not account for the uncertainty in the Elk Lake varve chronology. This is done in Figure 20 by replotting the apparent calibration curves for the minimum (lower curve), best (middle curve), and maximum (upper curve) varve ages. The dendrochronology curve is dotted. All three solid curves indicate that the carbonate correction is too great, but they diverge further out. The minimum curve supports Tauber's calibration curve but does not agree with the tree ring calibration. The maximum curve rises well above all three of the other calibration curves. The best varve age curve seems to follow the tree-ring curve most closely and again lends support to Stuiver's calibration curve. The Elk Lake varve chronology is too uncertain and the radiocarbon dates are too few and too scattered to provide an improvement to the previously published calibration curves, but the curves indicate that the true sediment age is within the varve chronology boundaries and close to the best varve age estimate. The radiocarbon dates are thus taken as confirming evidence of the annual nature of the varves and of the cumulative varve count. Henceforth, the varve chronology will be used for dating purposes because of its high resolution and its well constrained uncertainty.

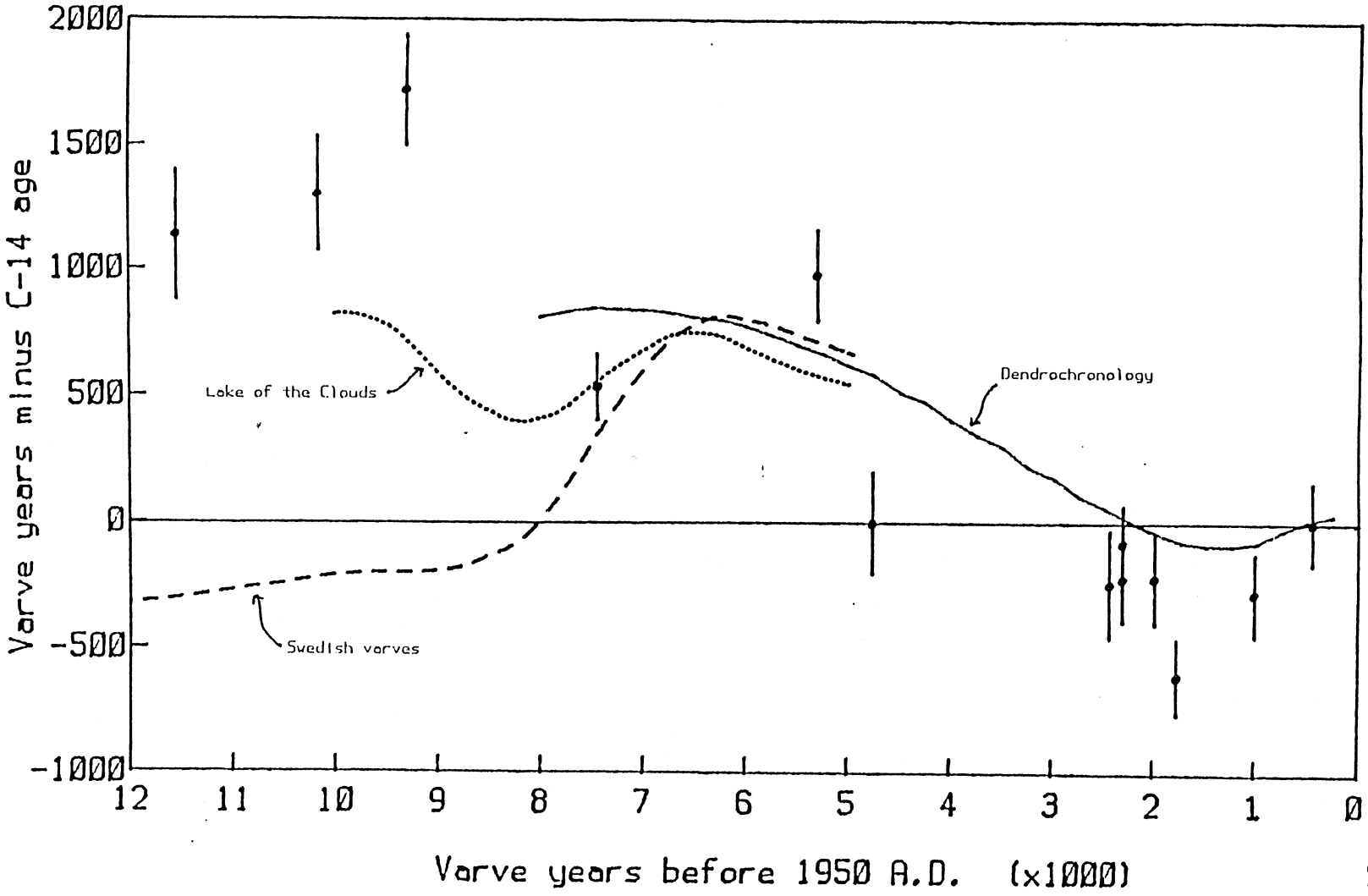
2000
1500
1000
500
0
-500
-1000
Varve years minus C-14 age
Lake of the Clouds
Dendrochronology
Swedish varves
12
11
10
9
8
7
6
5
4
3
2
1
0
Varve years before 1950 A.D. (x1000)

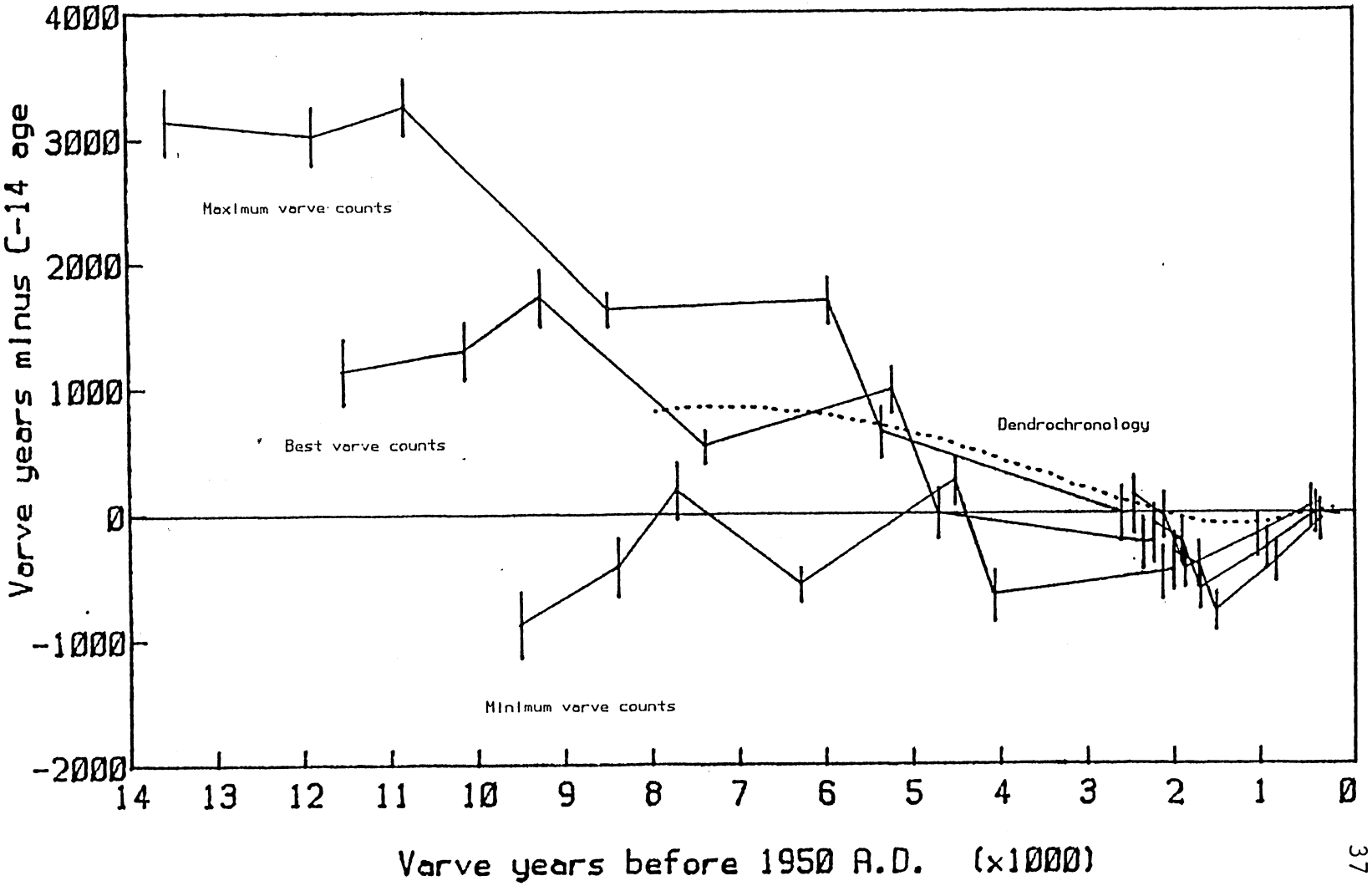
4000
3000
2000
1000
0
-1000
-2000
Varve years minus C-14 age
Maximum varve counts
Best varve counts
Minimum varve counts
Dendrochronology
14
13
12
11
10
9
8
7
6
5
4
3
2
1
0
Varve years before 1950 A.D. (x1000)

CHAPTER 5 : THE DIRECTIONAL MAGNETIC RECORD

A. Introduction.

The stratigraphic control and the varve chronology of the previous chapters provide a good foundation for the directional magnetic record. It is convenient to deal with the directional record in terms of the inclination (I) (angle down from vertical), and the declination (D) (angle east from north). Together, these two scalars uniquely define the direction of the paleomagnetic vector. Paleointensity, the length of the paleomagnetic vector, will be dealt with separately in the next chapter.

B. Rock magnetics.

Of importance to the directional record is the response of the samples to AF demagnetization. Figure 21a is a Zjiderveldt plot of the magnetic vectors from test pair 83b-3584 after stepwise increasing AF demagnetization. The +'s are projections of the magnetic vector on the horizontal plane, while the x's are projections on the vertical axis. The straight lines to the origin show demagnetization of the signal from stable magnetic grains, representing the field at the time of deposition. The elbows at the low field end of the curves, removed by 150 Oe, are from unstable magnetic grains. Plots of this sort led to the selection of 100 Oe as the uniform cleaning field for the 1982 cores. Numerous (~45) additional test pairs from the 1983 cores indicate that 150 Oe is a more appropriate cleaning field for these samples. The different cleaning fields for the 82 and 83 samples should have no noticeable effect on the results.

Figure 21b plots the normalized intensity of magnetization (solid lines) vs. demagnetizing field for the same test pair. The large field remaining at 150 Oe indicates that the majority of magnetic grains are stably magnetized. The dashed lines in Figure 21b show the demagnetization of ARM for the same pair. The similarity of shape between the NRM and ARM demagnetization curves is taken as preliminary support for the use of ARM as a normalization factor for paleointensity (Chapter 6). The median destructive field (MDF) of the NRM, 245 Oe for this pair, is a commonly used indicator of magnetic stability. Figure 22 is a plot of MDF vs. depth for test pairs from cores 83a and 83b. The magnetic record is uniformly stable throughout the lower section, with an increase in stability in the upper section due to the change in average magnetic grain size mentioned in Chapter 3.

Figure 21 (p. 40) - AF demagnetization of sample pair 83b-3584. The +'s (21a) are projections of the magnetic vector on the horizontal plane, while the x's are projections on the vertical axis. The values plotted are normalized to the NRM intensity of 1.3×10^{-4} emu. There is one mark for each of the demagnetization levels listed at the bottom. In 21b, the normalized total intensity is plotted vs. demagnetizing field for the NRM (solid lines) and ARM (dashed lines). The MDF derivation for the NRM is shown.

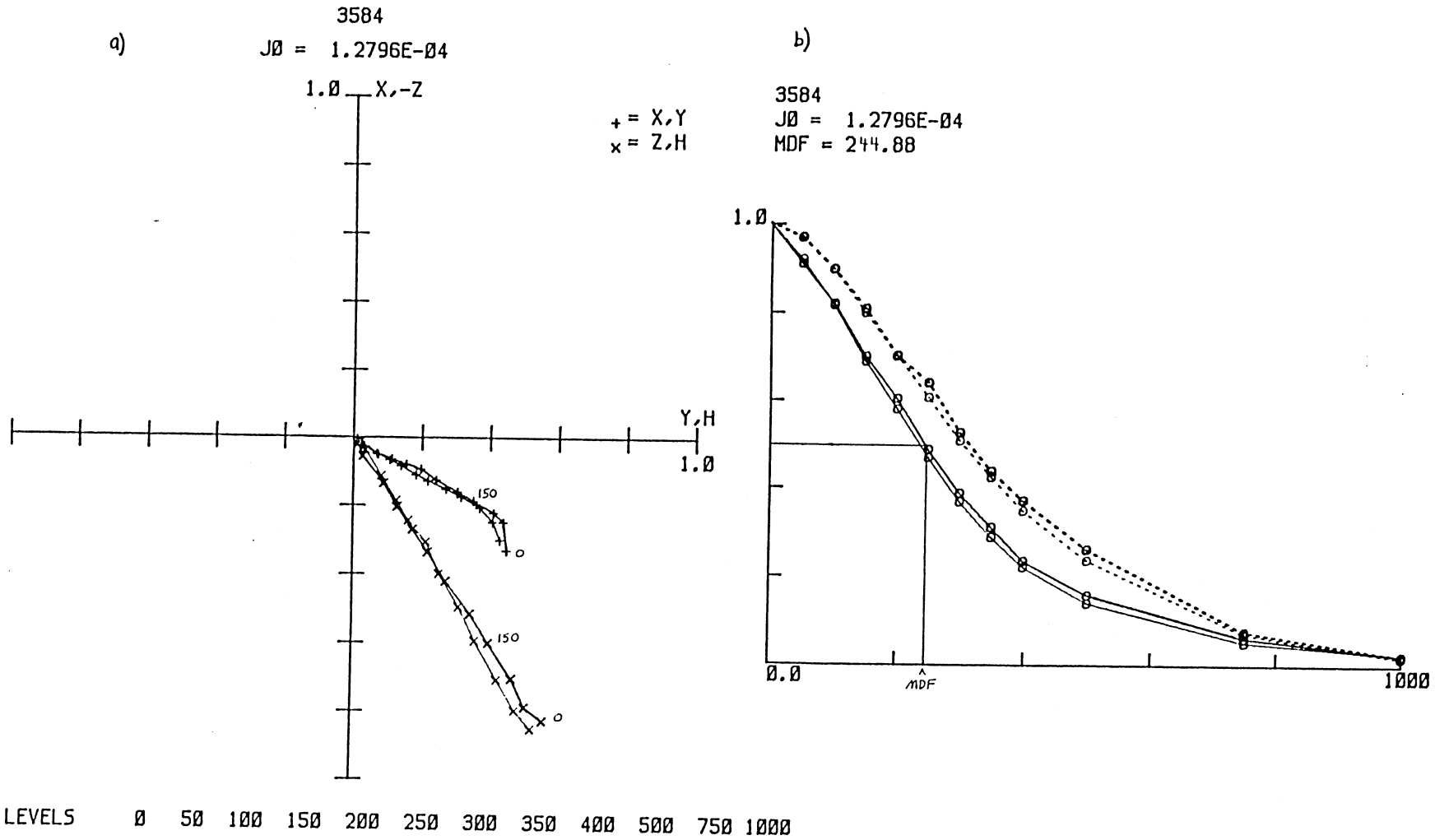
3584
a)
JØ = 1.2796E-Ø4
1.Ø
X,-Z
+ = X,Y
x = Z,H
Y,H
1.Ø
150
0
150
0
b)
3584
JØ = 1.2796E-Ø4
MDF = 244.88
1.Ø
Ø.Ø
MDF
1ØØØ
LEVELS Ø 5Ø 1ØØ 15Ø 2ØØ 25Ø 3ØØ 35Ø 4ØØ 5ØØ 75Ø 1ØØØ

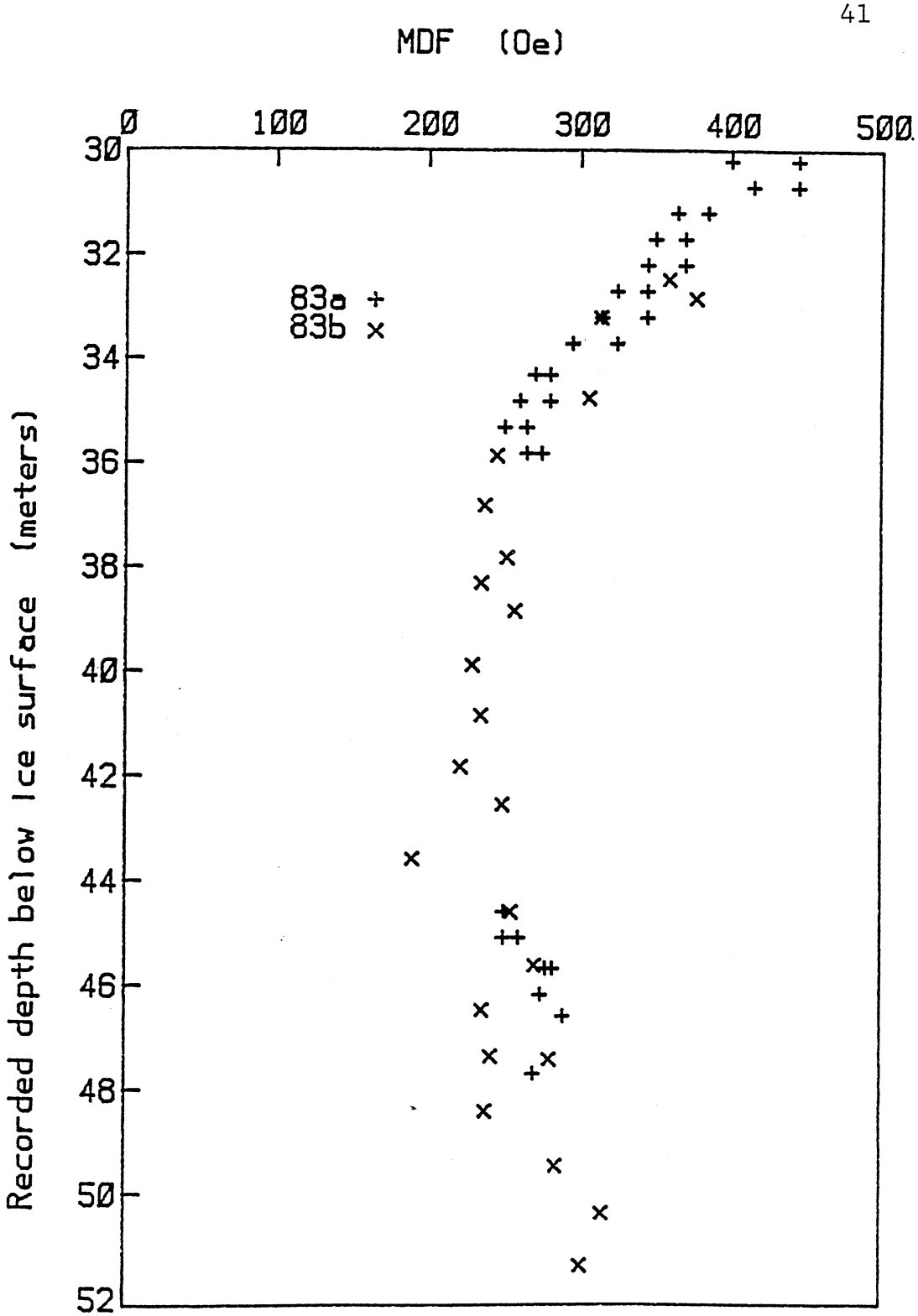

Figure 22 - MDF vs. recorded depth for test pairs from 83a and 83b.

C. Dealing with outliers.

Figures 23 and 24 present the I and D raw data from core 83a, magnetically cleaned at 150 Oe. Each line segment in the figures connects the two measurements from a given sample pair. Trends in the curves are apparent, but also apparent is noise in the signal as well as obviously errant pairs.

There are several possible sources of noise in the magnetic record. Imperfection in the signal recording process in the sediment can be appealed to, but both the integration time of this process and the integration time of the subsample width (~15 yr) should smooth any such noise. Most of the noise is thus probably due to disturbance during and subsequent to the field work. The common occurance of outliers at the top and bottom of individual core segments indicates distubance during coring. Additionally, rotational errors are quite possible during the subsampling process. A common method for dealing with outliers (King, 1983) is to select a reasonable (but arbitrary) cutoff value, beyond which data are eliminated. A more rigorous and satisfying method for dealing with outliers is developed in the next few paragraphs.

Figure 25 is a plot of the absolute values of the differences between the I_{150} values for the sample pairs plotted in Figure 23. Several pairs are certainly abnormal with regard to the difference between the two measurements, but visually choosing a cutoff value between normal and abnormal is clearly ambiguous. If we assume that the differences are normally distributed, we can analyse the variance among the points of Figure 25. Figure 26 is a histogram plot of the differences (not absolute value) plotted in Figure 25. The histogram approximates a normal distribution fairly well, except for the tails. Smooth curve a is the normal curve defined by the sample mean and standard deviation (std. dev.). This curve does not describe the data at all well because the variance is strongly a function of the outliers to the extreme left and right. But this provides a clue as to how to procede. We define the 'good' data as being normally distributed and described by the central portion of the histogram in Figure 26. Outliers are any points not thus accounted for.

Smooth curve b (Figure 26) is the best fitting normal curve to the central part of the histogram in the following sense. A new mean for the central portion is defined by the median of the values within 0.5 original std. dev. from the original mean. Using this new mean, a new std. dev. is calculated by step-wise reducing the original std. dev. until the ratio of the number of data points within two std. dev. of the mean to the number of data points within one std. dev. of the mean, originally close to 1.0, exceded 1.39. The outlier cutoff is chosen as 2.6 times the new std. dev. from the new mean. In this way, only 1% of

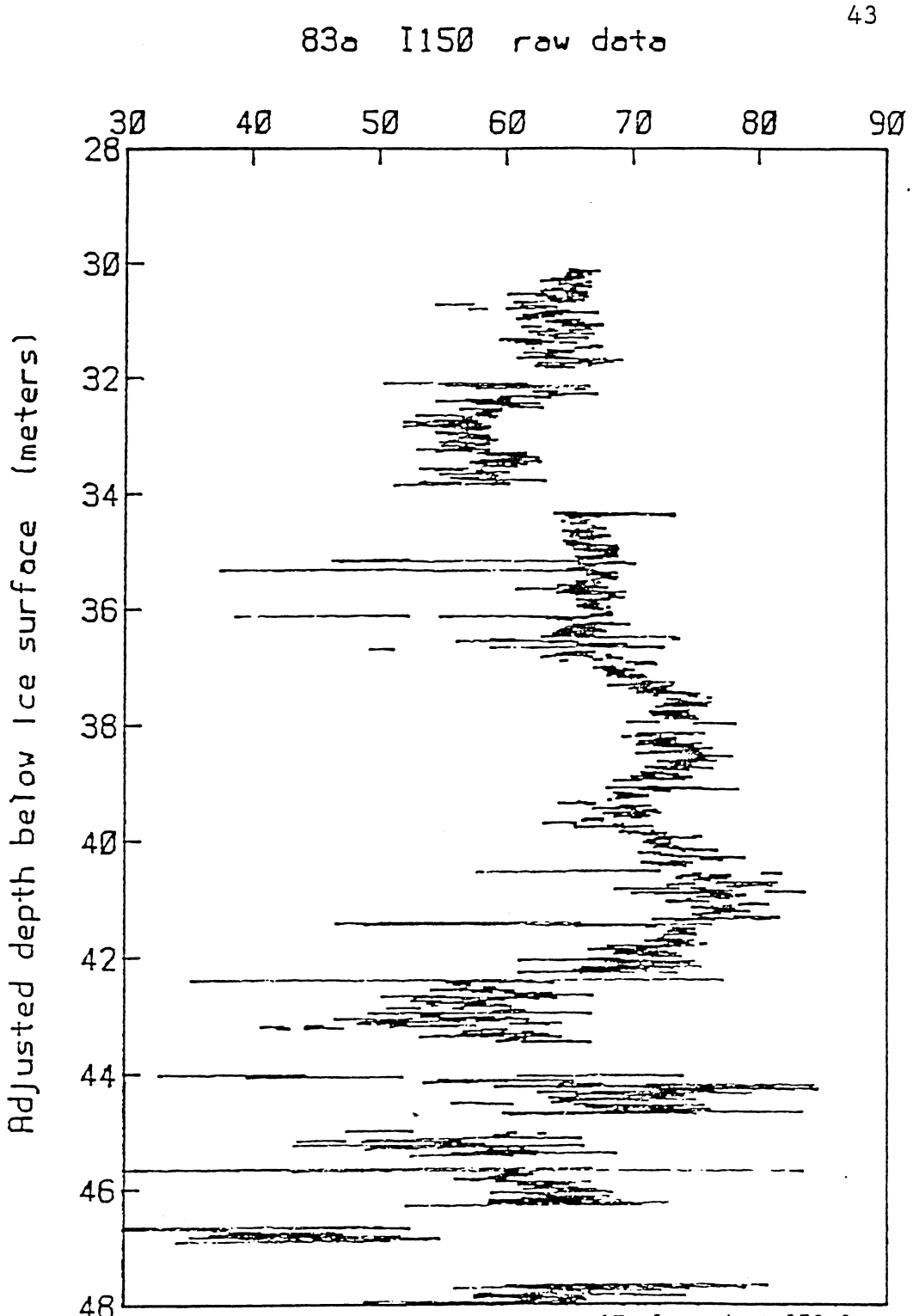

Figure 23 - 83a inclination data, AF cleaned at 150 Oe. Each line segment connects the two measured inclination values from a given sample pair. Horizontal axis scaled in degrees.

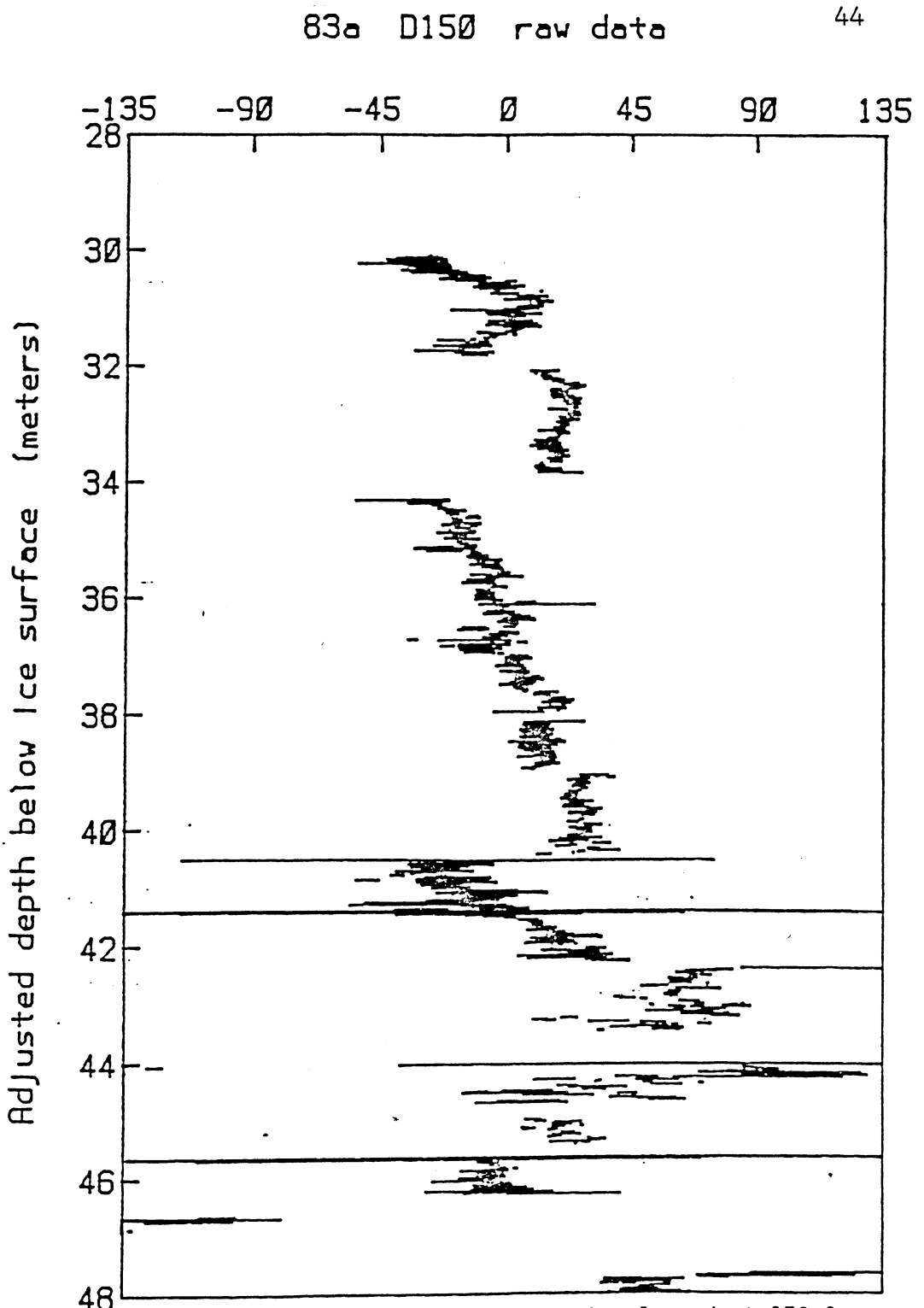

Figure 24 - 83a declination data, AF cleaned at 150 Oe. Each line segment connects the two measured declination values from a given sample pair. Horizontal axis scaled in degrees.

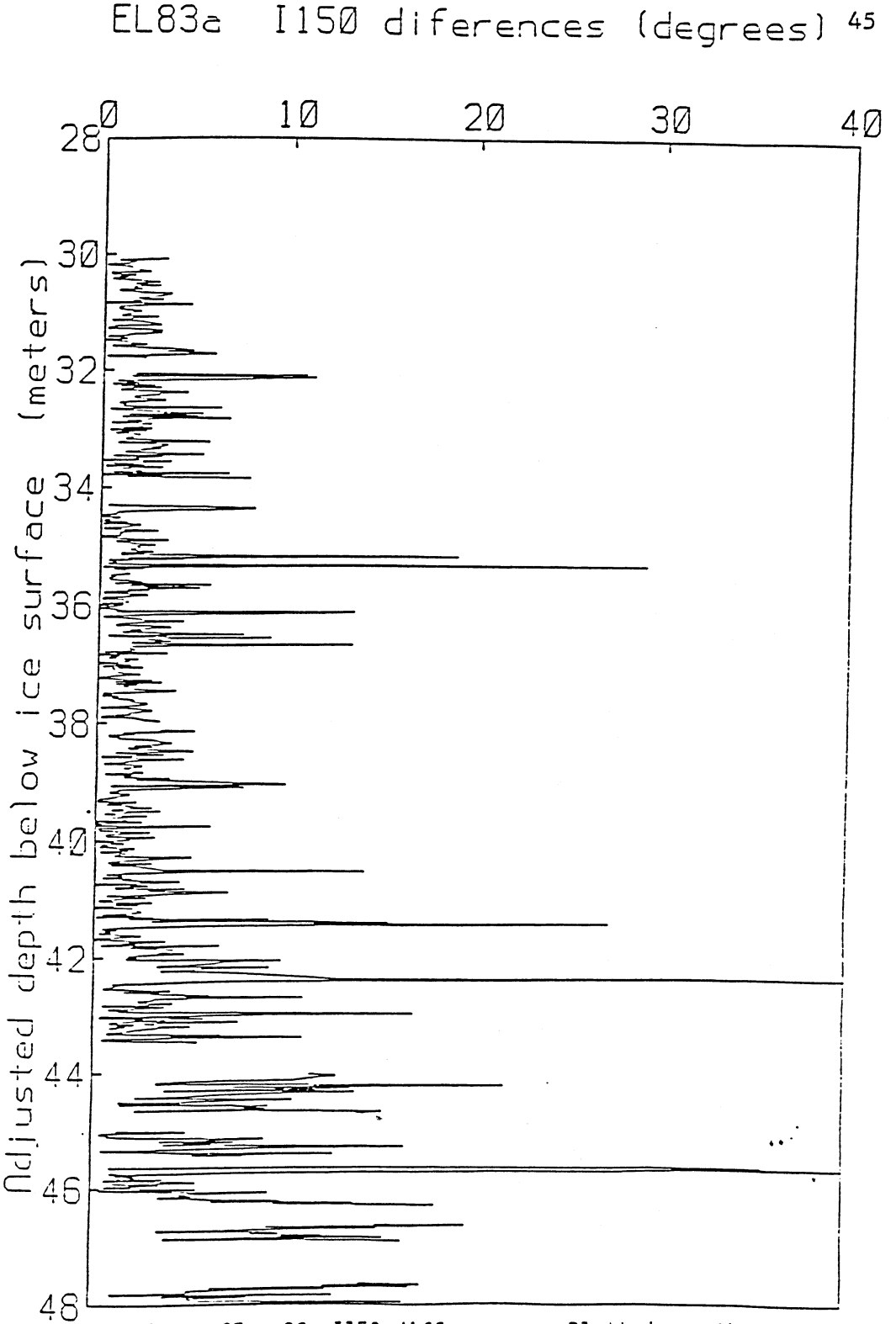

Figure 25 - 83a I150 differences. Plotted are the absolute values of the differences between the two measured inclination values from each pair plotted in Figure 23. Horizontal axis scaled in degrees.

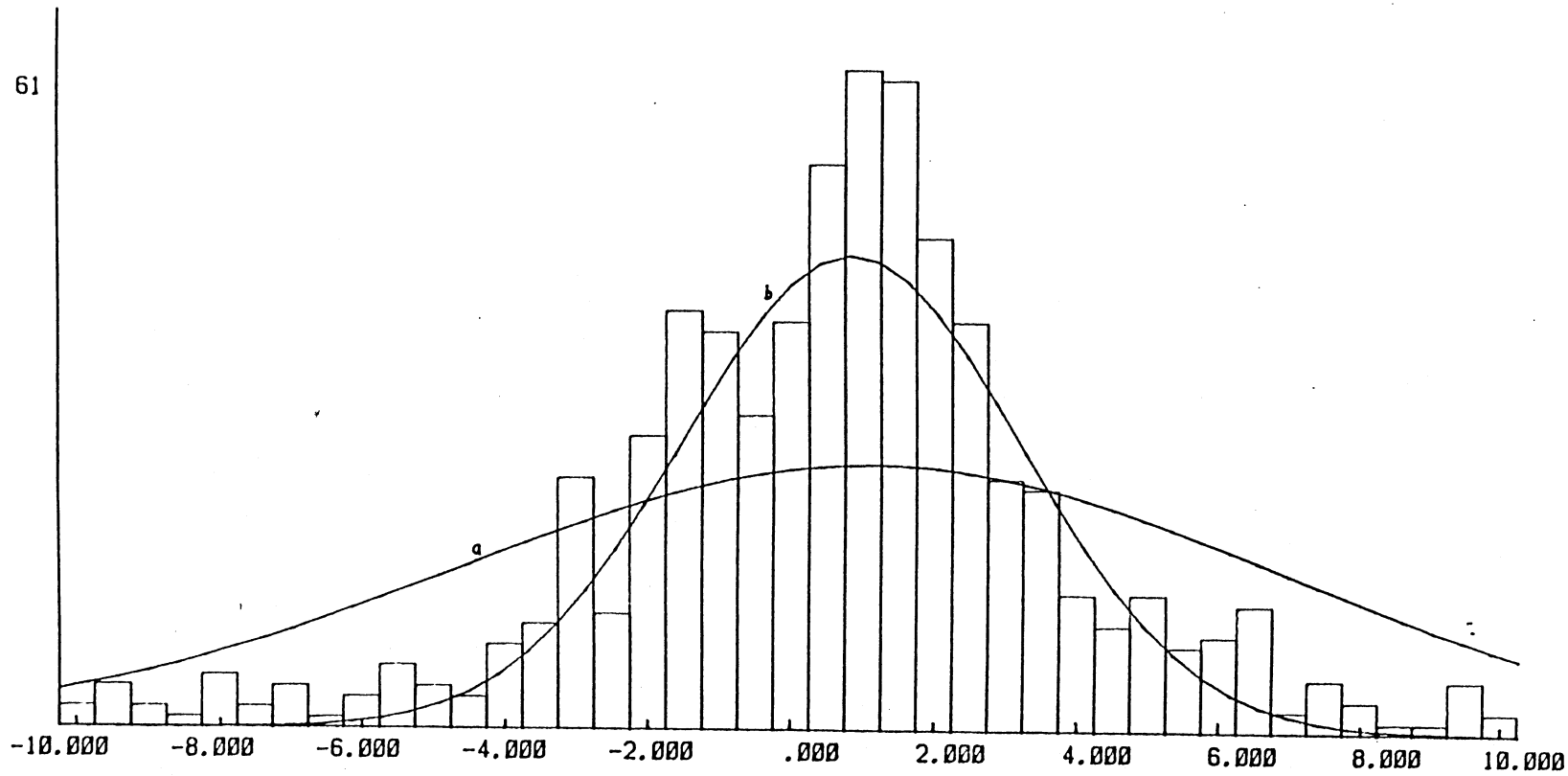

Figure 26 - Histogram plot of the 83a I150 difference data (Figure 25). Curve a is the normal curve defined by the sample mean and std. dev. Curve b is the best fitting normal curve to the central portion of the data, as detailed in the text.

the 'good' data should be eliminated along with the outliers. The same procedure was followed for the declination data, with any pair eliminated from either I or D eliminated from both.

In addition to pairs with divergent measurements, there are pairs for which the two measurements are similar but with a mean which is clearly abnormal. Thus, the above trimming procedure was repeated using as data the differences between the means of adjacent sample pairs. Again a new mean and std. dev. were derived and pairs more than 2.6 times the new std. dev. from the new mean were eliminated as outliers. Any pair which was eliminated from either I or D was eliminated from both. The twice trimmed I and D data for core 83a are presented in Figures 27 and 29. Several pairs which seem to be outliers remain because the two measurements are sufficiently close together and the pair has no adjacent pairs for evaluation of means. For comparison purposes, the pairs eliminated from the I and D curves are plotted in Figures 28 and 30. The details of the trimmings for all seven cores of interest are presented in Appendix 3. Of the original 2694 inclination pairs from the seven cores, 2075 remain after trimming. The trimming procedure removed 23% of the original data. It would be hard to justify such an extensive reduction of the data without an objective method for distinguishing outliers, but this points out the importance of having just such a method.

D. Stacking the data.

Given the stratigraphic control provided by magnetic susceptibility, the directional data from the multiple cores can be stacked with confidence. The inclination and declination data will be dealt with separately in some detail.

Figure 31 shows the color-coded inclination data from the seven cores considered in this study. The lines connect the inclination means of the paired data. Most of the records are coincident through the upper and middle sections (down to 41 m.), with much more divergence in the lower section. Importantly, most of the variance is between cores rather than within cores, i.e., common features, some of them very small scale (such as the jag to the right at 33.3 m), can be seen in multiple records, but the records are offset from one another, by as much as 15°. We can explain this in terms of non-vertical drives, but care must be taken in dealing with the offsets. The goal is to derive a record of the past variations in the local magnetic field, with limits of confidence. Three options present themselves: 1) take the data as they are, 2) throw away the bad data, and 3) slide the core segments over to match one another (i.e., cross-correlation). Taking the data as they are is

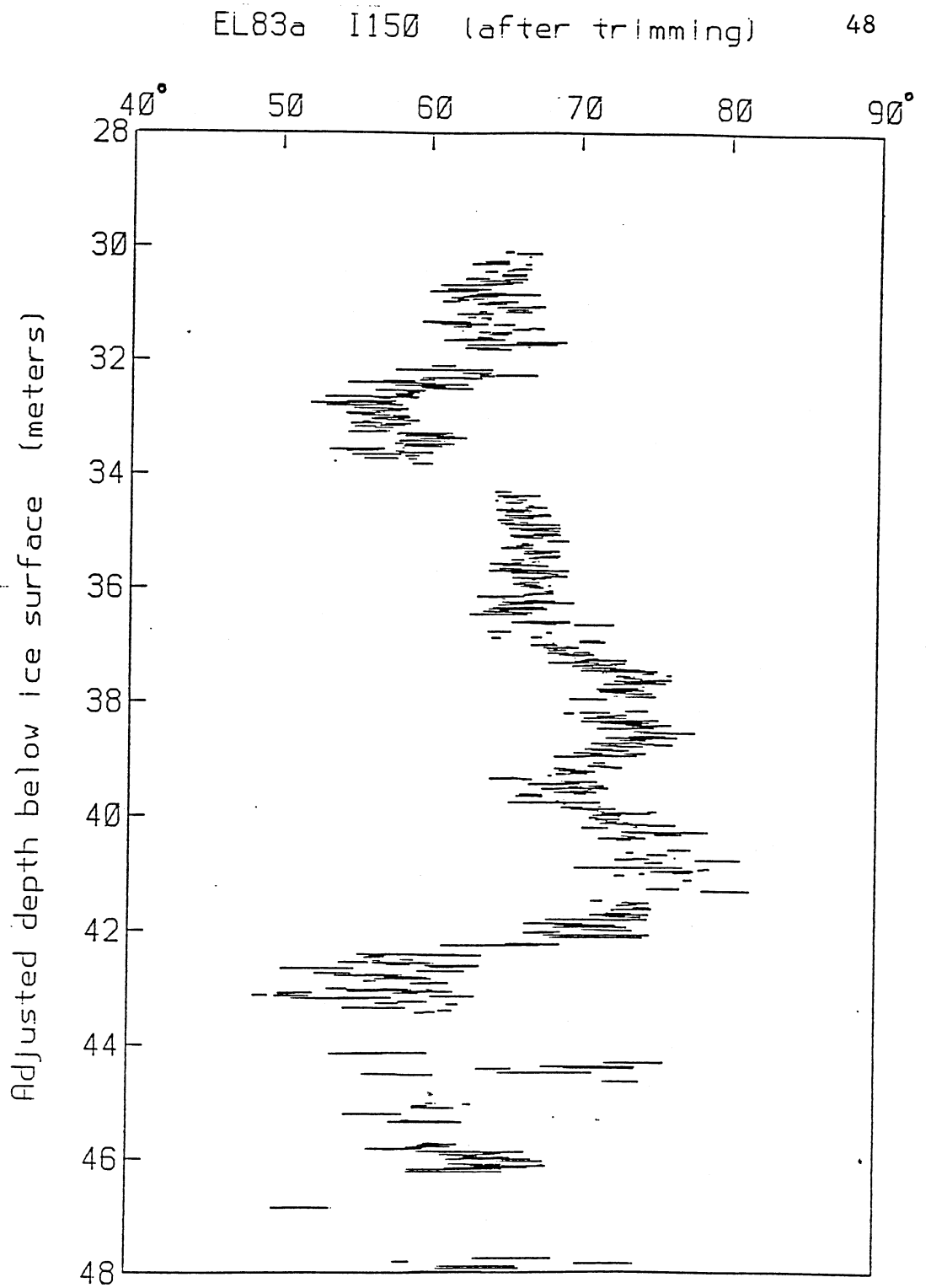

Figure 27 - 83a I150 trimmed data. Each horizontal line segment connects the two inclination measurements from a given pair, each pair remaining after the trimming procedure.

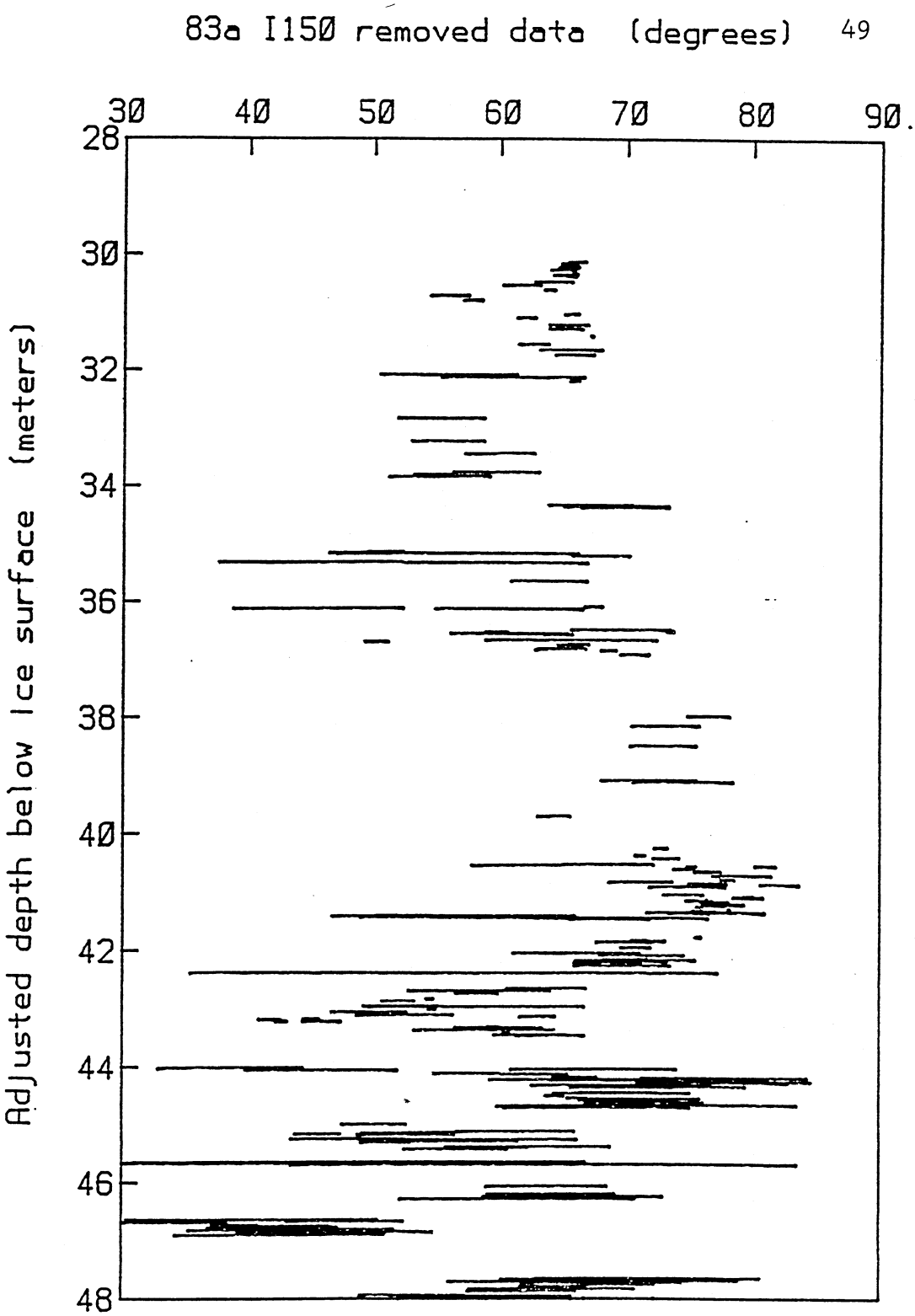

Figure 28 - 83a I150 removed data. Each horizontal line segment connects the two inclination measurements from a sample pair eliminated as bad data.

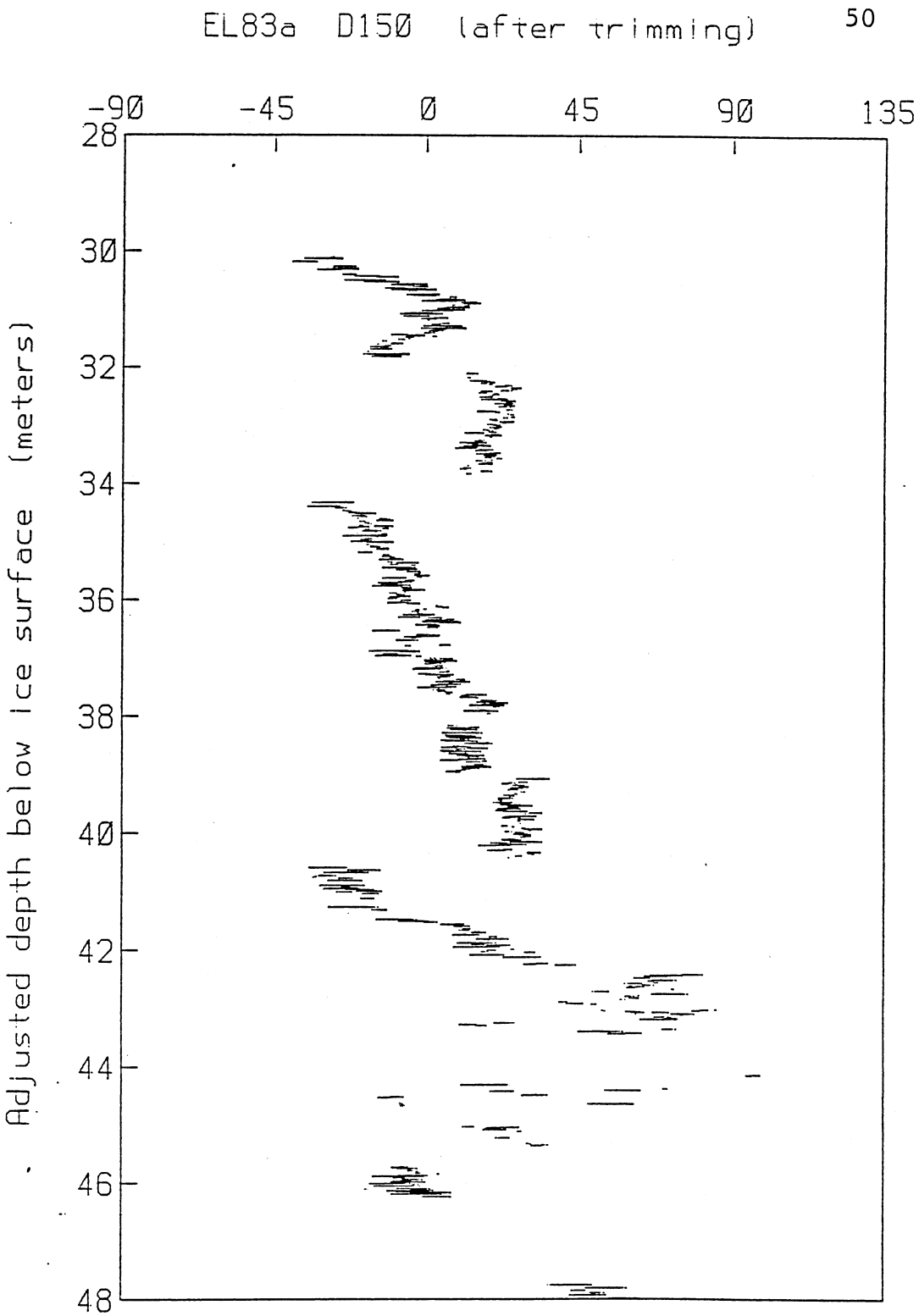

Figure 29 - 83a D150 trimmed data. Each horizontal line connects two declination measurements from a given sample pair, each pair remaining after the trimming procedure.

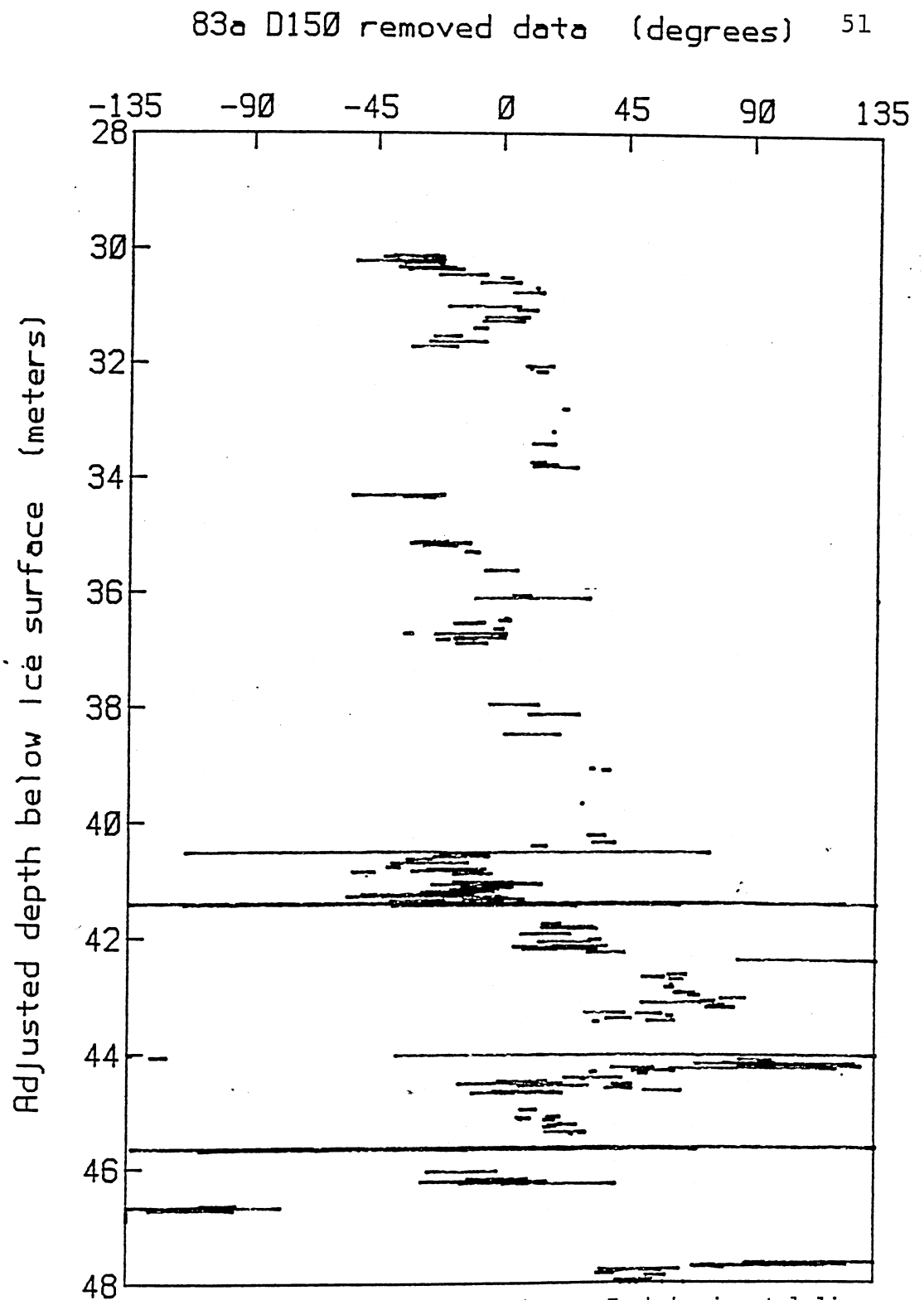

Figure 30 - 83a D150 removed data. Each horizontal line segment connects the two declination measurements from a sample pair eliminated as bad data.

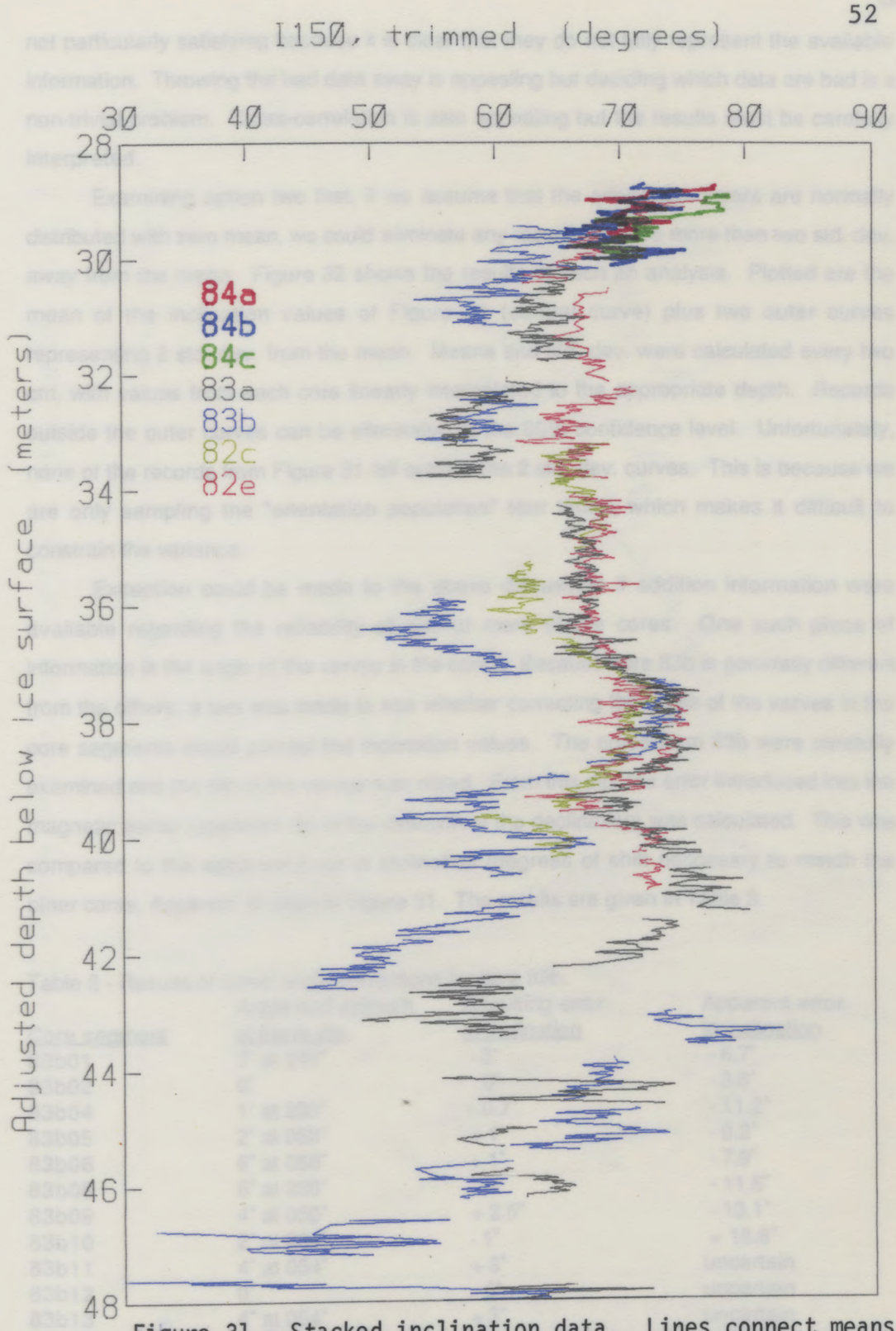

Figure 31 - Stacked inclination data. Lines connect means from paired measurements. Samples were cleaned at 100 Oe (82) or 150 Oe (83,84).

not particularly satisfying because it is clear that they do not fully represent the available information. Throwing the bad data away is appealing but deciding which data are bad is a non-trivial problem. Cross-correlation is also appealing but the results must be carefully interpreted.

Examining option two first, if we assume that the orientation errors are normally distributed with zero mean, we could eliminate any records that are more than two std. dev. away from the mean. Figure 32 shows the results of such an analysis. Plotted are the mean of the inclination values of Figure 31 (central curve) plus two outer curves representing 2 std. dev. from the mean. Means and std. dev. were calculated every two cm, with values from each core linearly interpolated to the appropriate depth. Records outside the outer curves can be eliminated at the 95% confidence level. Unfortunately, none of the records from Figure 31 fall outside the 2 std. dev. curves. This is because we are only sampling the "orientation population" four times, which makes it difficult to constrain the variance.

Exception could be made to the above discussion if addition information were available regarding the reliability of one or more of the cores. One such piece of information is the angle of the varves in the cores. Because core 83b is generally different from the others, a test was made to see whether correcting the angle of the varves in the core segments would correct the inclination values. The cores from 83b were carefully examined and the dip of the varves was noted. From this dip, the error introduced into the magnetic vector (apparent dip in the direction of the declination) was calculated. This was compared to the apparent error in inclination (degrees of shift neccesary to match the other cores, Appendix 4) seen in Figure 31. The results are given in Table 3.

Table 3 - Results of varve angle corrections for core 83b.

Core segment	Angle and azimuth of varve dip	Resulting error in inclination	Apparent error in inclination
83b01	3° at 240°	- 3°	- 6.7°
83b02	0°	0°	- 3.8°
83b04	1° at 233°	- 0.7°	- 11.2°
83b05	2° at 053°	+ 1°	- 0.2°
83b06	6° at 056°	+ 1°	- 7.9°
83b08	6° at 230°	0°	- 11.5°
83b09	4° at 050°	+ 2.5°	- 13.1°
83b10	2° at 234°	- 1°	+ 18.8°
83b11	4° at 054°	+ 3°	uncertain
83b12	0°	0°	uncertain
83b13	4° at 054°	+ 3°	uncertain
83b14	0°	0°	uncertain

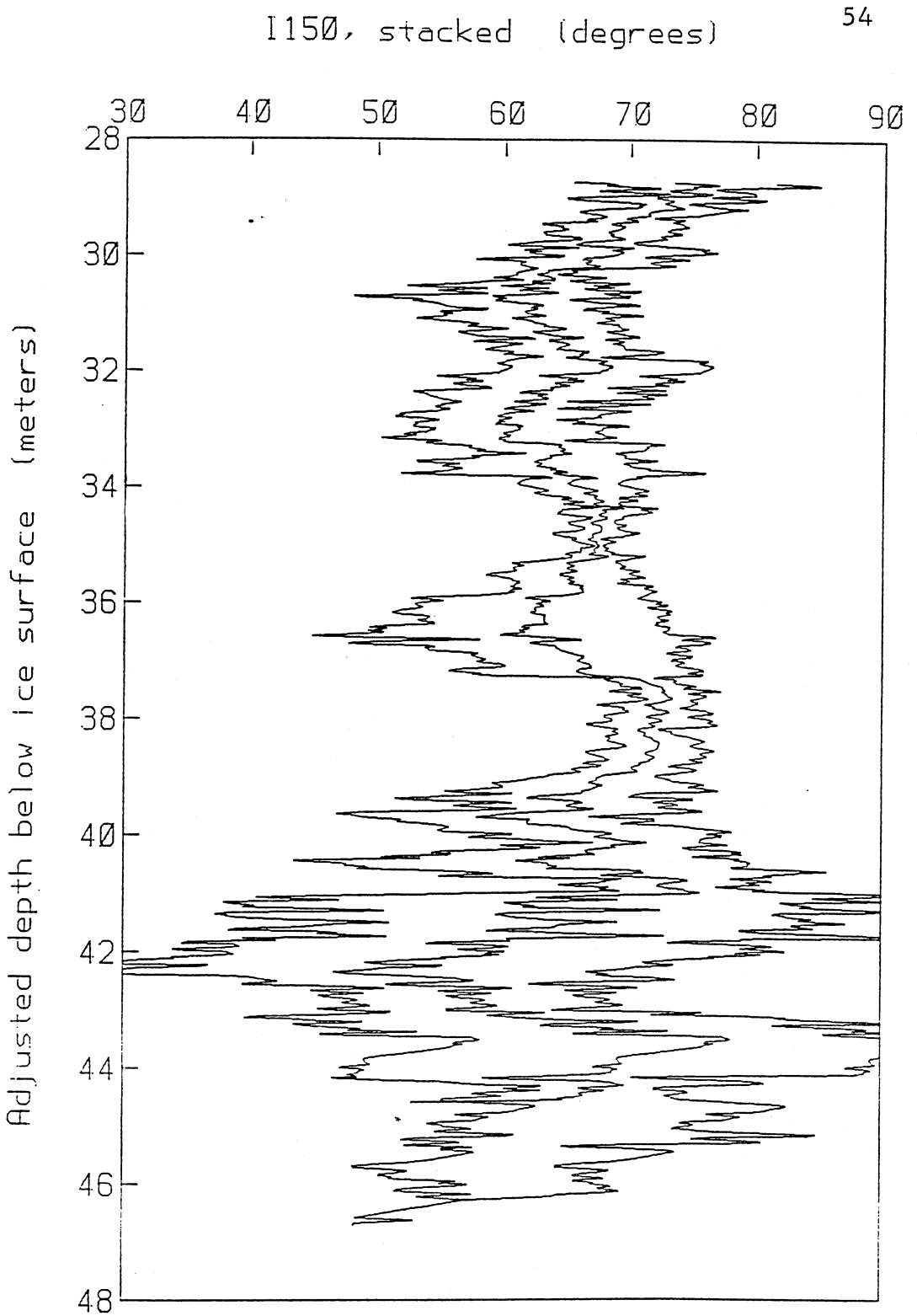

Figure 32 - I150 means of values from seven cores, with outer curves giving 95% confidence limits, defined by two std. dev. of teh stacked values.

The dip of the varves in the 83b cores is somewhat variable in both magnitude and direction. Since assuming no initial dip in the varves does not account for the variability in the inclination data, at least some variability is suggested in the true dip of the varves. Since the cores are taken in the vicinity of the steepest part of the lake bottom, a true dip of four or five degrees is not unreasonable. Certainly, the effort to correct the inclination data using the varve angles was not successful. Similar efforts for the other cores might be informative, but the varve dip angles are not adaquately known.

Thus, the only remaining tactic is cross-correlating the inclination values and shifting the cores to match one another. Since the depth scale is secured by magnetic susceptibility, the various core segments in Figure 31 were shifted to the left or right to minimize the sum of squares differences in the inclination values, with respect to a reference core segment. These shifts are recorded in Appendix 4 and the resultant curves are plotted in Figure 33. The initial reference core segment, 83a04, was chosen because it has average values for both I and D. Because of the gap at 32 m, across which no correlations can be made, an additional reference core was chosen, 83a01. Below 43 m, correlations are difficult because of the scarcity of data, so core segments below 83a12 and 83b10 must also be assumed correct. Given the assumed cores, all other core segments can be adjusted in series.

It is important to note the assumptions which have been made in cross-correlating the cores. The choosing of reference cores, while done in a reasonable way, is arbitrary. We do not know a priori which values of inclination are correct and which are incorrect. Shifting the inclination values of the core segments preserves the relative features within the cores, legitimate information in the data, but it arbitrarily alters the data with respect to an absolute reference. Therefore, a careful distinction must be made between the best estimate of the ***shape*** of the inclination function (relative inclination) and the best estimate of the actual ***value*** of the function (absolute inclination). The shape of the function is given in Figure 33; the best estimate of the value of the function is the mean shown in Figure 32, with each core segment unaltered and equally weighted. Figure 34 plots the mean value of the shifted inclination data with outer curves of 95% confidence defined by 2 std. dev. of the stacked data from the mean.

Henceforth, the shifted mean (Figure 34) will be taken as the best estimate of the inclination signal, with two regions of 95% confidence, one for the shape of the signal (Figure 34) and one for its value (Figure 32). These curves are shown, optimally smoothed, in Figure 35. The smoothing procedure is that described by Clark (1978). The

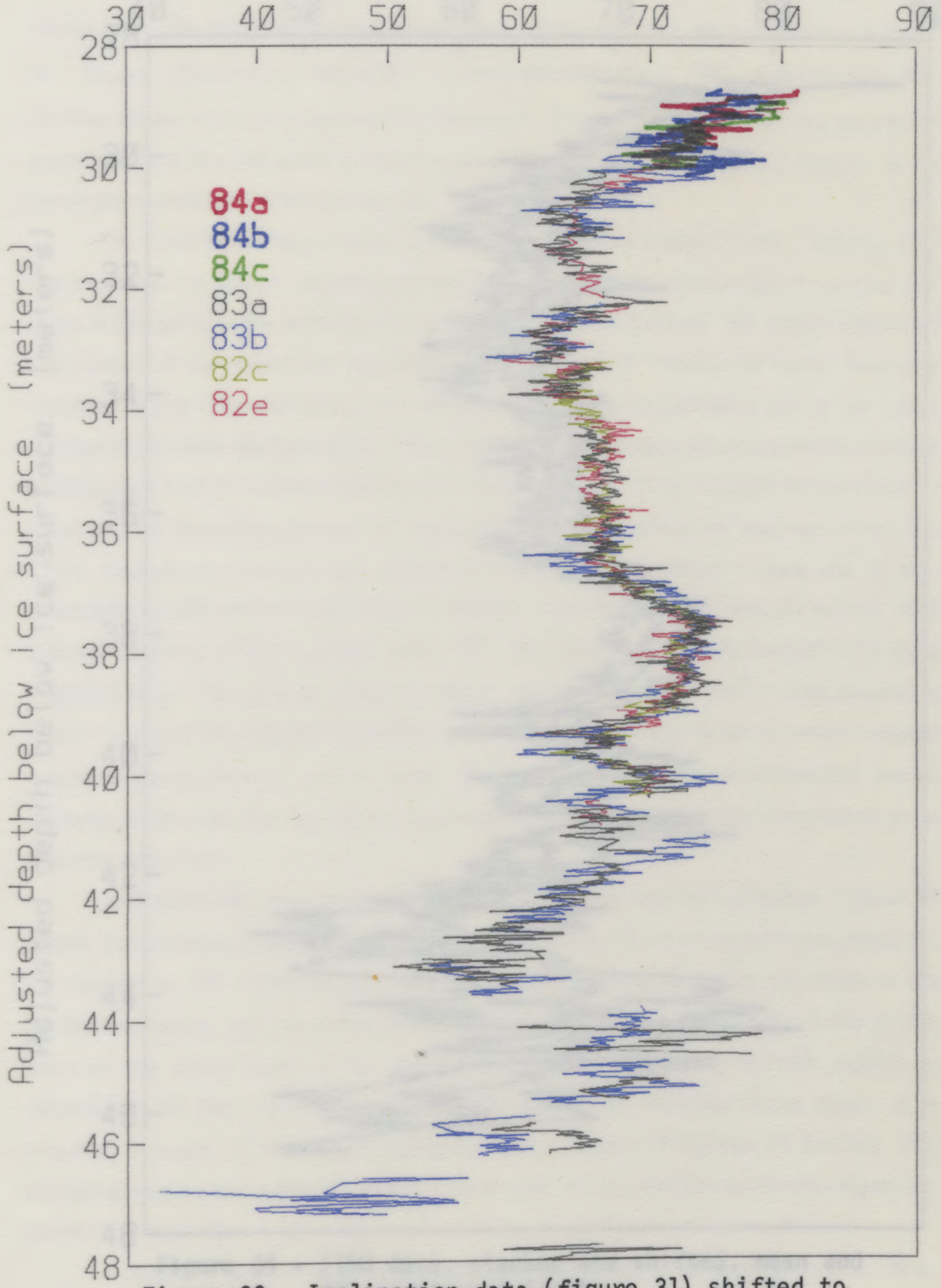

Figure 33 - Inclination data (figure 31) shifted to remove systematic errors in core orientation.

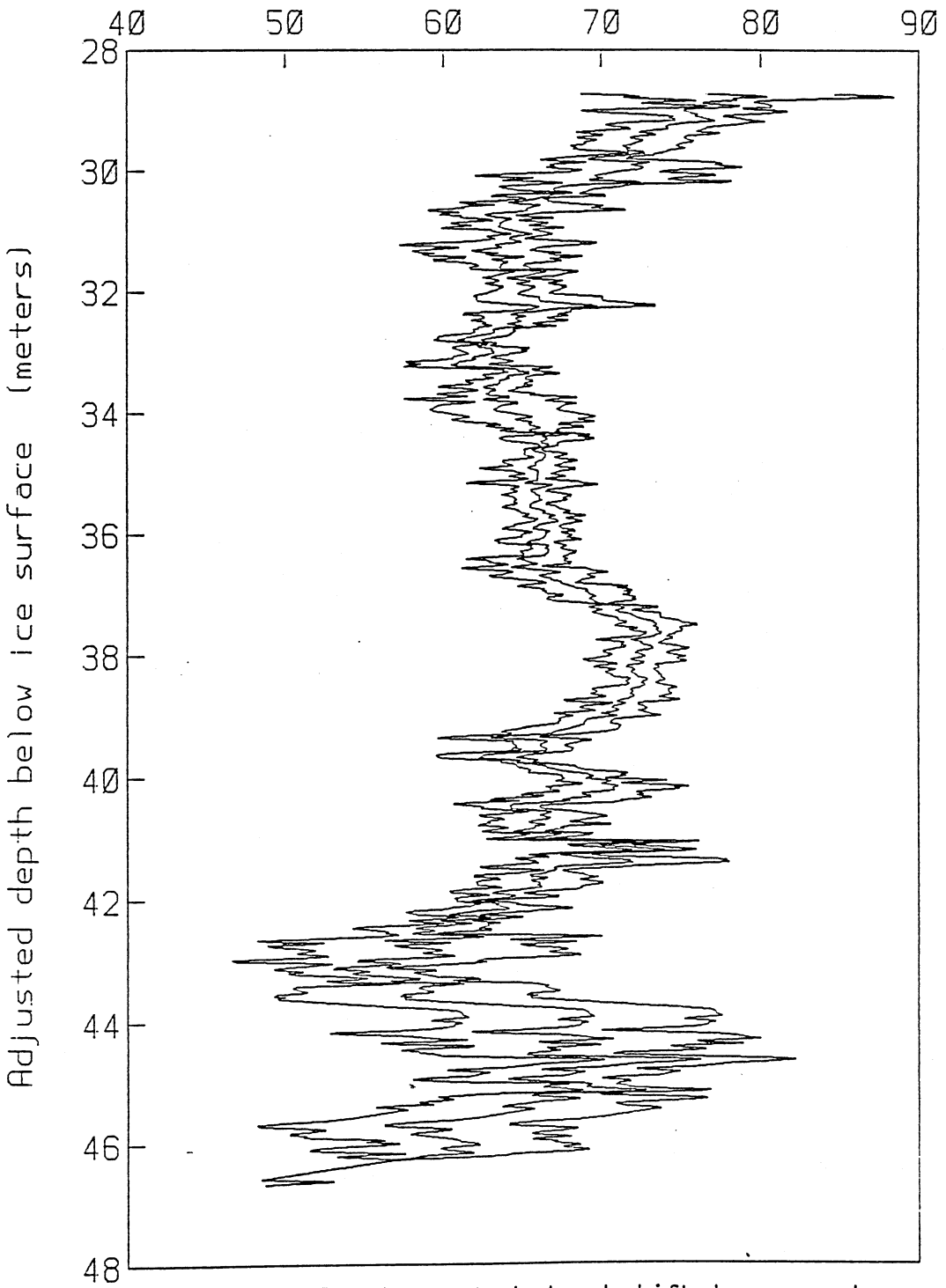

Figure 34 - I150 data, stacked and shifted, mean and 95% confidence limits.

data are partitioned into a test sample and an estimation sample. The optimum width for a triangular averaging window is that which, over a series of partitions, best predicts the test values using the smoothed estimation samples. The smoothed value at depth x is given by : $[\Sigma_{y=0...n}$ (value at y ÷ bandwidth * (1-|(x-y)÷bandwidth|)$_+$)]. The $_+$ indicates that only positive values of (1-|(x-y)÷bandwidth|) are used. The bandwidth defines the degree of smoothing and the half width of the triangular window. For the Elk Lake data, a 12 cm bandwidth was shown to be appropriate.

The Clark smoothing method is designed to remove random noise, retaining only true signals in the curves. Additional information regarding the differentiation of signal and noise is contained in the record of the inclination change at 33.3 m. The shifted data from this portion of the record are plotted in Figure 36 (p. 61). Since the same change is recorded in two different cores from different years, it is undoubtedly due to an actual change in the local magnetic field. The 4° change in inclination occurs between adjacent sample pairs over a maximum distance of 4 cm. (≈ 25 yrs). This indicates that the 'lock in zone' and the integration time for the magnetic recording process are less than 4 cm. and 25 yr. respectively, the limits of resolution in the magnetic record. Thus, the 12 cm. smoothing window should easily remove spurious signals from the magnetic record. Any features resolved at this degree of smoothing should represent true changes in the local magnetic field. The 'lock in' depth (the depth at which the 4 cm lock in zone occurs) is about 10 or 20 cm, based on relative water content and the depth at which reliable magnetic measurements can be made. Thus, the sediment should accurately record changes in the field, but with a time lag (magnetic signal younger than the sediment) of less than 100 years.

Declination has been dealt with in exactly the same way as inclination. Figure 37 shows the declination data, with the lines connecting the means of paired measurements, AF cleaned at 100 (1982) or 150 (1983,1984) Oe. Figure 38 shows the mean of the declination values with the outer curves representing the 95% confidence limits (2 std. dev.) on the actual value of the declination function. One core segment, 83b01, is recorded in the field notes to be misaligned and was not included in the mean. It is included, however, in the shifted composite curves plotted in Figures 39 and 40. The smoothed mean and confidence limits for the shape and value of the declination signal are plotted in Figure 41.

A couple of notes must be made about cross-correlating the declination data. First, while the gap at 32 m was a minor problem in the inclination match, it is a major question in

Figure 35 (p. 60) - Optimally smoothed I_{150} mean and limits of confidence. The center curve is the best estimate of the inclination signal. The outer (light weight) curves are the limits of 95% confidence on the value of the signal (absolute inclination). The remaining two curves define the limits of confidence in the shape of the curve (relative inclination). The dashed curve at 65.1° is the expected axial dipole average inclination value.

Figure 36 (p. 61) - Detailed view of the inclination change at 33.5 m. The x's are the mean inclination values for sample pairs from core 82e. The o's are the mean values for pairs from core 83a. The minimum resolution of the magnetic record (4 cm, ≈25 yr.) is defined by assuming that the actual field change is a step function.

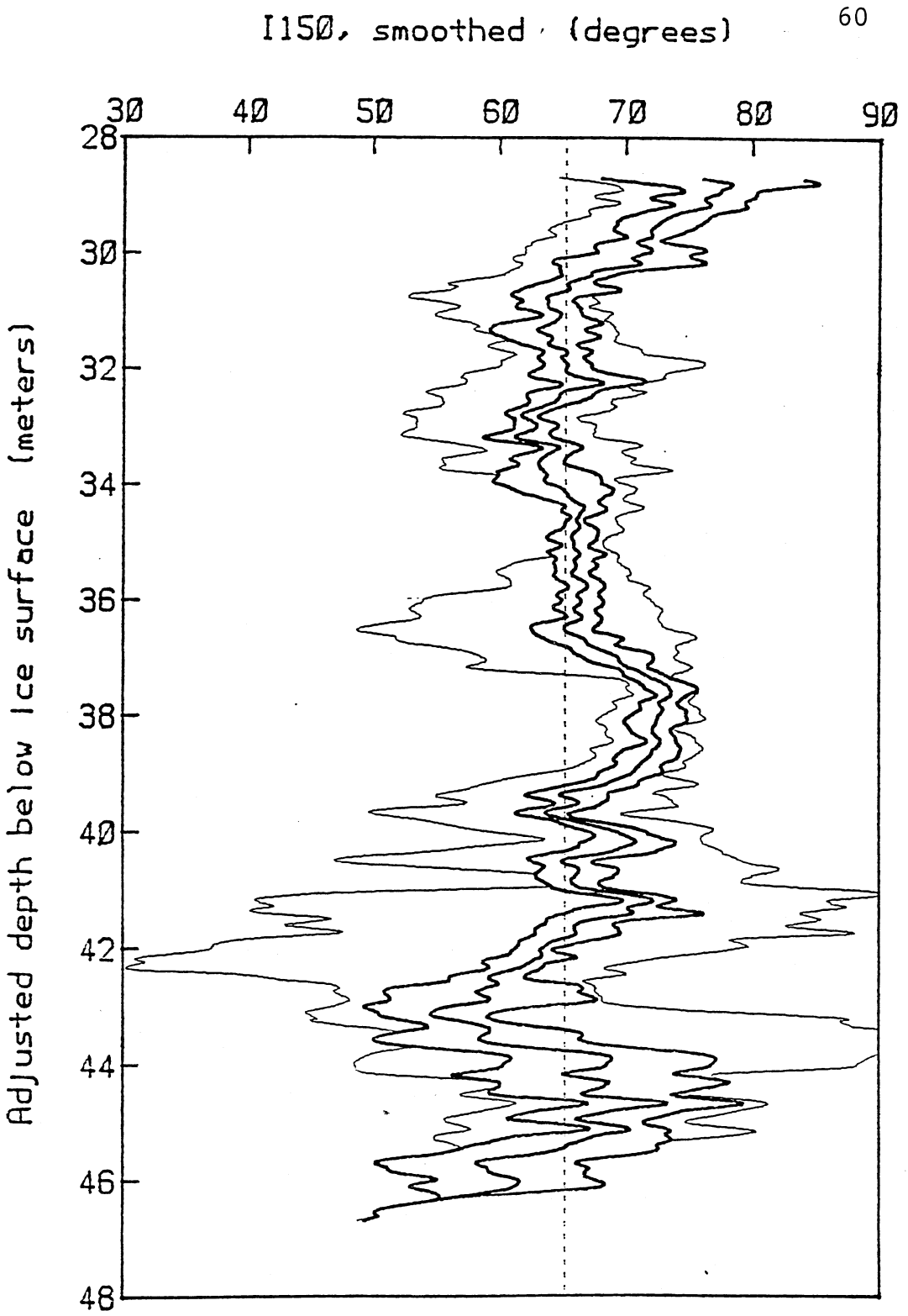
I150, smoothed (degrees)
30
40
50
60
70
80
90
28
30
32
34
36
38
40
42
44
46
48
Adjusted depth below ice surface (meters)

Figure 35.

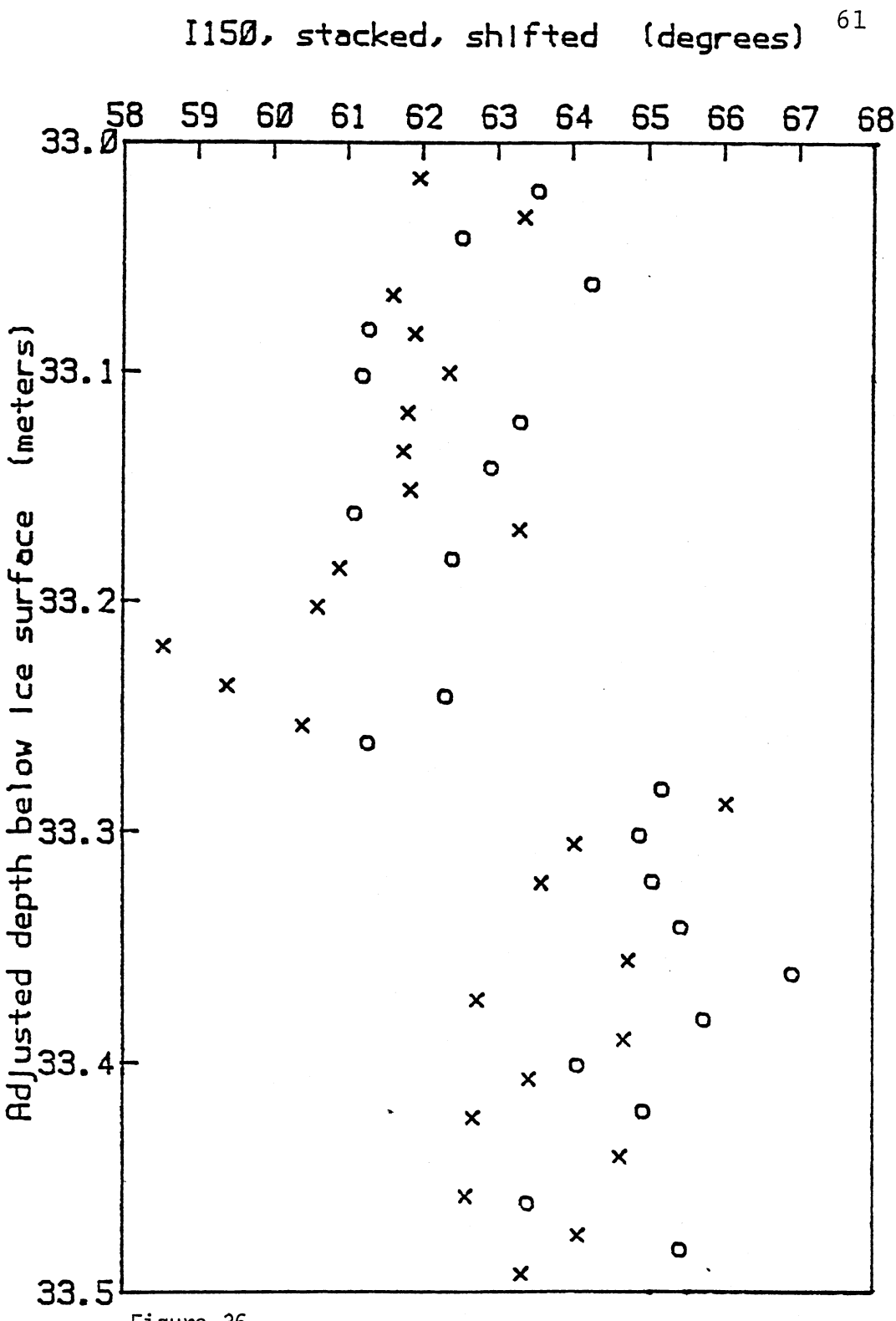
I150, stacked, shifted (degrees)
58
59
60
61
62
63
64
65
66
67
68
33.0
33.1
33.2
33.3
33.4
33.5
Adjusted depth below ice surface (meters)

Figure 36.

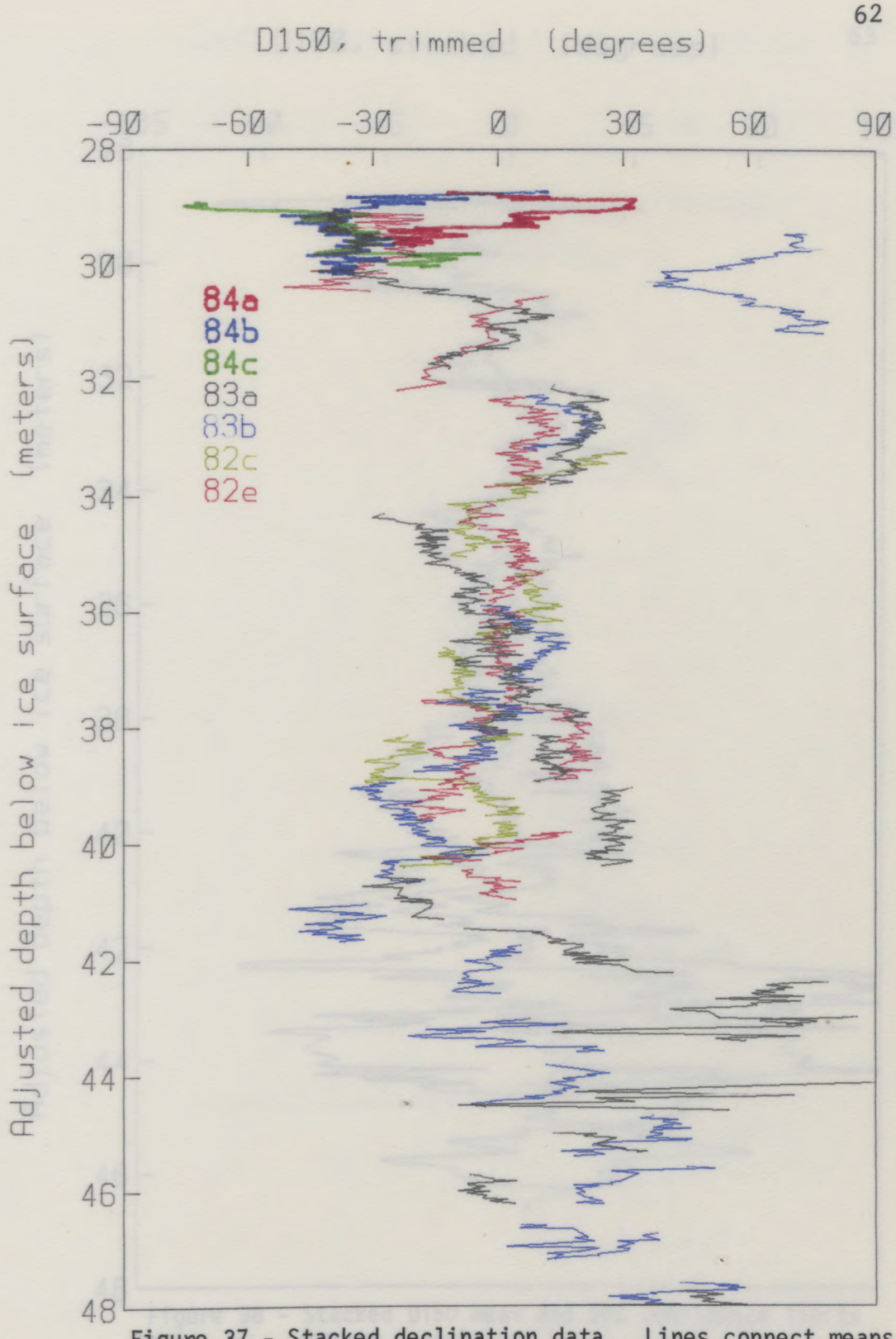

Figure 37 - Stacked declination data. Lines connect means from paired measurements. Samples were cleaned at 100 Oe (82) or 150 Oe (83,84).

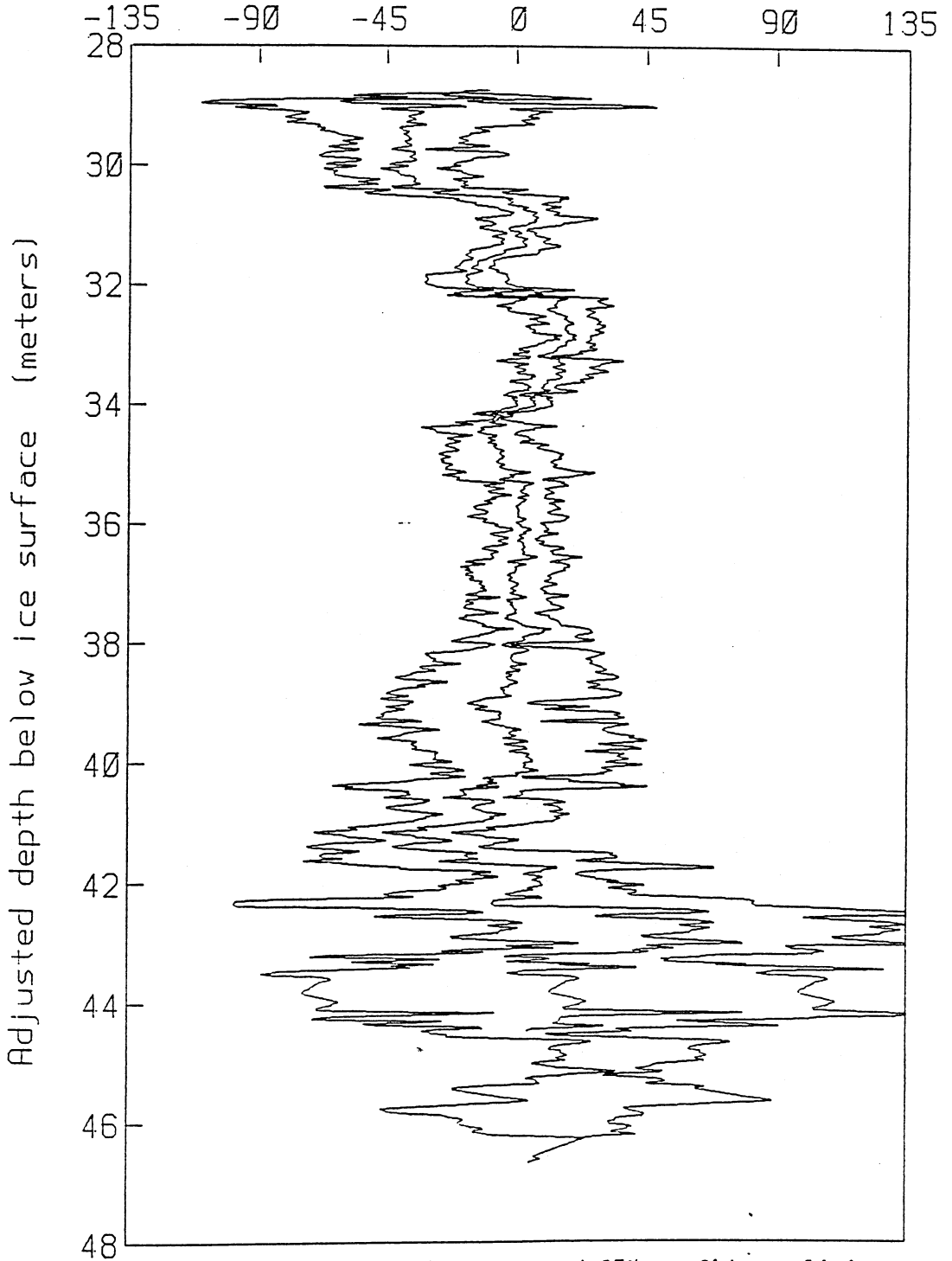

Figure 38 - Stacked D150 mean and 95% confidence limits (2 std. dev.).

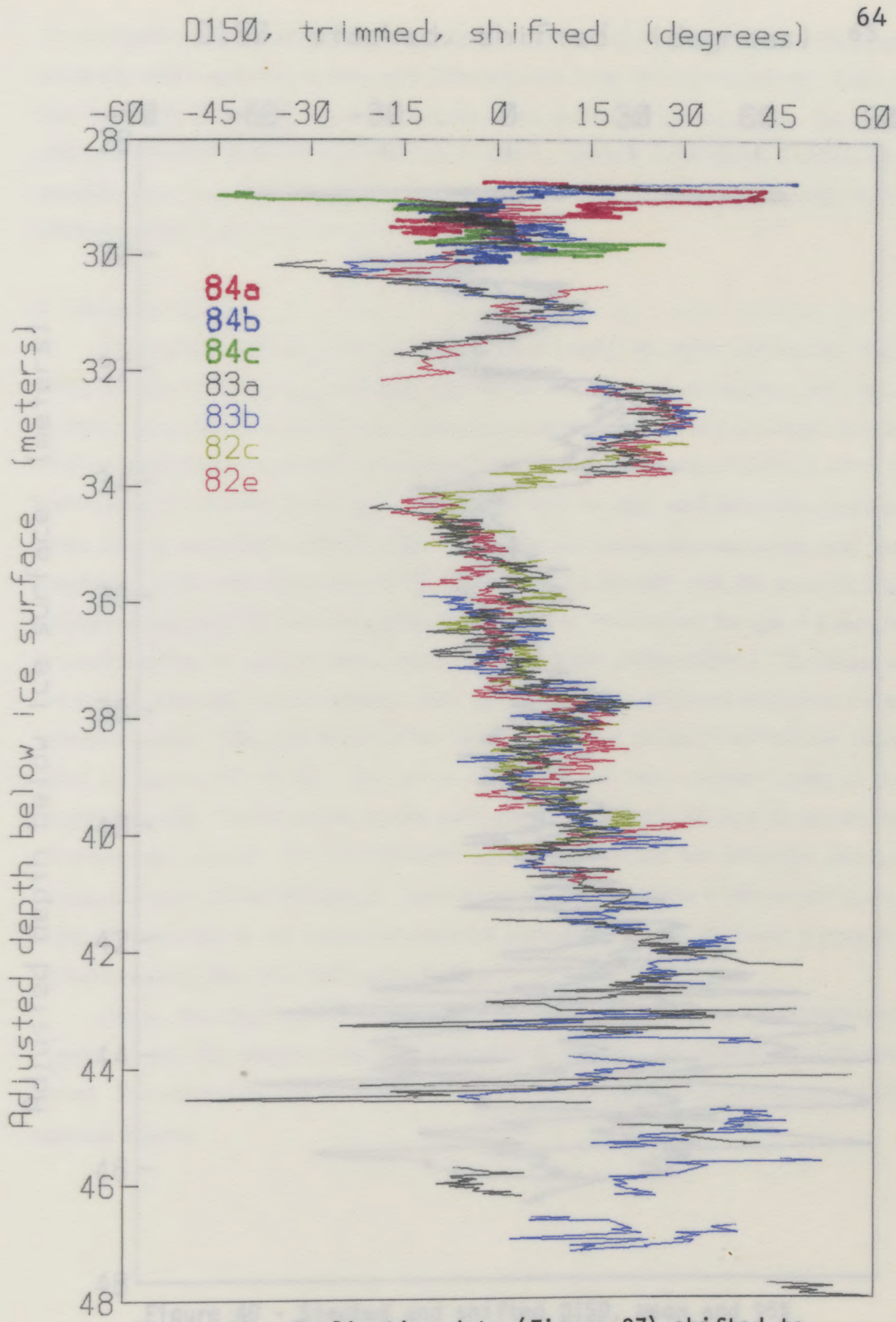

Figure 39 - Declination data (Figure 37) shifted to remove systematic errors in core orientation.

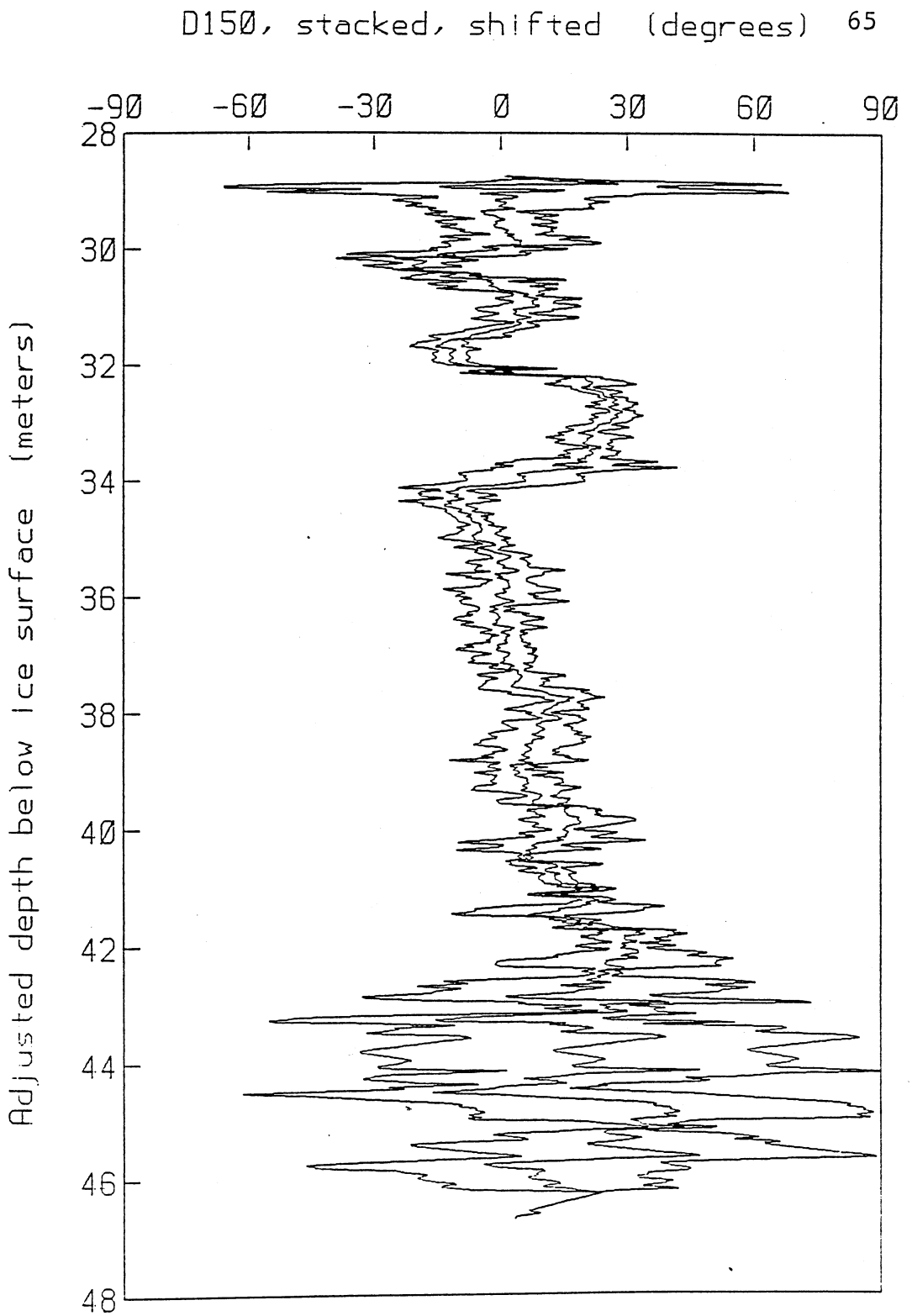

Figure 40 - Stacked and shifted D150, mean and 95% confidence limits.

the declination match. There appears to be a major shift in declination right in this gap. Since the shift is apparent in two cores (83a and 82e) it has not been removed. Rather, core segments 83a04 and 83a01 were again taken as fixed references. Also, the major shift in declination at 34m is recorded only in 82c01. There is evidence for a shift in 83a and 82e, but it is accentuated in 82c. It is unfortunate that these important points in the declination record are so poorly covered.

E. Dating the curves.

The stacked, shifted, and smoothed curves of I and D vs. depth can now be dated using the varve chronology, facilitating time series analysis and comparison with other records. The limits of confidence for the I and D curves, derived at such length above, must be reconsidered at this point since thay have been derived relative to depth, which is known without significant uncertainty. In plotting I or D vs. age, each data point could be given an age uncertainty (vertical axis) in addition to the signal uncertainty, with the resulting curves washing out most of the resolution in the records. But this assumes that the ages of the samples are independent of one another, when in fact the age of a sample is constrained by the younger sample above it and the older sample below it. The shape of the curves is known; the uncertainty in the age scale simply stretches the curves by an unknown amount. Thus, the means of the I and D curves are plotted three times vs. varve years in Figures 42 and 43. The center curves are the best estimate dating of the magnetic signals. The left curves are the minimum age curves and the right curves are the maximum age curves. The true sediment age is between the two extremes and our previous analysis of the radiocarbon dates suggests that it is close to the central curve. Although stretching of the curves between the extremes need not be linear, it must be smoothly varying given the stratigraphic control.

Hence, the smoothed curves of Figures 35 and 41, with the possible stretching of Figures 42 and 43, represent the final derivation of the Elk Lake directional magnetic record. The limits of confidence allow true features in the signal to be distinguished from spurious signals.

Figure 41 (p. 68) - D150 data, optimally smoothed with limits of 95% confidence. The inner curve is the best estimate of the declination signal. The outer (light weight) curves define the limits of 95% confidence for the value of the curve (absolute declination). The remaining two curves define the limits of 95% confidence for the shape of the signal (relative declination). The dashed line at 0° is the expected axial dipole average declination value.

Figure 42 (p. 69) - Smoothed inclination means vs. varve years. The uncertainty in the age scale is accounted for by plotting three curve sets, one minimum (left), one maximum (right) and one best fitting (center). The horizontal axis is scaled with reference to the center set with the left and right sets shifted 50°.

Figure 43 (p. 70) - Smoothed declination means vs. varve years. The uncertainty in the age scale is accounted for by plotting three curve sets, one minimum (left), one maximum (right) and one best fitting (center). The horizontal axis is scaled with reference to the center set with the left and right sets shifted 180°.

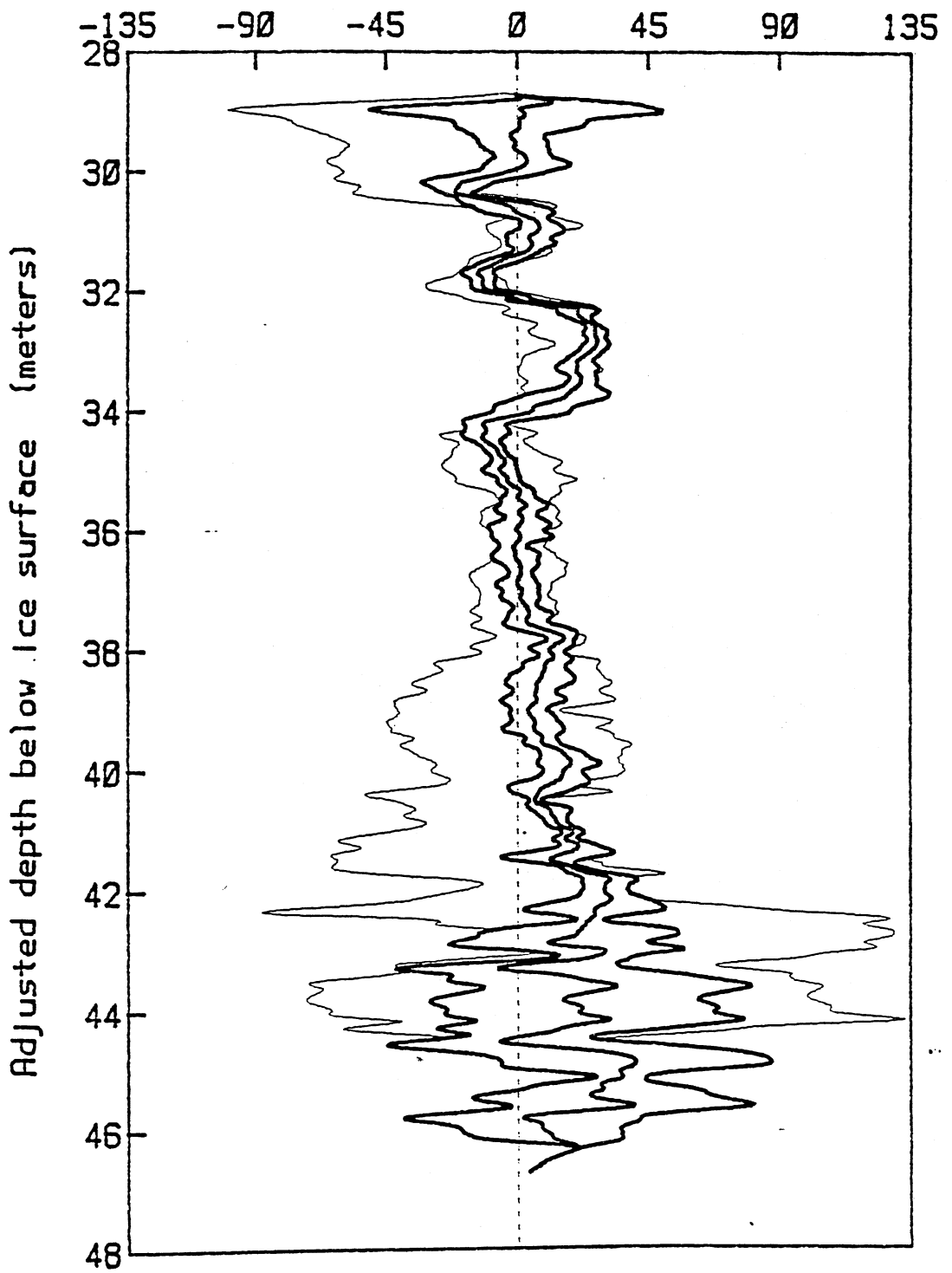
D150, smoothed (degrees)
-135
-90
-45
0
45
90
135
28
30
32
34
36
38
40
42
44
46
48
Adjusted depth below ice surface (meters)

Figure 41.

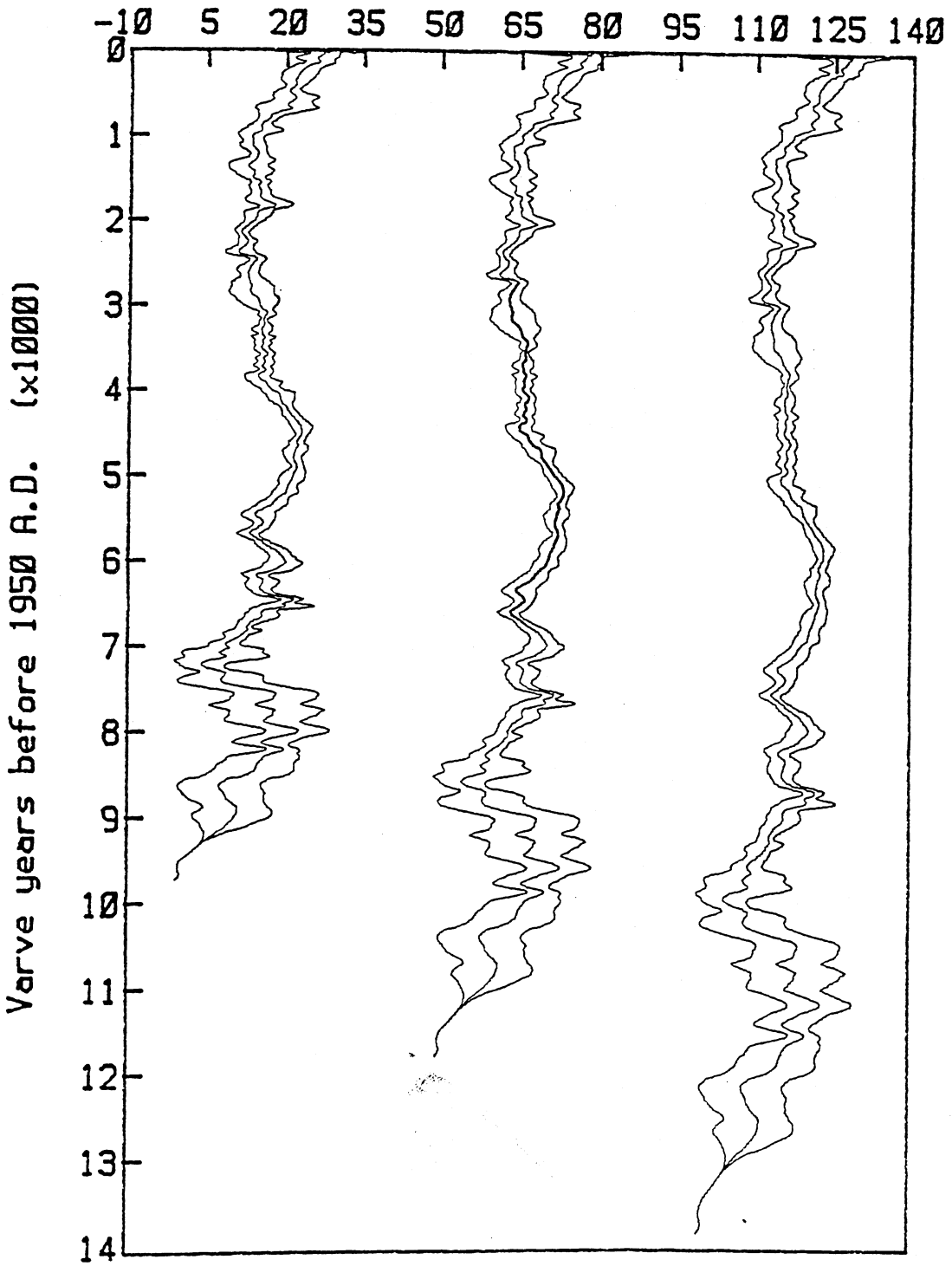
I150, smoothed (degrees)
-10 5 20 35 50 65 80 95 110 125 140
0 1 2 3 4 5 6 7 8 9 10 11 12 13 14
Varve years before 1950 A.D. (x1000)

Figure 42.

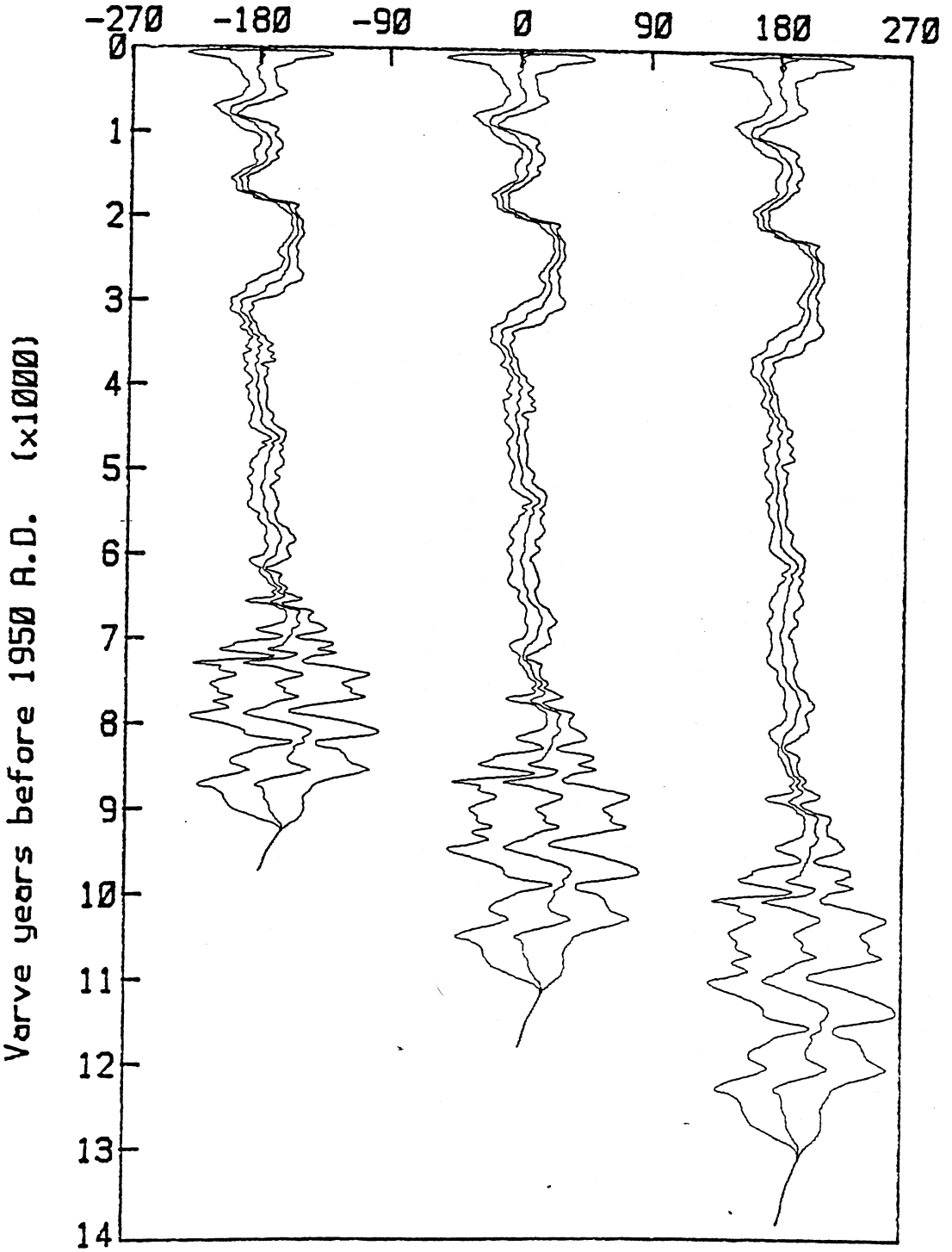
D150, smoothed (degrees)
-270
-180
-90
0
90
180
270
0
1
2
3
4
5
6
7
8
9
10
11
12
13
14
Varve years before 1950 A.D. (x1000)

Figure 43.

CHAPTER 6 : PALEOINTENSITY

A. Introduction and rock magnetics.

This chapter details an effort to derive relative paleointensities from the sediments of Elk Lake. The length of the paleomagnetic vector (paleointensity) is dealt with separately from the directional record because it is a function of several additional variables. While the direction scalars are quite robust with respect to changes in magnetite grain size or concentration, or changes in the intensity of the ambient field, the intensity of the DRM is strongly dependent on all of these variables. Because of the changes in magnetite grain size and concentration, paleointensities cannot be derived with much confidence at the present time. However, the results presented give strong evidence that the Elk Lake sediments do contain useful paleointensity information, and therefore, hope for the future.

Johnson et al. (1948) first demonstrated that the intensity of magnetization of redeposited sediments is dependent on the strength of the ambient field at the time of deposition. The dependence was shown to be linear for fields less than about 4 Oe. Stacey (1972) explained this field dependence in terms of two competing forces, the aligning force of the ambient field, and the randomizing force of Brownian motion. Given a uniform (or at least simple) and very well known grain size distribution, and the temperature at the time of deposition, and assuming that Brownian motion is the predominant randomizing force, it is possible to derive the paleofield intensity from the sediment remanence using Stacey's theory. With any complexity of grain size distribution, the problem becomes much more difficult, and the method is invalid if forces other than Brownian motion significantly impede grain alignment.

More practical methods of deriving paleointensities fall into two categories, resettling and normalization. Resettling of sediments under known conditions dates back to Johnson et al. (1948). If the redepositional environment sufficiently mimics the original environment, then the redepositional remanence, acquired in a known field, can be used to calibrate the original remanence. Since no laboratory method can exactly reproduce the original depositional conditions, reasonable approximations which are convenient to use have been sought. Slow depositions over long periods of time have been tried (Barton and McElhinny, 1979) as well as depositions of dilute (King, 1955; Lèvi and Banerjee, 1976) and concentrated (Kent, 1973; Graham, 1974) slurries. Tucker (1980,1981) has made a siginicant contribution with his work on SRM (stirred remanent magnetization),

giving evidence that stirring in a known field can be used to calibrate intensities for a range of sediment types. All of these methods suffer from inevitable differences between original and laboratory conditions, and from the fact that each small individual sample cannot be resettled.

For these reasons, much effort has been invested in a search for an appropriate normalizing parameter for paleointensity. The problem is difficult because the remanent intensity of sediments is related to at least three factors other than the paleofield strength : the composition of the magnetic minerals, the concentration of magnetic minerals, and the magnetic mineral grain size. Parameters which have been tried include IRM (isothermal remanent magnetization) (Johnson et al., 1948), SIRM (saturation isothermal remanent magnetization) (Nakajima and Kawai, 1973), and initial susceptibility (Harrison, 1966). But the parameter which appears to best mimic the field dependence of DRM is ARM (Johnson et al., 1975; Levi and Banerjee, 1976; Lund, 1981). King et al. (1983a) have carefully detailed the range of sediment types for which ARM responds similarly to DRM. They define three conditions necessary for NRM/ARM to reflect relative paleointensity : 1) the dominant magnetic mineral must be magnetite, 2) the maximum magnetite concentration must be less than 20 times the minimum concentration, and 3) the magnetite particle size range must be between 1 and 15 microns.

The first two criteria are easily met by the entire Elk Lake sediment section, but the third presents problems. Figure 44 is a plot of ARM/X (average of all cores) vs. adjusted depth. Since ARM affects small magnetite grains more than large, and X affects large grains more than small, the ratio ARM/X is a useful measure of relative grain size in magnetite (King et al., 1982). The dramatic rise in ARM/X at 31.5 m indicates a marked decrease in the average magnetite grain size above this transition. Since the change is due entirely to a rise in ARM (Figure 8), a dramatic increase in the concentration of small grains is indicated. There is evidence for a second rise in ARM/X at 29 m., but the sediment above this point represents only the upper 100 years of the record. In the following paragraphs, two problems are examined : 1) the nature of and the reason for the transition at 31.5 m, and 2) the effect of the grain size transition on paleointensity estimates.

The circles plotted in Figure 44 locate samples studied in detail to define the nature of the transition. In addition, a Franz Magnetic Separator was used to extract the magnetic minerals from large bulk samples from above and below the transition. Hysteresis parameters were measured for the separates and the test pairs. Curie temperature

Figure 44 (p. 74) - ARM/X vs. adjusted depth. ARM/X is inversely related to magnetite grain size so that the average magnetite grain size is smallest for the upper three meters. ARM is measured in emu (xE-6) while X is measured in emu/Oe (xE-5). The circles represent individual samples from the sample pairs used to investigate the change in magnetite grain size.

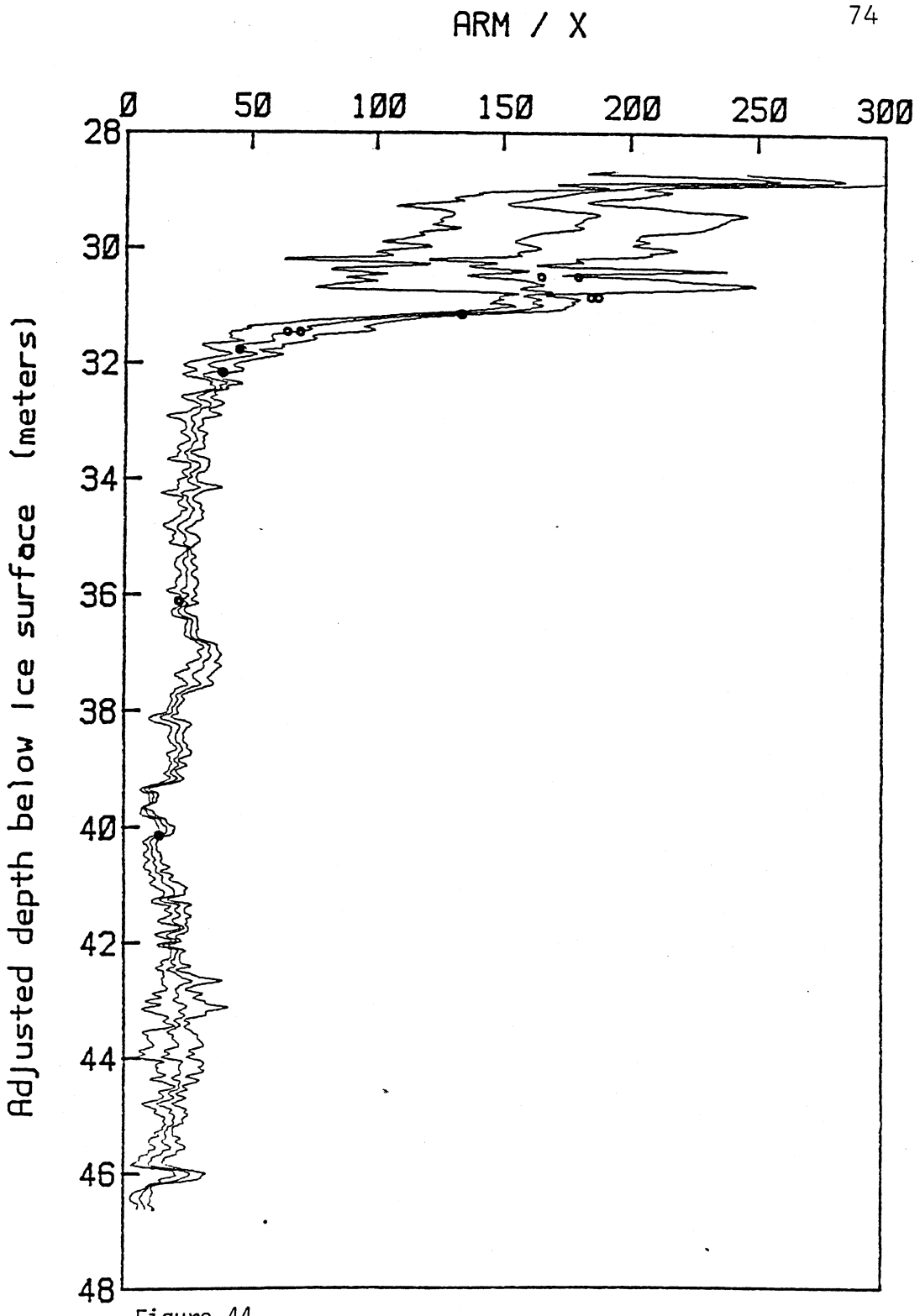
ARM / X
0
50
100
150
200
250
300
28
30
32
34
36
38
40
42
44
46
48
Adjusted depth below ice surface (meters)

Figure 44.

determinations were made on the separates and IRM acquisition was measured on the test pairs. Figure 45 plots the IRM acquisition curves for the test pairs. The rise to saturation at about 1200 Oe is characteristic of magnetite. The different curve shapes reflect the different grain sizes but there is no evidence of any other magnetic phase such as hematite. Figure 46 is the preheating hysteresis loop for magnetic separate a2 from above the transition, measured on a vibrating sample magnetometer (VSM). The figure caption explains the various parameters measured from the loop. Figure 47 shows the Curie temperature determination on the same sample, also measured on the VSM. The Curie temperature of ≈580° C is characteristic of magnetite. The difference between the Curie temperatures on the heating and cooling cycles is due to thermal lag in the measuring system, the true Curie temperature estimate being the average of the two. There is no evidence of any thermally induced change of phase in the magnetite on either the heating or cooling cycles. Figures 48 and 49 show the corresponding hysteresis and Curie determinations for magnetic separate b1 from below the transition. Table 4 summarizes the results obtained from the test pairs and separates.

Table 4 - Rock magnetic parameters from test pairs and separates.

Sample	Varve years	Js	Jrs	Hc	Hcr	Jrs/Js	Hcr/Hc	ARM/X	Tc
83a3050a	980	.0385	.0145	244.6	557.0	.3762	2.277	33.0	
b								35.9	
3086a	1211	.0378	.0139	231.2	527.0	.3673	2.279	37.5	
b								36.9	
3114a	1415	.0294	.0103	215.1	467.0	.3489	2.171	26.8	
b								26.7	
3146a	1601	.0175	.0047	166.4	414.0	.2691	2.650	13.9	
b								12.9	
3178a	1770	.0151	.00315	100.0	404.0	.2086	4.04	9.1	
b								9.1	
3218a	2002	.0137	.00307	143.7	379.0	.2239	2.638	7.8	
b								7.8	
3590a	4143	.0384	.00488	≈92	306.0	.1270	3.326	4.5	
b								4.4	
4034a	7080	.0488	.00425	≈78	298.0	.0871	3.821	3.0	
b								2.9	
above-1	<1000	.40	.032	≈320	75.0	.080	4.27		586
above-2	<1000	.47	.037	315	74.0	.078	4.26		583
below-1	>2000	.53	.026	262	48.5	.049	5.40		589
below-2	>2000	.43	.017	247	42.4	.040	5.83		585

Unit key for Table 4. Js and Jrs are measured in emu (electromagnetic units). Hc and Hcr are measured in Oe (Oersteds). Tc is measured in °C.

Figure 45 (p. 77) - IRM acquisition. IRM acquisition for the test pairs across the transition, normalized to the IRM at 10 kOe, is plotted vs. applied field. All of the samples rise to saturation by about 1500 Oe, indicative of magnetite. The slightly different shapes of the curves reflects the change in grain size. There is no evidence for significant amounts of other magnetic phases such as hematite.

Figure 46 (p. 78) - a2 hysteresis. The curves marked 'a' show the full field hysteresis properties of magnetic extract a2. The sample magnetization above about 4000 Oe is the saturation magnetization, Js. The curves marked 'b' show the central portion of the loop with the vertical scale expanded 10x and the horizontal scale expanded 100x. The intercept of the curves with the vertical axis is the saturation remanent magnetization, Jrs, while the intercept with the horizontal axis is the coercive force, Hc. The fourth parameter, the coercivity of remanence (Hcr), is the back field necessary to average the remanence to zero. It cannot be determined directly from the hysteresis loops.

Figure 47 (p. 79) - a2 Curie temperature. Sample magnetization is plotted vs. temperature in °C for heating and cooling (see arrows) of the sample. The magnetization disappears at the Curie temperature. The offset between the heating and cooling curves is due to thermal lag in the temperature measuring system. The average of the two yields a Curie temperature of ≈580 °C. The noise in the cooling curve signal is due to physical breakup of the sample pellet. The return to the starting point on the cooling curve indicates that there is no chemical or phase change during heating. All indications are that the predominant magnetic mineral is pure magnetite.

Figure 48 (p. 80) - b1 hysteresis. The pre-heating hysteresis curves for magnetic separate b1 are shown. See the caption of Figure 46 for discussion, with the exception that for the 'b' curves, the horizontal expansion is x10 rather than x100.

Figure 49 (p. 81) - b1 Curie temperature. The Curie point determination for magnetic separate b1 is shown. See caption of Figure 47 for discussion.

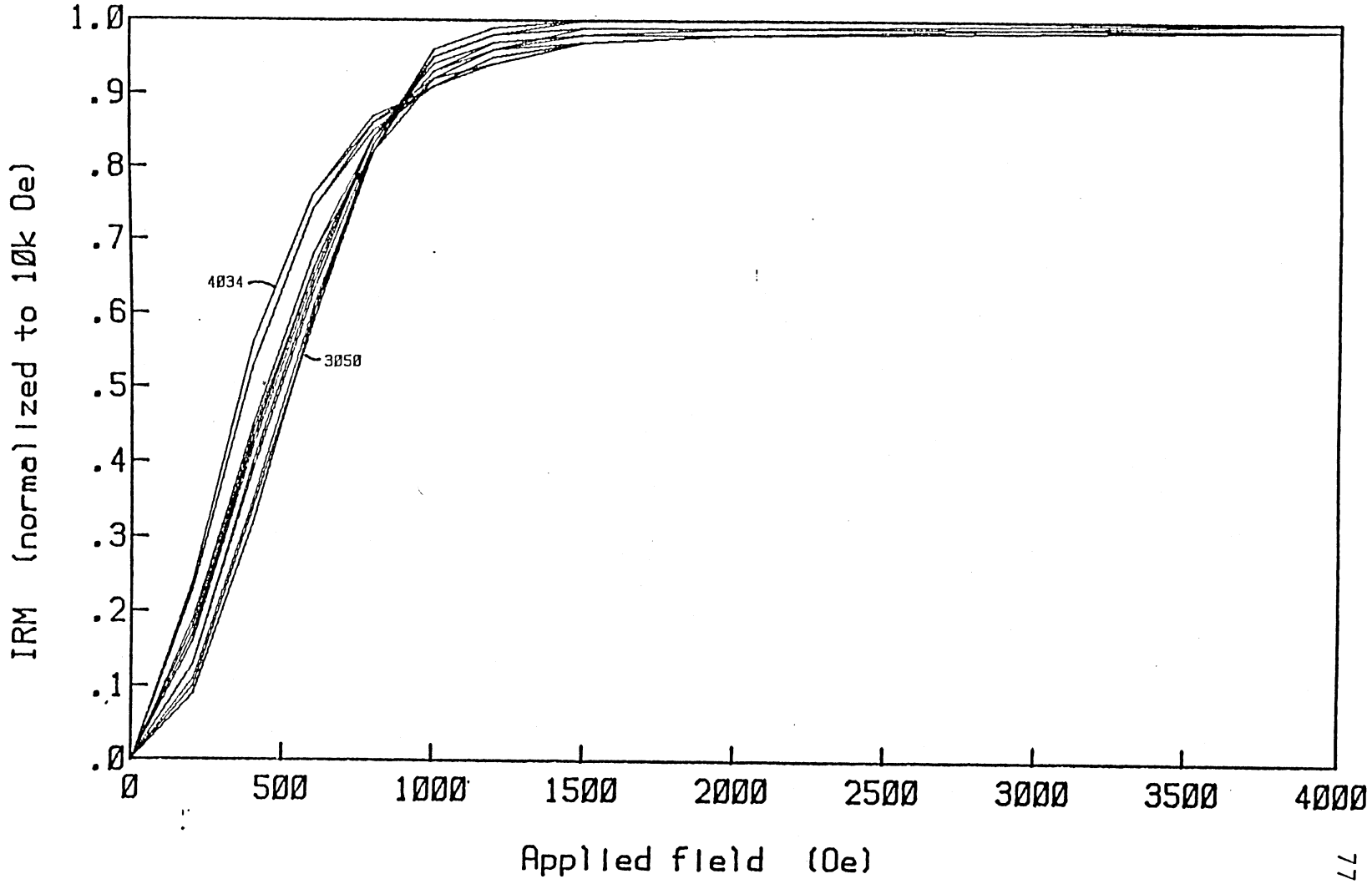
1.0
.9
.8
.7
.6
.5
.4
.3
.2
.1
.0
IRM (normalized to 10k Oe)
4034
3050
0
500
1000
1500
2000
2500
3000
3500
4000
Applied field (Oe)

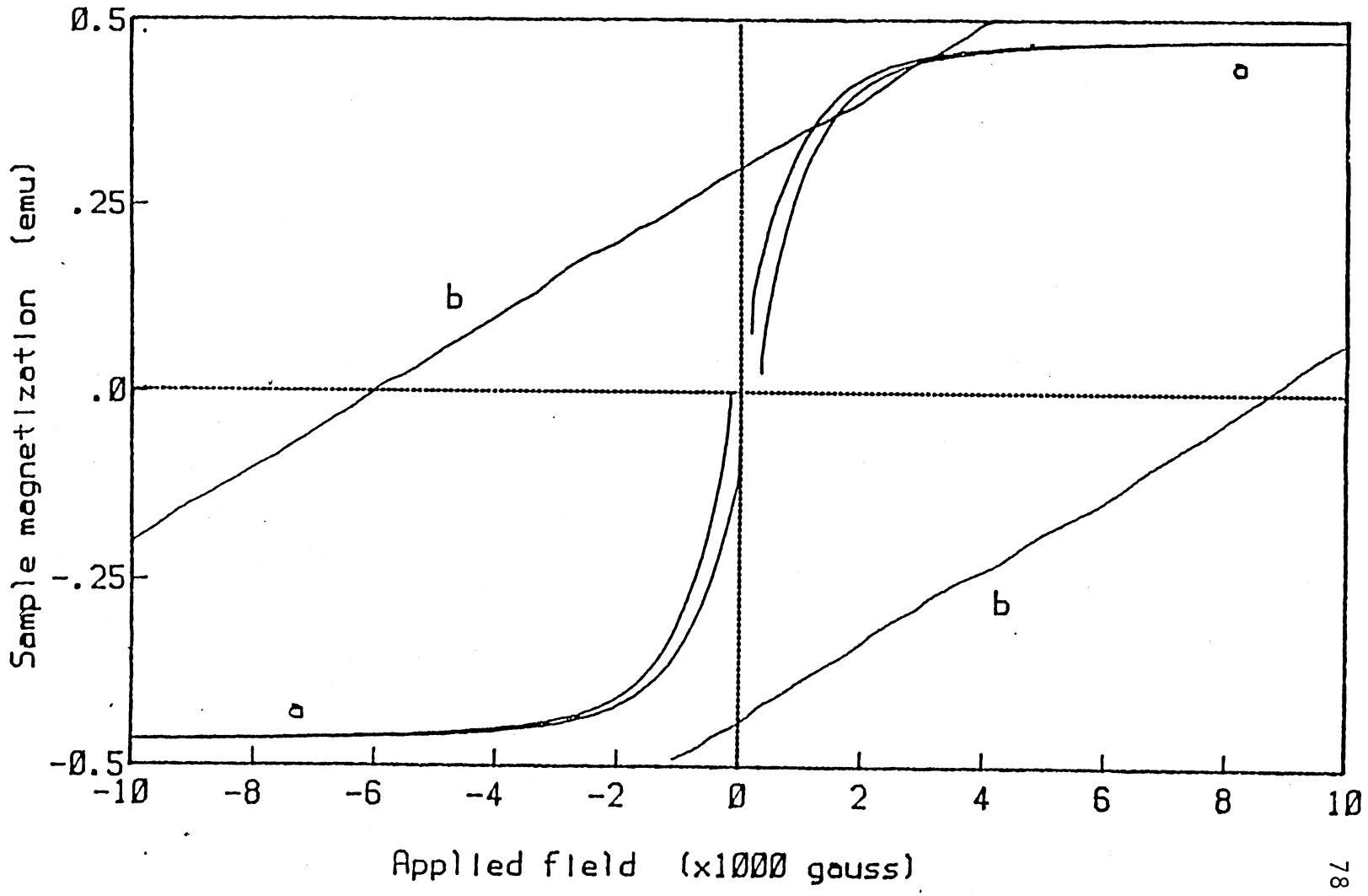
0.5
.25
.0
-.25
-0.5
-10
-8
-6
-4
-2
0
2
4
6
8
10
Sample magnetization (emu)
Applied field (x1000 gauss)
a
b
a
b

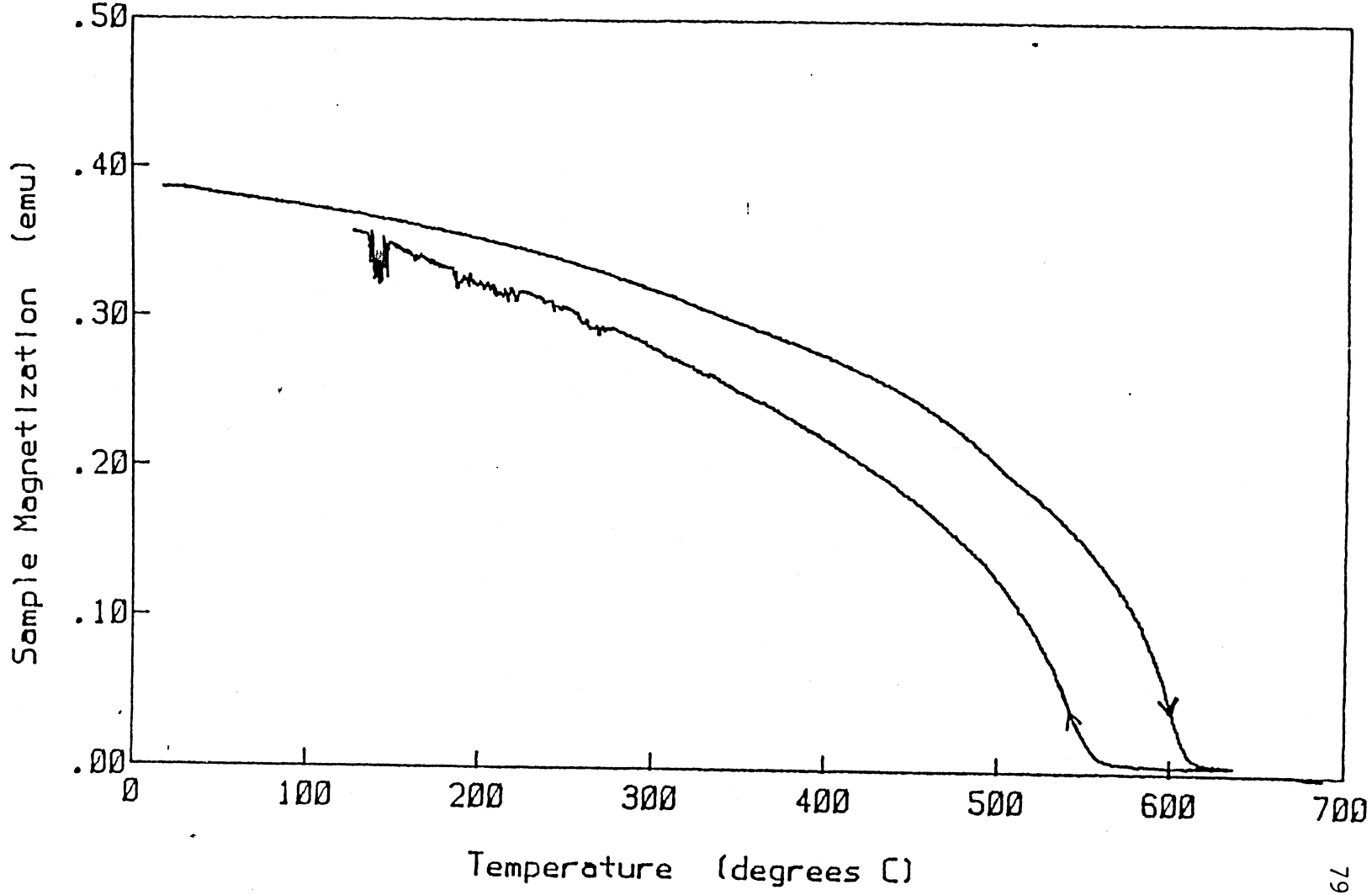
.50
.40
.30
.20
.10
.00
Sample Magnetization (emu)
0
100
200
300
400
500
600
700
Temperature (degrees C)

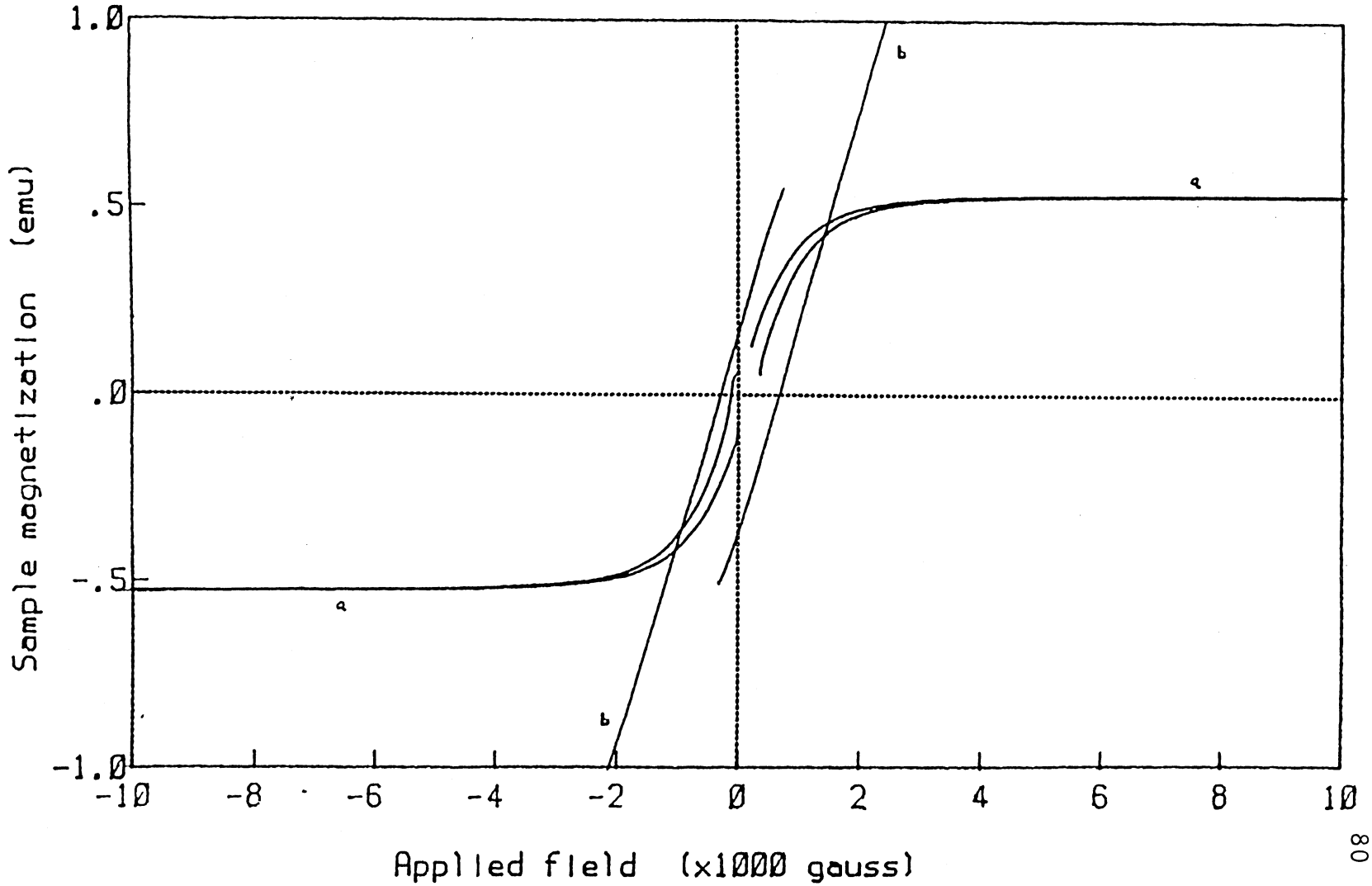
1.0
.5
.0
-.5
-1.0
Sample magnetization (emu)
-10
-8
-6
-4
-2
0
2
4
6
8
10
Applied field (x1000 gauss)
a
a
b
b

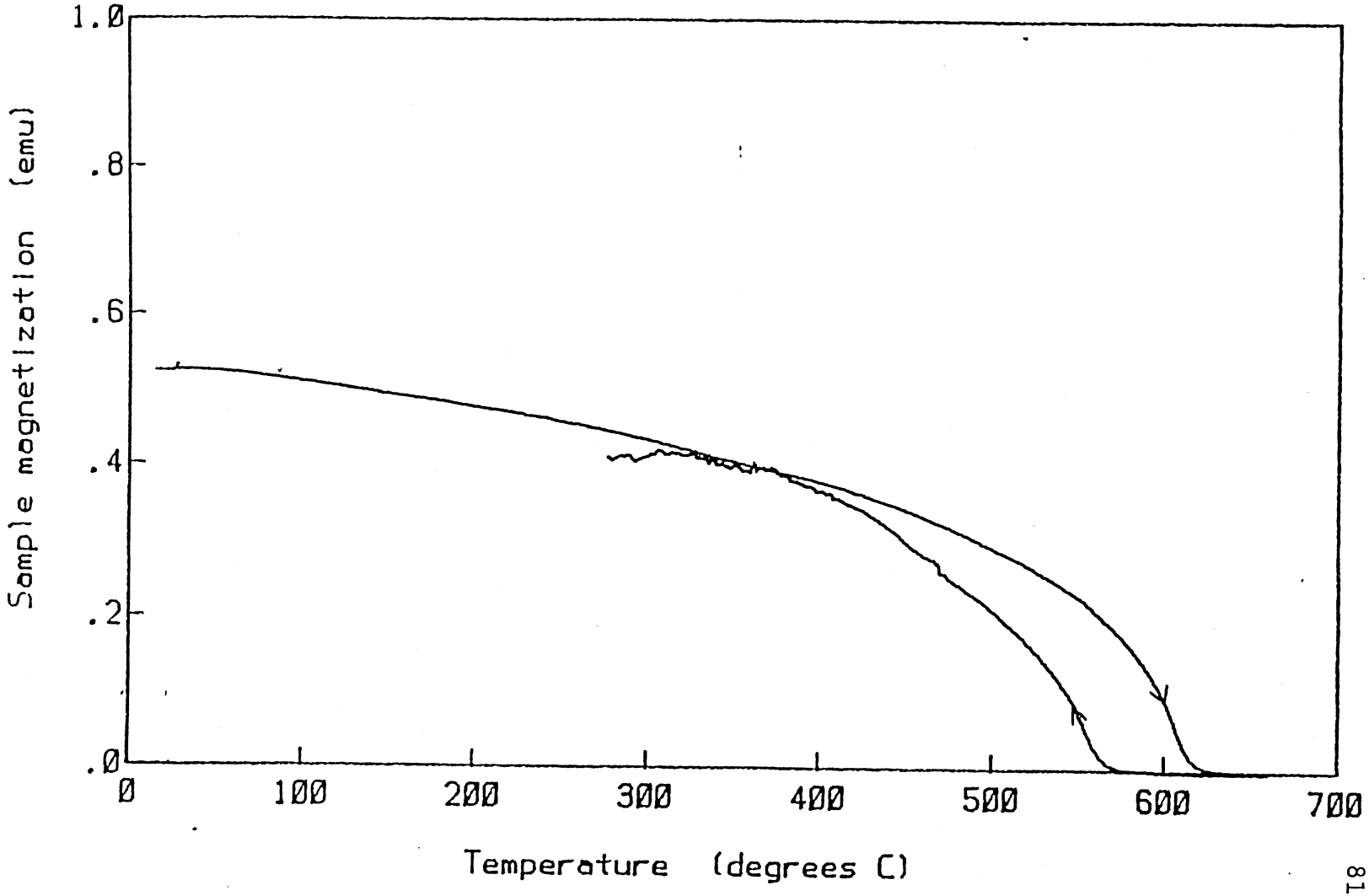
1.0
.8
.6
.4
.2
.0
Sample magnetization (emu)
0
100
200
300
400
500
600
700
Temperature (degrees C)

The Curie temperatures and the IRM acquisition curves indicate that magnetite is the dominant magnetic mineral throughout the sediment section. The Js values indicate that the maximum concentration of magnetite in the sediment (above the transition) is about five times the minimum concentration (below the transition). Thus, the first two of King et al's. (1983a) requirements for the ARM normalization method are fullfilled by the Elk Lake sediment. The remaining requirement is that the average magnetite grain size be between 1 and 15 microns.

The hysteresis parameters are related to magnetite grain size as shown in Figure 50 (Day et al., 1977). The three regions, labeled SD, PSD, and MD represent the different domain states, single domain, psudo-single domain and multi-domain. SD grains are magnetized entirely in one direction, while MD grains are divided into many regions whose magnetizations oppose one another. PSD grains are multi-domain grains with few enough domains (<10) so that their behavior is similar to that of single domain grains. Grains with different domain states have different magnetic properties and stability characteristics. PSD grains are magnetically stable and commonly occuring so they contribute significantly to the stable remanence of many sediments, including those from Elk Lake. Also shown in Figure 50, as the dotted rectangle, are the parameter limits listed by King et al. (1983a) as defining the grain size range 0-15 microns. The trend in values in Figure 50 from sample 4034 to 3050 confirms the earlier evidences of a decrease in average magnetite grain size through the transition. Sample 3178 is anomalous for an unknown reason. Also plotted in Figure 50 are the hysteresis properties of the magnetic separates, plotted as +'s (above) and x's (below). The same grain size trend is seen between these samples, but they are shifted significantly to larger sizes with respect to the test pairs. This indicates that the magnetic separation process extracts large grains more efficiently than small grains. Other workers have also found this to be the case (Karlin and Levi, 1985a). The sample pairs below the transition meet King et al's requirements for the ARM normalization method. The samples above the transition, while safely in the PSD range, do not meet the requirements. The King et al. boundaries are uncertain because they are derived from scattered data and because sediment samples have a distribution of grain sizes rather than a single grain size. Even so, Figure 50 indicates that care is required in deriving relative paleointensities for the samples above and across the transition.

An explanation for the origin of the transition might give a clue as to how to procede. Two facts must be accounted for, the decrease in average magnetite grain size and the 500% increase in total magnetite content through the transition. An obvious possibility is

Figure 50 (p. 84) - Domain states of test pairs and separates. The hysteresis parameters are related to magnetic domain state in magnetite as shown by Day et al. (1977). The circles plot the results from the test pairs across the grain size transition. A clear movement towards larger grains with depth is seen, as predicted by the ARM/X curve. The dotted box defines the King et al. boundaries for the grain size range 0 to 15 microns, for which the ARM normalization method is thought to be valid. The samples above the transition, while fimly in the PSD range, fall outside the King et al. boundaries. The magnetic separates from above and below the transition are plotted as +'s and x's respectively. The same grain size trend is seen in the separates, but the magnetic separation process has resulted in a bias towards the larger grain size fraction, making these data less reliable.

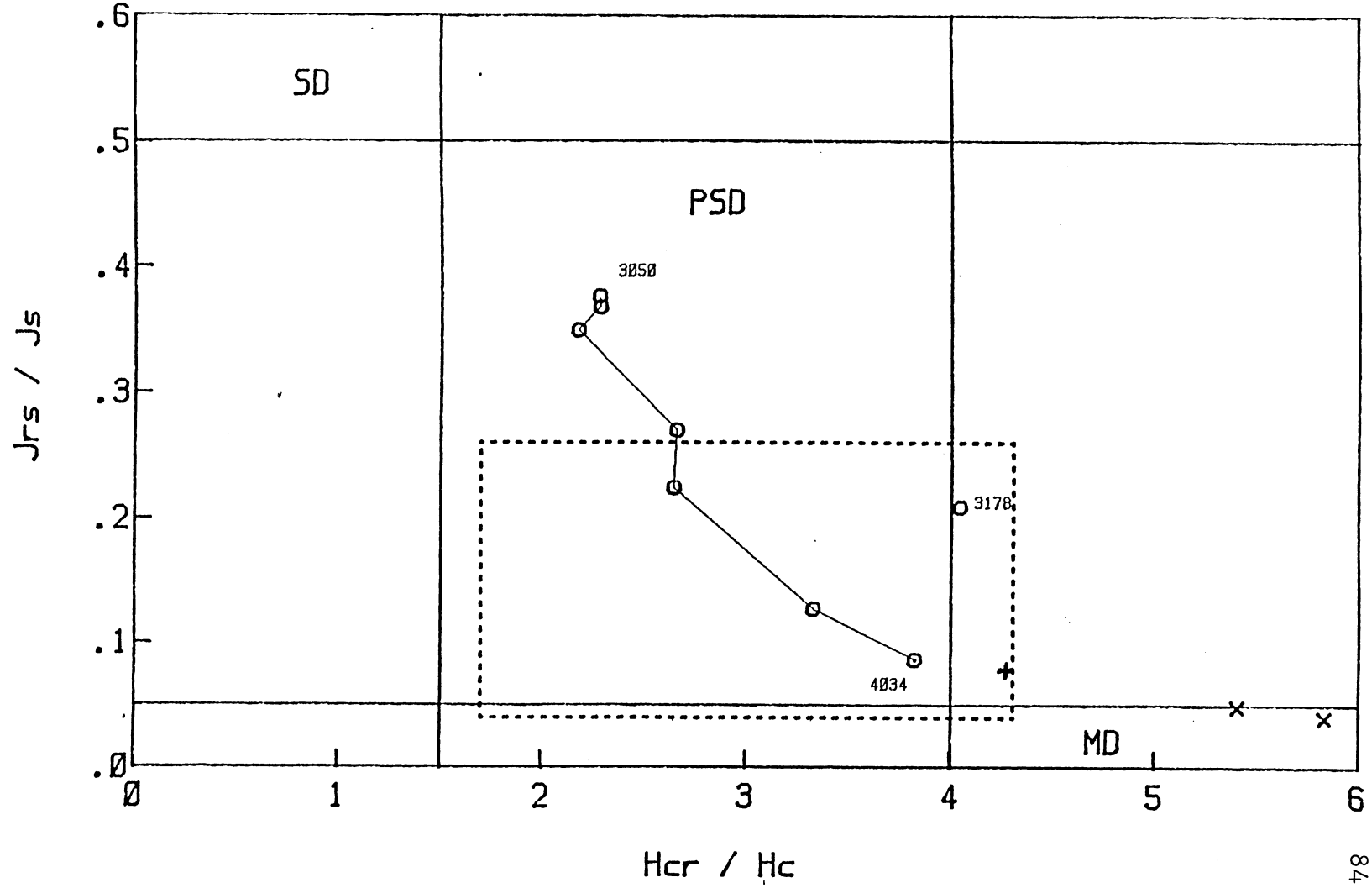
SD
PSD
MD
3050
3178
4034
.6
.5
.4
.3
.2
.1
.0
0
1
2
3
4
5
6
Jrs / Js
Hcr / Hc

that there was a sudden influx of small grained magnetite into the lake 1500 years ago and this influx has continued to the present. It is difficult to document a climatological or erosional change in the lake environment capable of producing such a large change in both average magnetite grain size and total influx. The only apparent source for such an influx of fine grained magnetite is magnetotactic bacteria. Certain species of bacteria produce SD magnetite grains which they use for navigational purposes (Kirschvink and Gould, 1981). If such bacteria suddenly appeared in the lake 1500 years ago, they could produce a significant amount of fine-grained magnetite, (Kirschvink and Lowenstam, 1979; Towe and Moench, 1981), enough to account for the observed changes.

However, even if magnetotactic bacteria are present in Elk Lake, we cannot argue for their sudden appearance in the lake because of a second and more likely explanation for the observed changes, namely, that magnetite is being dissolved in the sediment. Karlin and Levi (1983, 1985a) have demonstrated very similar magnetic behavior in continental shelf sediments and have argued rather convincingly that it is due to the reduction and dissolution of magnetite associated with diagenesis of organic material. As the magnetite dissolves, the average grain size appears to coarsen with depth because the fine grains are completely eliminated. This explanation is favored over the bacterial influx proposal because while the ARM/X diagram (Figure 41) seems to indicate a step function in grain size, the MDF diagram (Figure 22) and the trend in hysteresis properties (Figure 50) show a much more gradual change in the magnetic properties of the sediment.

Karlin and Levi (1985a, 1985b) have argued that such dissolution of magnetite in the sediment should have little effect on the directional magnetic record, but that paleointensity studies are precluded because of the loss of remanent intensity. Thus the prospects for deriving paleointensities from the sediments of Elk Lake seem rather bleak. King et al. argue that the ARM normalization method will not work above or through the transition because the average magnetite grain size is too small above the transition and because of the change in properties through the transition. Karlin and Levi on the other hand argue that paleointensities cannot be reliably derived even below the transition because of the changes which have occured in the sediment. But perhaps all is not lost. The King et al. boundaries are based on scattered data and may be too conservative. Karlin and Levi have thrown out paleointensities aprori, but since the field dependence of sediment magnetization is based on the degree of alignment of magnetic grains, if the directional record is preserved through the dissolution process, the field dependence of remanent intensity should also be preserved. Selecting an appropriate normalizer for the

remanence may be difficult, but there is no reason to discard the intensity record at the outset.

B. The remanent intensity record.

Figure 51 plots the mean of the NRM/ARM ratios from the seven cores, along with the limits of 95% confidence, calculated from the std. devs. of the stacked data. Sample pairs which were eliminated from I and D in Chapter 5 were eliminated from the intensity data, but no additional pairs were removed. Figure 21b and similar diagrams from other test pairs both above and below the transition indicate that ARM affects the different grain size fractions similarly to DRM. ARM is thus useful for normalizing out the major effects on NRM of the change in magnetite content, and the minor effects due to sample volumn variability. The work of King et al. and Karlin and Levi indicate that properly calibrating the NRM/ARM ratio for paleointensity may be difficult.

Two methods are available for calibrating the NRM/ARM curve to estimate paleointensity and to determine how to deal with the grain size transition. One method is to estimate the relationship between NRM/ARM and ambient field strength by resettling. The stirring (SRM) method of Tucker (1981,1982) is the most promising and is used here. The second is to compare the NRM/ARM record with absolute paleointensity records from lava flows and archeological samples.

Bulk sediment samples from above and below the grain size transition were reconstituted by adding water and were redeposited in a series of known fields. The rewetted samples were poured into cylinders 3 in. in diameter by 4 in. high. Holes in the cylinders, blocked with filter paper, allowed the sediment to gradually lose water. After about 24 hr., the samples were dry enough for the DRM to be stabily established and for the sediment to be subsampled and measured. The DRM's were measured at various demagnetization steps and then ARM's were imparted and measured, also at several demagnetization steps. Figures 52 and 53 plot typical demagnetization results for the resettled DRM's for material from above and below the transition. The straight line portions of the Zjiderveldt diagrams represent the remanence acquired during resettling. The straight lines do not go to the origin, indicating that a portion of the magnetic grains are not aligned by the resettling field. This is difficult to explain since the non-realigned grains are very stable magnetically, suggesting that they are small grains which should be easily realigned. It is possible that a number of small grains are not realigned because they are locked into "clumps" of organic matter which are not broken up during rewetting. The ARM

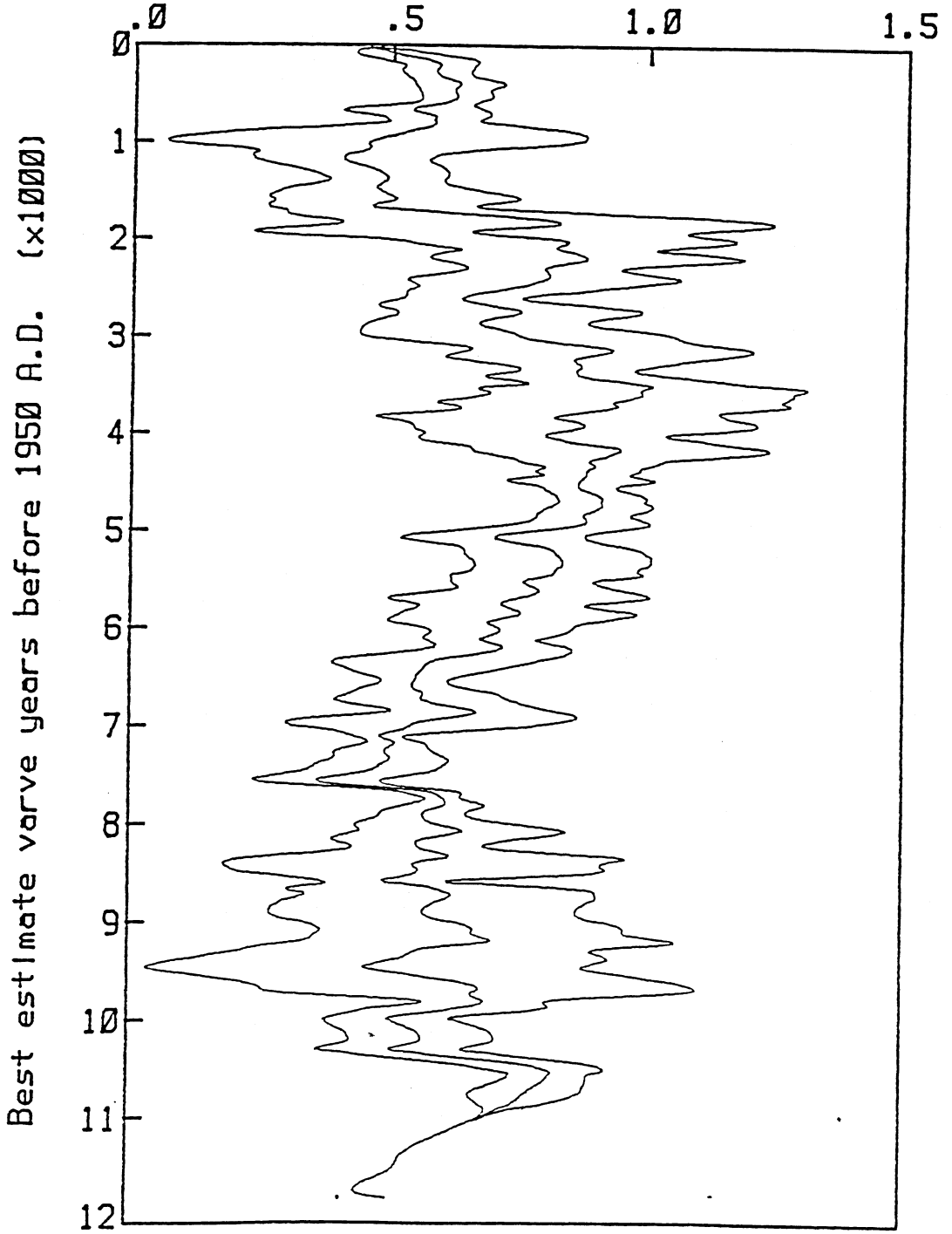

Figure 51 - NRM/ARM smoothed curves. The central curve plots the ratio of NRM150 to ARM150 (.25 Oe DC field), smoothed with a 12 cm. bandwidth. The outer curves are the smoothed 95% limits of confidence.

demagnetization curves are also shown in Figures 52 and 53. The ARM curves are similar to the NRM curves, indicating that in general, the two remanences should affect the different grain size fractions similarly.

Figure 54 plots the DRM_{150}/ARM_{150} results for four separate resettling fields. The samples from above the transition are plotted as x's and the samples from below the transition are plotted as o's. At each field, four cylinders of each sediment type were resettled. Each data point represents the average value for two samples from a given cylinder. The x results at 0.8 Oe are clearly anomolous and have not been used in the analysis. The most likely reason for the low results is a too low initial water content. Water content was shown to have no effect on the results as long as a certain minimum value was exceded. The DRM/ARM values are clearly field dependent, indicating that the NRM of the sediment should be related to the paleo-field strength. The straight lines plotted through the points have noticably different slopes. The best fitting straight line to the samples from above the transition is: DRM/ARM = Field (0.63183) + (0.006). The best fitting straight line through the samples from below the transition is: DRM/ARM = Field (0.3388) - (0.06425). These equations can now be used to calibrate the NRM/ARM values from Figure 51 to derive the paleofield intensity. Unfortunately, the results obtained for the paleofield intensity (0.7 Oe for the present field, 0.94 Oe at 500 years ago, 2.6 Oe at 2200 years ago, and 3.1 Oe at 3800 years ago) are not at all reasonable values for the paleofield strength (see Figure 55). It appears that the resettled NRM's are less than the corresponding original NRM's. This is further evidence that some of the grains are not being realigned. Further work on the SRM method may yield useful results, but only if the sediment can be reconstituted to its original condition.

The second method for calibrating the NRM/ARM curves is simply to compare the curves with information about paleofield strength from other sources. This is done in Figure 55. Plotted along with the NRM/ARM central curve, arbitrarily calibrated to a modern value for NRM/ARM of 0.5, are the smoothed curves representing lava flow data from the western United States (Champion, 1980), archeomagnetic data from Arizona (Bucha et al., 1970), and the worldwide archeomagnetic compilation of Barton et al. (1980). There is a fair amount of difference between the three reference curves used. The western U.S. and Arizona data show a common peak at about 800 years, but the ages of the next low and high are not coincident. The fit of these two with the worldwide data is even worse. This is due partly to the fact that most of the worldwide data is from Europe and also to the fact that the worldwide curve is smoothed with a 1000 year window.

Figure 52 (p. 90) - Demagnetization curves for resettled samples from above the transition. The left diagram shows the directional data from successive demagnetization steps of the DRM. The straight line portions represent the magnetization acquired during resettling. That the curves do not trend towards the origin indicates that not all of the magnetic grains have been realigned during the resettling process. The left diagram shows the loss of remanent intensity upon demagnetization for the DRM's (solid lines) and the ARM's (dotted lines). The curves are not identical, but they indicate that ARM is effecting roughly the same grain size fractions as DRM.

Figure 53 (p. 91) - Demagnetization curves for resettled samples from below the transition. See Figure 52 caption for discussion.

Figure 54 (p. 92) - Dependence of resettling remanence on depositional field. The DRM/ARM ratio is plotted against the resettling field for sediment from above (x's) and below (o's) the transition. The x values at 0.8 Oe are anomolously low and are not used in calculating the best fitting straight line. While the DRM's are field dependent, they do not reasonably calibrate the Elk Lake NRM/ARM curves. This implies that the resettling technique does not fully remobilize all of the magnetic grains.

Figure 55 (p. 93) - Comparison of paleointensity data. The central NRM/ARM curve from Elk Lake is plotted as the dark, solid line. The worldwide archeointensity compilation of Barton et al. (1982) is plotted as a light, solid line. The dotted line is the lava flow data from the western U.S. from Champion (1980). The dashed line is the archeomagnetic data from Arizona from Bucha et al. (1970). The reference curves are normalized to the modern field value. The Elk Lake curve is plotted assuming a modern value of 0.5 for NRM/ARM.

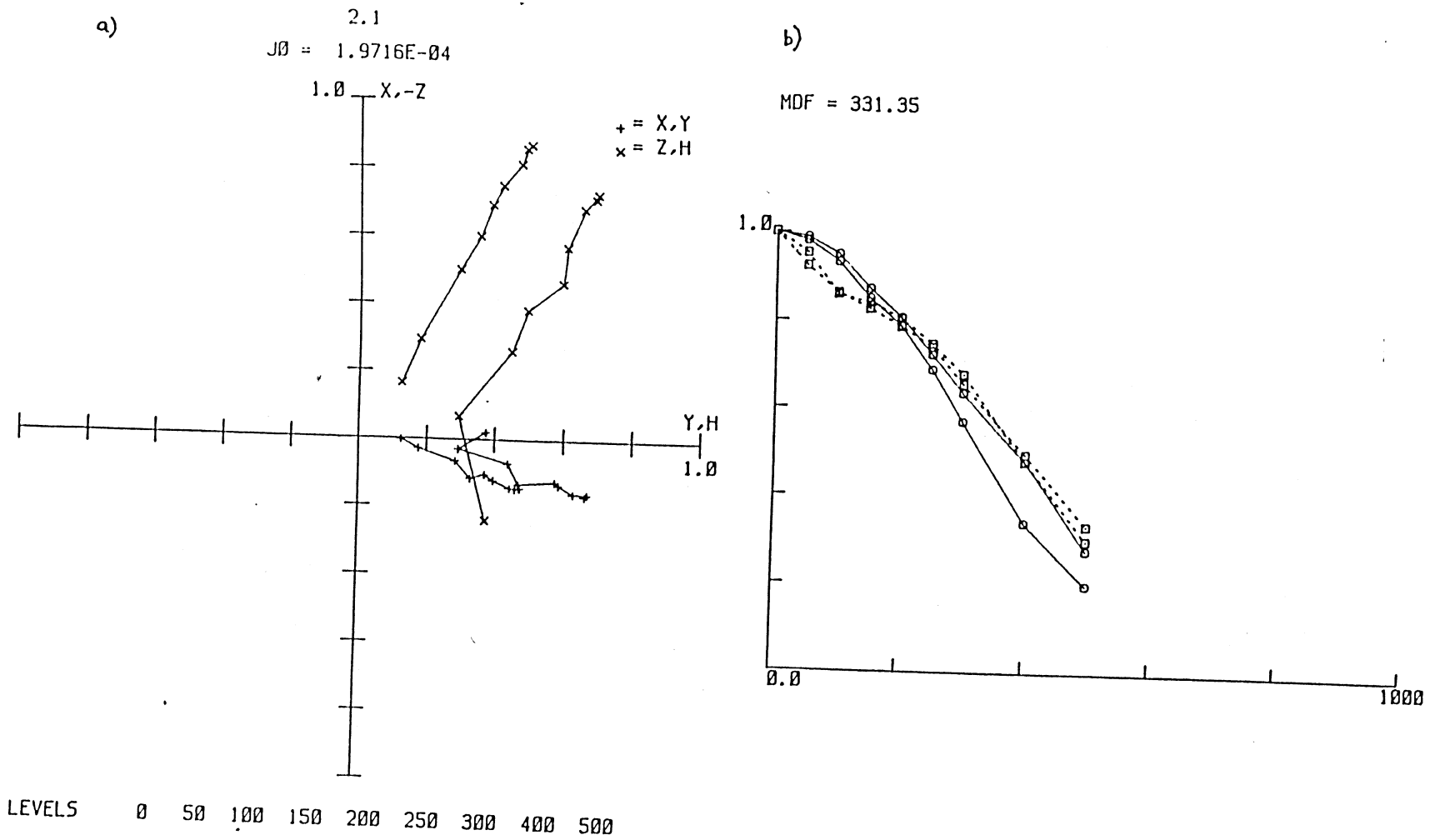
a)
2.1
JØ = 1.9716E-04
1.Ø
X,-Z
+ = X,Y
× = Z,H
Y,H
1.Ø
LEVELS 0 50 100 150 200 250 300 400 500
b)
MDF = 331.35
1.Ø
Ø.Ø
1000

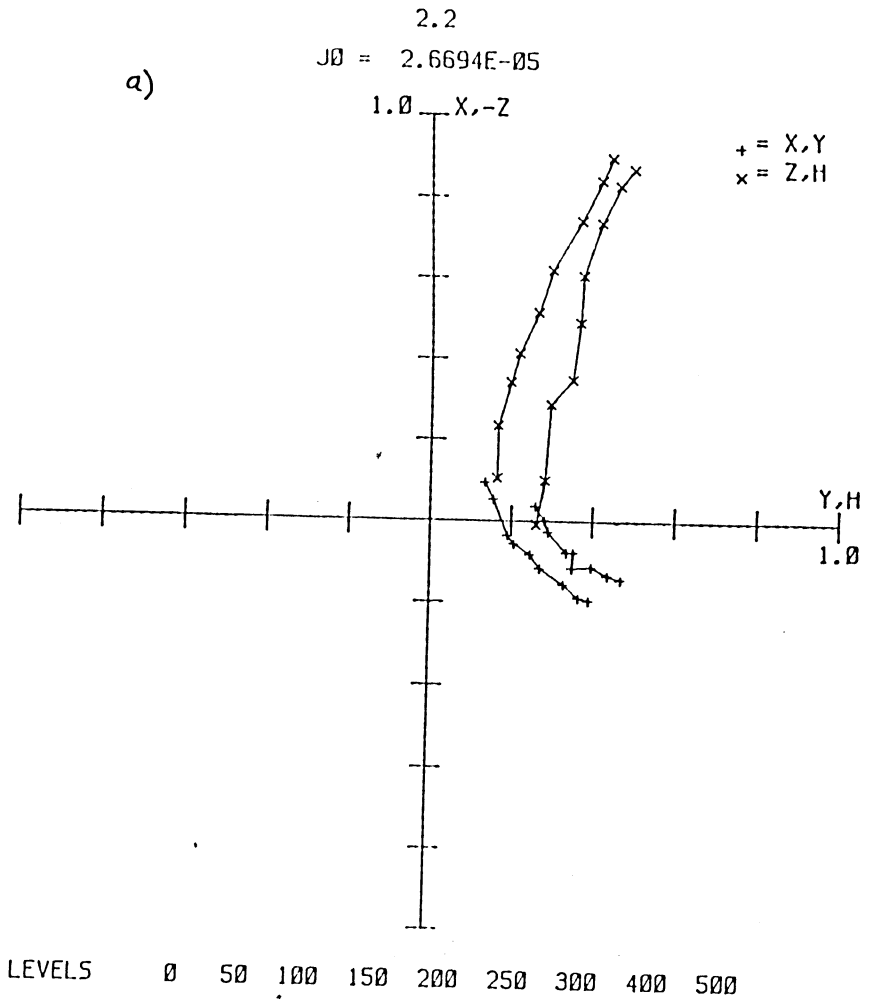
2.2
J0 = 2.6694E-05
a)
1.0
X,-Z
+ = X,Y
× = Z,H
Y,H
1.0
LEVELS 0 50 100 150 200 250 300 400 500

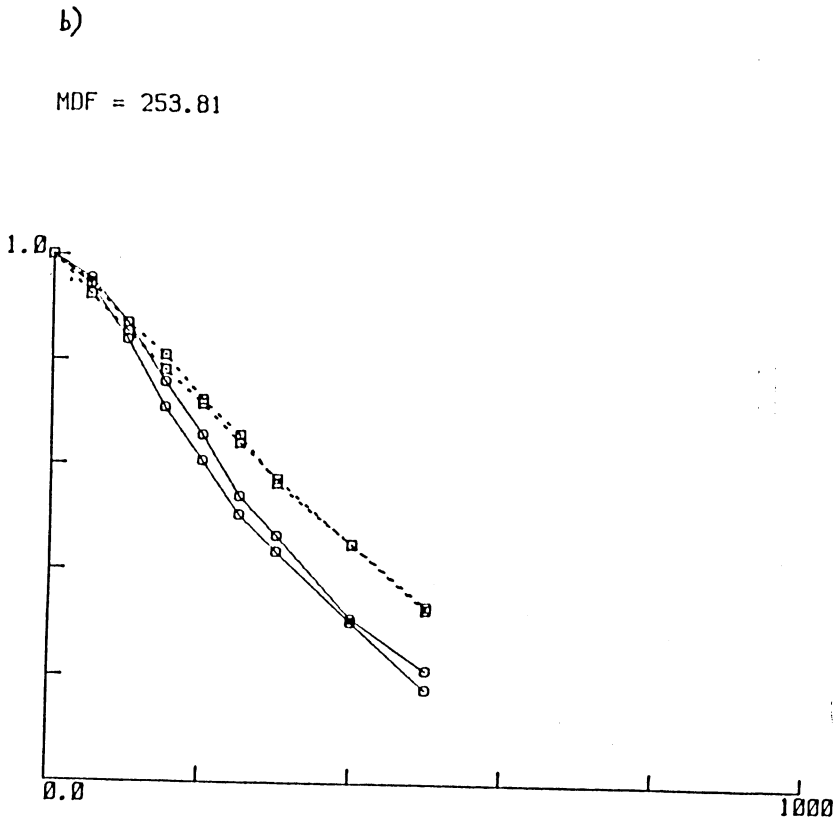
b)
MDF = 253.81
1.0
0.0
1000

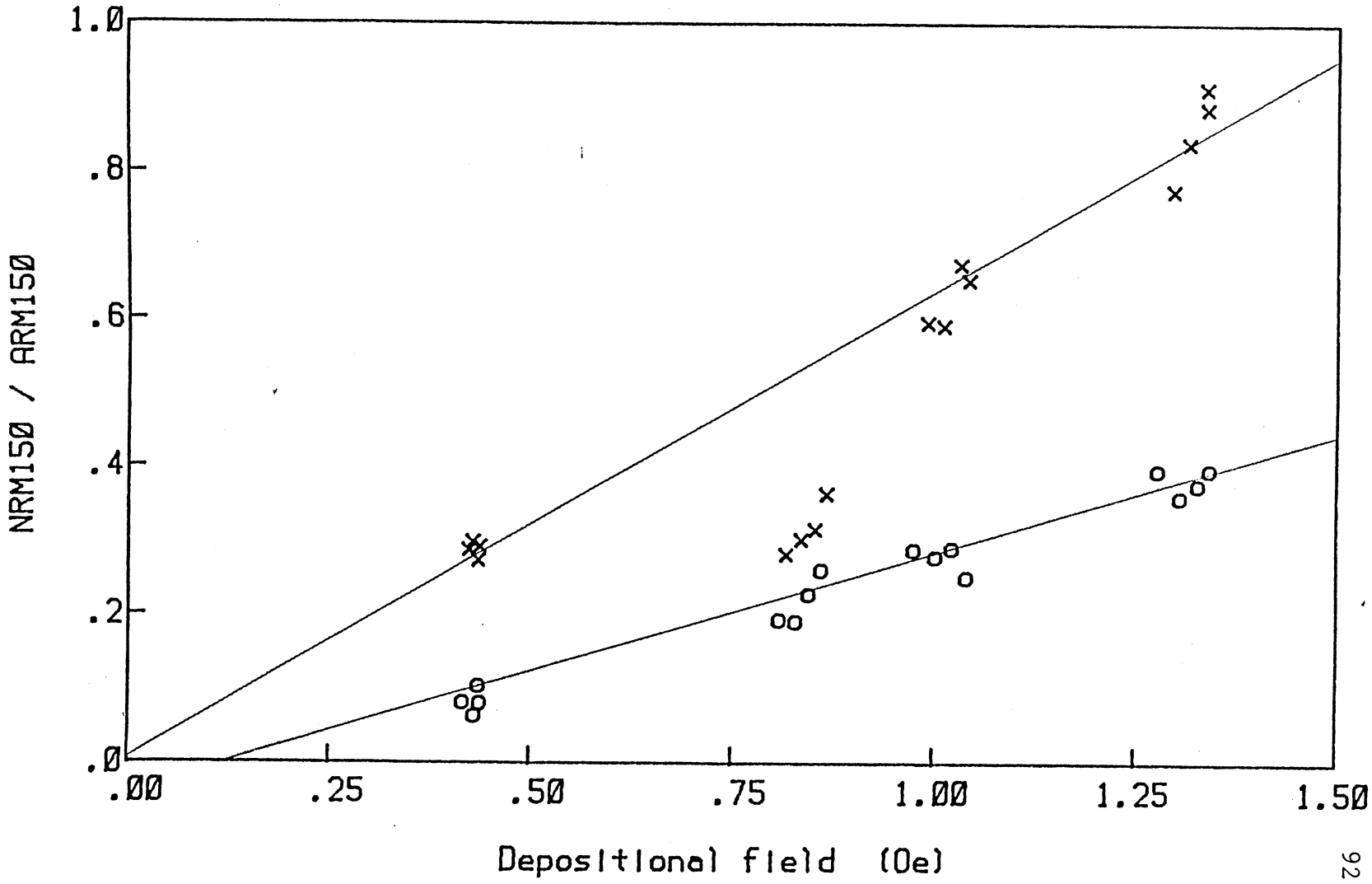
1.Ø
.8
.6
.4
.2
.Ø
NRM15Ø / ARM15Ø
.ØØ
.25
.5Ø
.75
1.ØØ
1.25
1.5Ø
Depositional field (Oe)

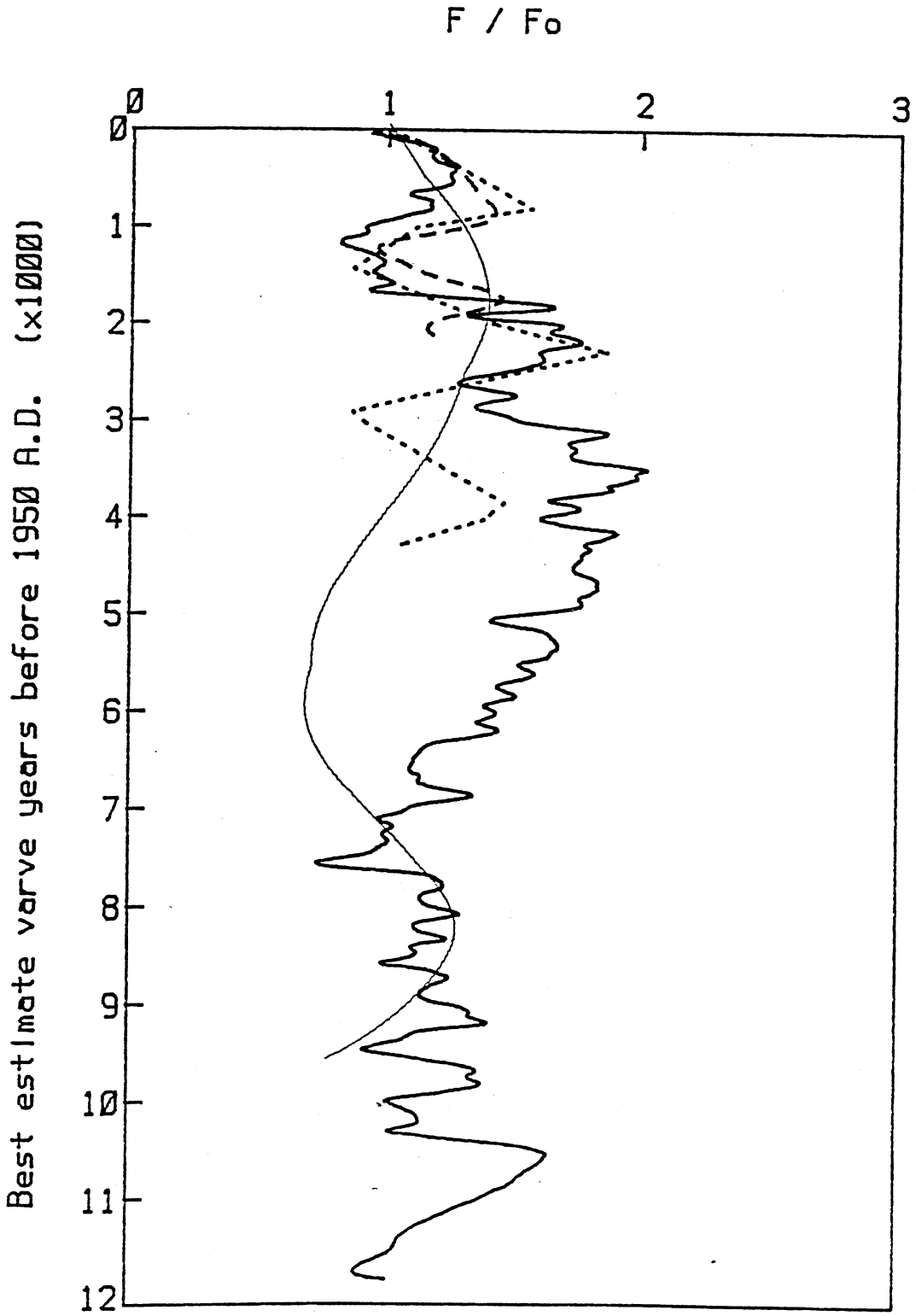
F / Fo
0
1
2
3
0
1
2
3
4
5
6
7
8
9
10
11
12
Best estImate varve years before 1950 A.D. (x1000)

Figure 55.

The locations of the peaks and troughs in the Elk Lake curve correlate well with the Champion curve, with a phase shift of about 500 years. The phase shift looks like a small eastward drift, but it is undoubtedly due to errors in the ^{14}C dating of the lava flows. The lower value of the 800 year peak in the Elk Lake data is consistent with King et al.'s evidence that the smaller grains are more sensitive to ARM, and are thus over normalized. This effect of changing grain size on ARM appears to continue down to at least 4000 years, since the Elk Lake curve is continually rising to this point while Champion's data are simply oscillating. This trend reflects the a continuing dissolution of magnetite down to at least this level, as seen in the MDF data (Figure 22). This suggests that MDF may be an appropriate parameter for removing the effect of the grain size change on the NRM/ARM ratio. What is needed is a parameter that is not dependent on sample volume or magnetite concentration, but is dependent on magnetite grain size. MDF is just such a parameter.

The MDF curve has thus been used to further normalize the NRM/ARM curve as shown in Figure 56. The rising trend has been removed from the Elk Lake data and the relative amplitudes of the first three peaks and troughs are in rough agreement with those of Champion. Full theoretical justification for this MDF normalization is certainly not available at present, but it appears that while ARM accounts for changes in magnetite concentration, the MDF corrects for the effect of grain size changes on ARM.

If the Elk Lake curve in Figure 56 is reasonably representative of the paleofield strength, several conclusions can be drawn. First, the high amplitude ocsillations of period about 1200 years, seen in the upper 4000 years, do not continue below 4000 years. This is exactly what is seen in the Elk Lake declination record (Chapter 7). Also, below 4000 years the field appears to be weaker than at present, with a gradual rise between 7000 and 4000 years ago.

C. Conclusions.

While paleointensities cannot be derived from the Elk Lake data with much confidence at the present time, several conclusions can be drawn. First, while there is strong evidence that magnetite is being dissolved with depth in the sediment column, as described by Karlin and Levi, their total disclaimer with regard to paleointensity is not warranted. The magnetic signal in Elk Lake is clearly still representative of the paleofield strength, and given a reliable calibration method, paleointensities can be derived. Second, while King et al's criteria for application of ARM normalization may be appropriate for chemically stable sediments, they are not sufficient for sediments in which magnetite is

Figure 56 (p. 97) - NRM/ARM normalized by MDF/MDFo. The solid curve plots (NRM/ARM)*(MDF/MDFo) vs. varve years, where MDFo is the MDF value at zero age. The MDF normalization appears to account for the grain size dependence of ARM because the relative amplitudes of the peaks and troughs compare well with Champion's data (dotted curve). The Champion curve is plotted as F/Fo with horizontal axis limits of 0.0 and 2.0. Without firmer theoretical justification for MDF normalization, the Elk Lake curve cannot be confidently considered to represent relative paleointensity.

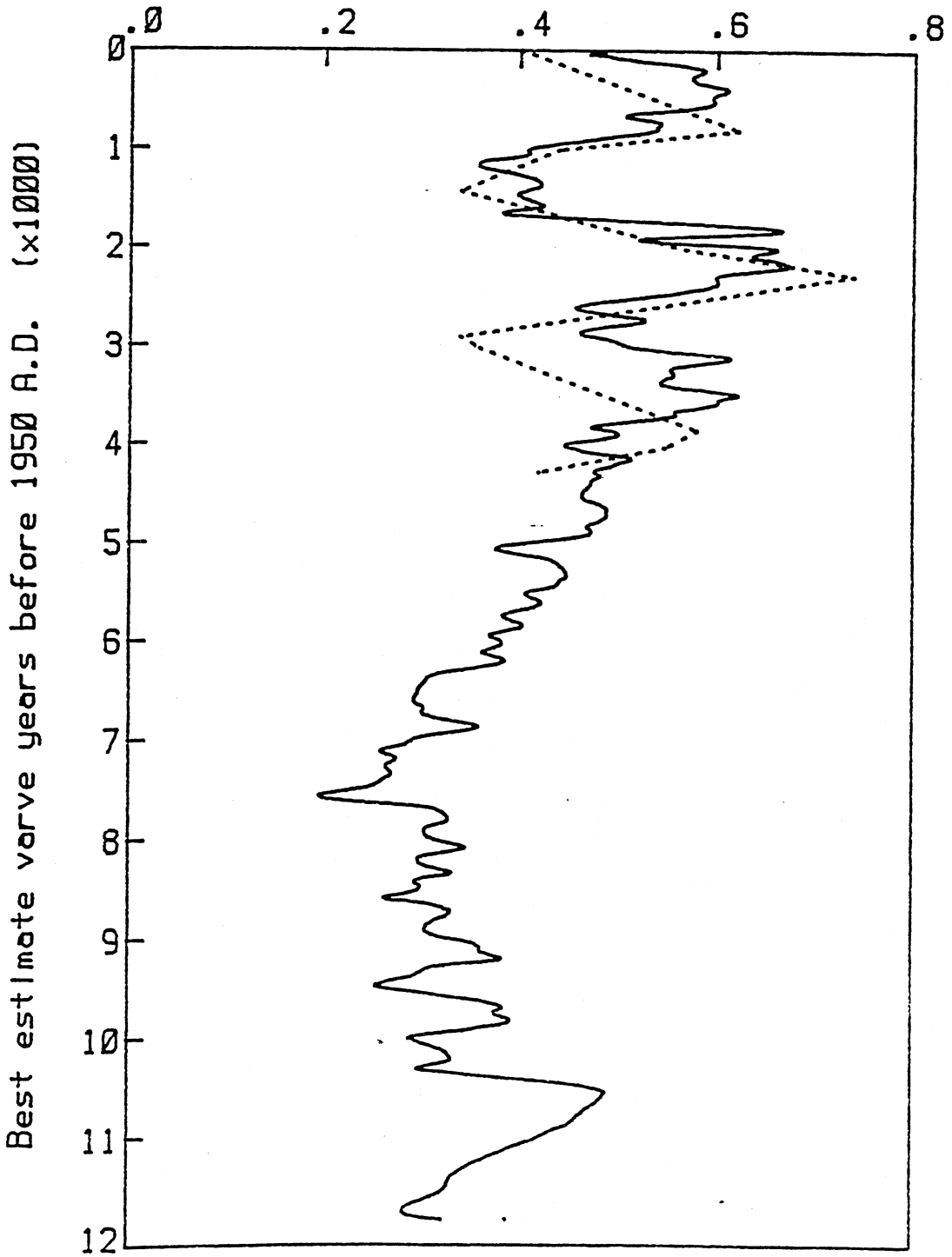
NRM/ARM * MDF/MDFo
.0
.2
.4
.6
.8
0
1
2
3
4
5
6
7
8
9
10
11
12
Best estimate varve years before 1950 A.D. (x1000)

Figure 56.

being dissolved. The sediments just below the grain size transition in Elk Lake pass the King et al. test for ARM normalization, but the continued dissolution of magnetite seen in the hysteresis and MDF properties, and evidenced in the NRM/ARM curves, are not seen in ARM or in ARM/X. Since MDF appears to better reflect gradual changes in magnetite grains size, it deserves further attention as both a grain size calibration and as a calibration for sediment paleointensities.

CHAPTER 7 : IMPLICATIONS

A. Introduction.

This chapter examines the implications and applications of the Elk Lake paleomagnetic record to four interdependent subjects: our understanding of the history of the magnetic field in central North America, the validity of the axial geocentric dipole hypothesis, fluid motions in the earth's core and dynamo models, and the nature of secular variation and the prominence of westward drift. Introductions to each of these topics will be given at the beginning of the appropriate sections. Except where specifically noted, the ages referred to are the best estimate varve ages and the limits of confidence shown are for the shape of the curves, the internal lines of Figures 35 and 41.

B. The history of the central North American magnetic field.

While few if any archeomagnetic measurements have been made on central North American samples, the large number of lakes in the region has allowed a good paleomagnetic record to be developed. Several records are available from the Great Lakes (see Mothersill, 1983 for review), but the dating of the records is so poor that they are of limited use for carefully defining the history of changes in the field. Creer and Tucholka (1982) have used the radiocarbon dates from Lund's (1981) Minnesota lake studies to date the Great Lakes records and produce paleomagnetic 'type curves' for the region. Because of the assumptions involved, it is doubtful whether the Great Lakes data add significantly to the Minnesota records.

Figure 57 plots the I and D curves and estimated paleointensity curve from Elk Lake (solid lines) with the smoothed equivalent curves from Lake St. Croix on the Minnesota - Wisconsin border (Lund and Banerjee, 1985). To first order, the curves are very similar, indicating that both lakes have faithfully recorded the changes in the magnetic field. There are differences in the shape of several features, such as the declination feature at 2500 years, which is a peak at St. Croix but a plateau at Elk Lake, and there are differences in the timing of prominent features. Above 3000 years ago, the St. Croix record lags the Elk Lake record by about 300 years. This difference is greater than the uncertainty in the varve counts at this level and is undoubtedly due to errors in the radiocarbon time scale from Lake St. Croix. The Elk Lake varve chronology significantly improves our estimation of the age of the prominent features in the upper portion of the record. Below 4000 years, the St. Croix record leads the Elk Lake record by some 350 years (seen in inclination). This

Figure 57 (p. 101) - Paleomagnetic records of Elk lake and Lake St. Croix (Lund and Banerjee, 1985). The confidence limits for inclination and declination are plotted for Elk Lake (solid lines) and Lake St. Croix on the Minnesota-Wisconsin border (dotted lines). Also plotted are the relative paleointensity estimations from the two sites (NRM/ARM for Lake St. Croix, and NRM/ARM*MDF/MDFo for Elk Lake). The Elk Lake data are plotted against the best estimate varve years while the Lake St. Croix data are radiocarbon dated. The Lake St. Croix inclination data are shifted five degrees to the right to account for the difference in latitude between the sites.

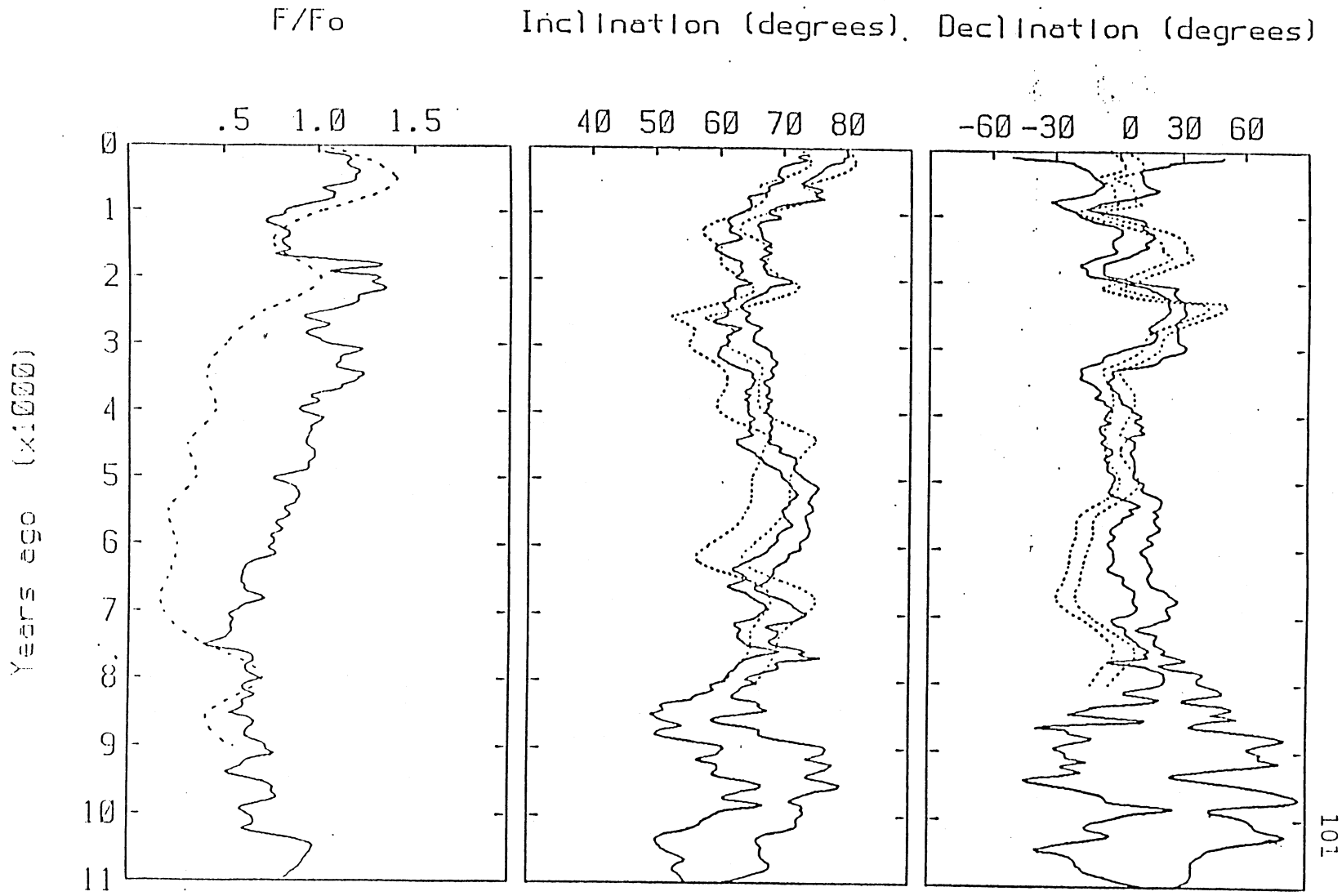
F/Fo
.5 1.0 1.5
Inclination (degrees)
40 50 60 70 80
Declination (degrees)
-60 -30 0 30 60
Years ago (x1000)
0 1 2 3 4 5 6 7 8 9 10 11

is at the limit of varve resolution at 4000 years and beyond resolution at 7000 years so the difference can be accounted for saying that too many varves have been counted in this region. But because true uncertainties in the radiocarbon time scale are difficult to estimate and may be as large or larger than those for the varve chronology, the varve ages are preferred and most of the discrepancy is again attributed to errors in the radiocarbon dates.

Except for the differences in dating, the only major difference between the records is in declination below 5000 years. While the St. Croix data is within the limits of confidence for absolute declination for the Elk Lake record (Figure 41, p. 68), the shapes of the curves (relative declination) are significantly different. For the following reasons, the Elk Lake curves are preferred. 1) The Elk Lake record is based on four cores down to 7700 years whereas the St. Croix record is based on two cores. 2) While cross-correlation methods have been used in the construction of both records, the St. Croix cores were poorly oriented azimuthally and the declination adjustments were more severe. 3) The shift in St. Croix declination at 5200 years, which produces most of the observed offset is recorded in only one core segment. 4) This portion of the St. Croix record is from a very low sedimentation rate (low resolution) section at the very bottom of the record where uncertainties are greatest (note the Elk Lake record below 8500 years). These evidences are not conclusive, so comparison with other records is appropriate. Unfortunately, at present this is not very fruitful. The Creer and Tucholka (1982) declination type curve agrees with the St. Croix curve but this is not surprising since the St. Croix data is fundamental to the type curve. The Great Lakes records (Mothersill, 1983) which were added to the St. Croix data to produce the type curve are quite variable and can be taken to support either or neither of the two curves. King (1983) has carefully derived the declination records from two lakes from the eastern U. S. which cover the time span from 5000 to 7000 years. The records from both Sandy Lake and Seneca Lake show a west to east trend from 5000 to 7000 years, in support of the Elk Lake record.

The discussion of chapter 6 makes it clear that much work remains to be done before relative paleointensity results can be reliably derived from lake sediments, but the F/Fo curves of Figure 57 (NRM/ARM for Lake St. Croix, NRM/ARM*MDF/MDFo for Elk Lake) do show common long term trends of decrease to 7000 years ago, increase to about 1000 years ago, and decrease to the present.

In summary, the Elk Lake paleomagnetic record has added significantly to our understanding of the recent changes in the magnetic field in central North America, both

the nature of the changes and their ages. The correspondence betweeen the magnetic records from different lakes speaks for the value of lake sediment paleomagnetic records in general and for the fidelity of the Elk Lake and Lake St. Croix records in particular.

C. The axial geocentric dipole hypothesis.

Foundational to much of paleomagnetism, especially that done on older rock samples, is an assumption about the nature of the geomagnetic field called the axial geocentric dipole hypothesis (McElhinny, 1973, p. 22). The hypothesis assumes that at any particular location, the magnetic field will average over time to that of a simple dipole at the center of the earth, aligned with the rotational axis. The hypothesis is particularly fundamental to plate motion reconstructions (using samples much older than those from Elk Lake of course) where average inclinations from numerous samples from a given formation are assumed to represent the axial dipole inclination at the time when the remanence was acquired. Any discrepancy between the sample mean inclination and the expected inclination at the site latitude is assumed to arise from a change in site latitude due to plate motion since the time of remanence acquisition. The critical factor is the length of time needed to average the field to that of a centered axial dipole. If the axial geocentric dipole hypothesis is not valid over the time spanned by the set of paleomagnetic samples averaged, then the plate reconstruction may be in error. There is theoretical support for the axial dipole hypothesis in that the field generating dynamo is thought to be strongly dependent on the Coriolis force, which is associated with the rotational axis. There is also circumstantial support for the hypothesis from the success of plate reconstruction efforts. However, recent work indicates that inclinations different from that of the axial dipole may persist for significant periods of time.

The Elk Lake data, being continuous and very well dated, can be used to check the axial geocentric dipole hypothesis in a limited sense. One limitation is the 12,000 year record, which is very short compared to the time scale of plate motions. This is not as serious a limitation as it might seem, however, since the assumption of an axial dipole average inclination is often made for time periods of a few thousands of years (McElhinny, 1973, p. 23). A greater limitation is presented by the question of whether the last 12,000 years of magnetic field history are 'normal' with respect to the longer history of the field. The Elk Lake record would not be representative if the worldwide field has been 'abnormal' for the last 12,000 years, or if there are unusual features in the Elk Lake local area.

With these limitations in mind, the time stationarity of the Elk Lake record can be

examined. For the axial geocentric dipole hypothesis to be valid for the past 12,000 years, the I and D values should average to the dipole values. Figures 58 and 59 replot the smoothed I and D curves vs. the best estimate varve chronology. Also plotted are the I and D values expected for an axial geocentric dipole, 65.1° and 0°, respectively. The average relative inclination for the 12,000 year record is 66.2 ± 3.4°, which is not significantly different from the axial dipole value. Over the last 8500 years where the record is better constrained, the average inclination is 67.7 ± 2.5°, just barely significantly different from the axial dipole value. When confidence limits for the absolute inclination average (Figure 35) are calculated, the significance disappears. The lack of difference between the Elk Lake average inclination and the expected axial dipole inclination suggests that the axial geocentric dipole hypothesis is valid for periods greater than 12,000 years. It is also evidence for an absence of inclination errors in the depositional process. It is noteworthy that the average inclination value is greater than the axial dipole average because other workers have reported shallower than expected average inclinations (Liddecoat and Lund,1983). It has been argued (Liddecoat and Lund, 1983) that the common occurrance of shallower than expected inclinations reflects a true characteristic of the earth's field in recent times, but the Elk Lake data does not support this contention. Possible explanations for the discrepancy include 1) a systematic error in the Elk Lake inclination data, 2) systematic errors in the other records and 3) underestimated uncertainties for the other records. Given the carefully calculated uncertainties for the Elk Lake record, which is qualitatively better than many other records, the third possibility deserves further attention.

The average declination value for the entire 12,000 year record is 9.8 ± 13.8°. For the last 8500 years, the average declination is 5.9 ± 8.3°. Neither of these is significantly different from the axial dipole value of 0°.

An additional requirement for the validity of the axial geocentric dipole hypothesis, is that there should be no long term trends in the records. This is not the case at Elk Lake as is shown in Figure 60 which plots the central I and D curves, smoothed with a sliding triangular window with a 3000 year bandwidth. Any features in the record of duration less than about 3000 years have thus been filtered out of the records. Also plotted for reference is the MDF normalized paleointensity estimation curve (Figure 56, p. 97), also smoothed with a 3000 year window. The inclination and declination records clearly indicate the presence of long term trends. Modeling of the curves with drifting dipoles suggests a period of at least 28,000 years, if the trends represent real periodic features in the magnetic field. Without additional evidence for the long term trends, the possibility of

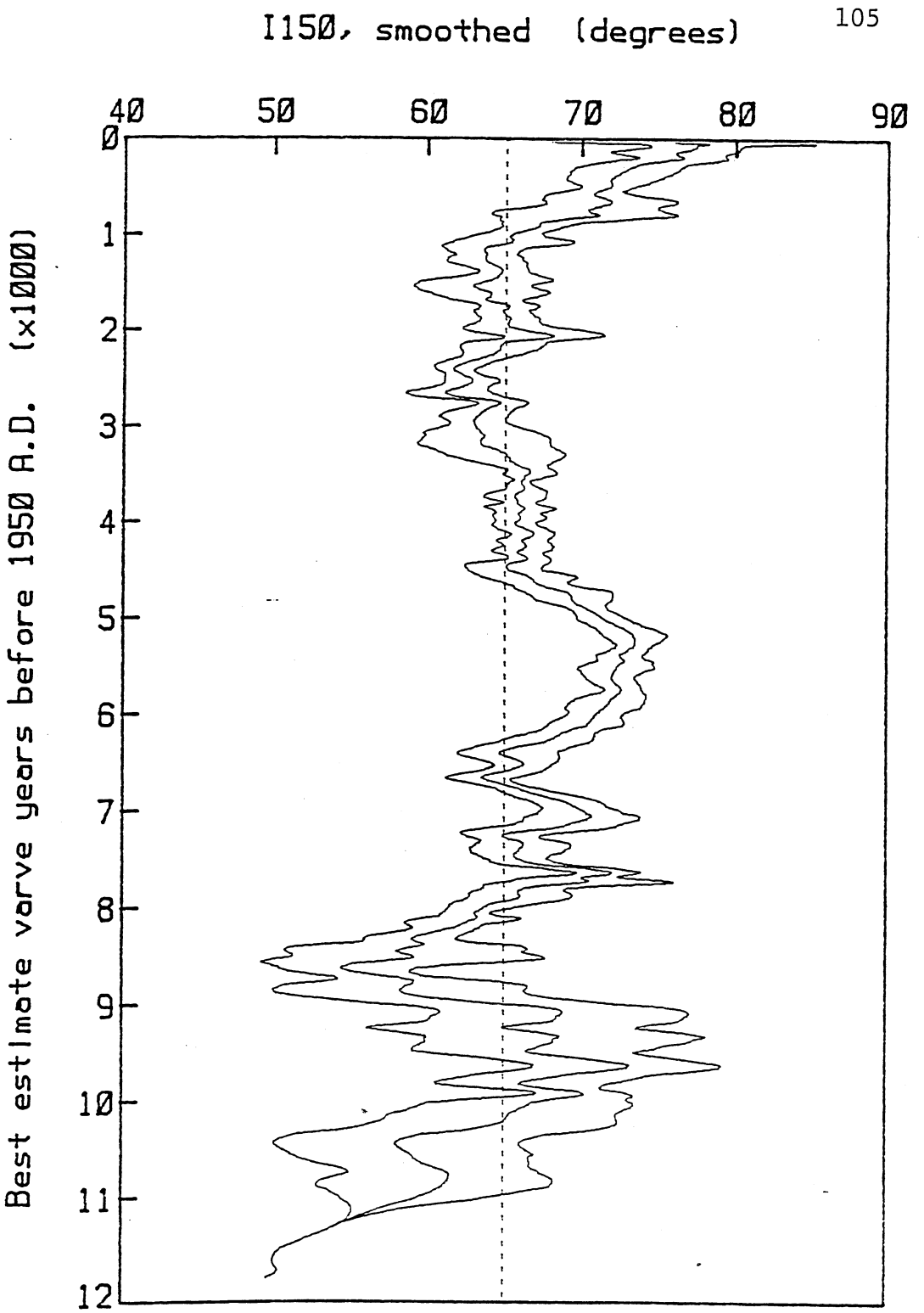

Figure 58 - Elk Lake smoothed inclination vs. best estimate varve years. The dashed line is the expected axial geocentric dipole inclination of 65.1° for the site latitude.

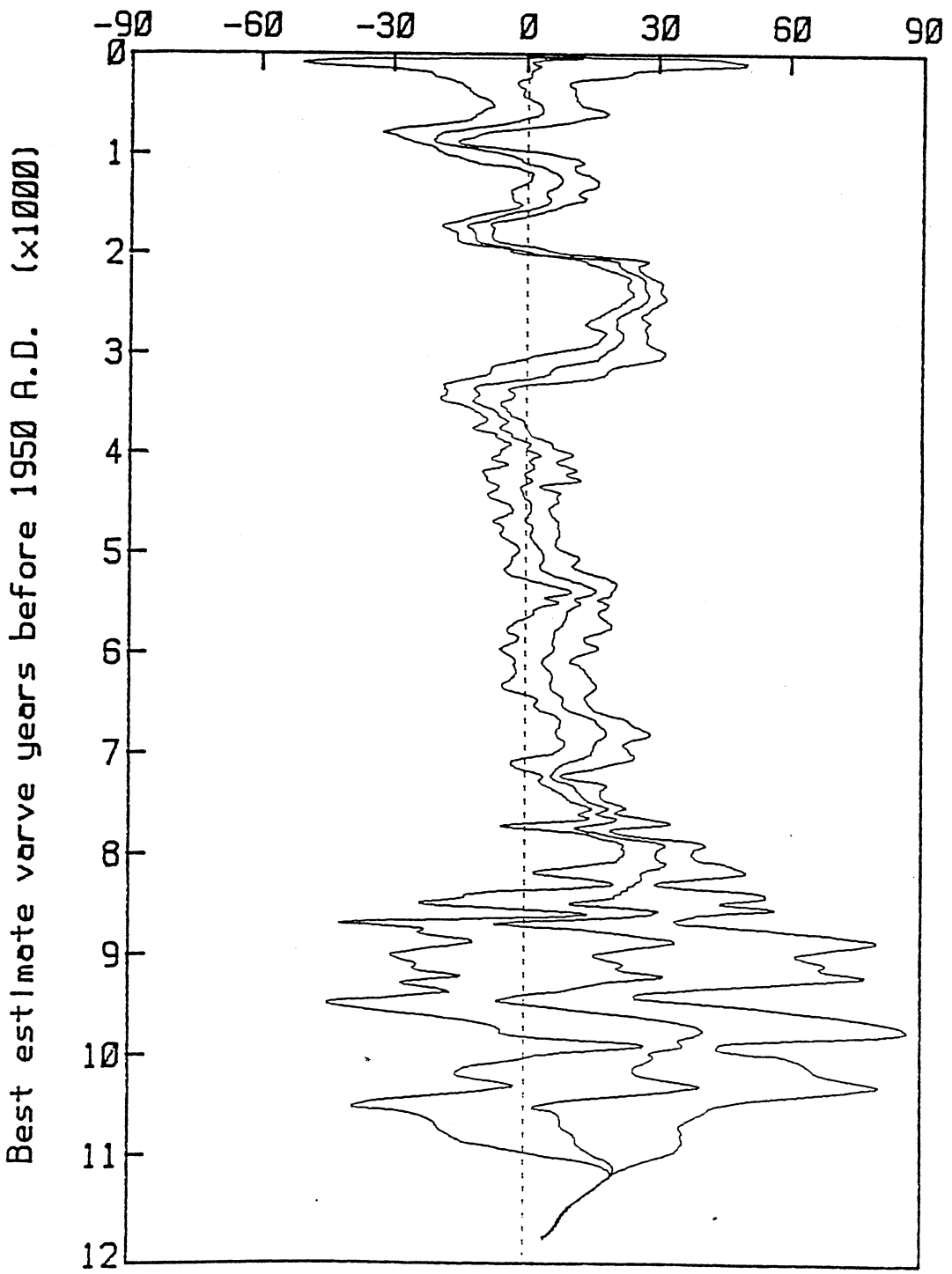

Figure 59 - Elk Lake smoothed declination vs. best estimate varve years. The dashed line is the expected axial geocentric dipole declination of 0°.

Figure 60 (p. 108) - Elk Lake low frequency trends. Plotted are the inclination, declination, and relative paleointensity estimate curves from Elk Lake, smoothed using a triangular window of 3000 year bandwidth. The high frequency components have been filtered out, leaving only the long term trends in the data.

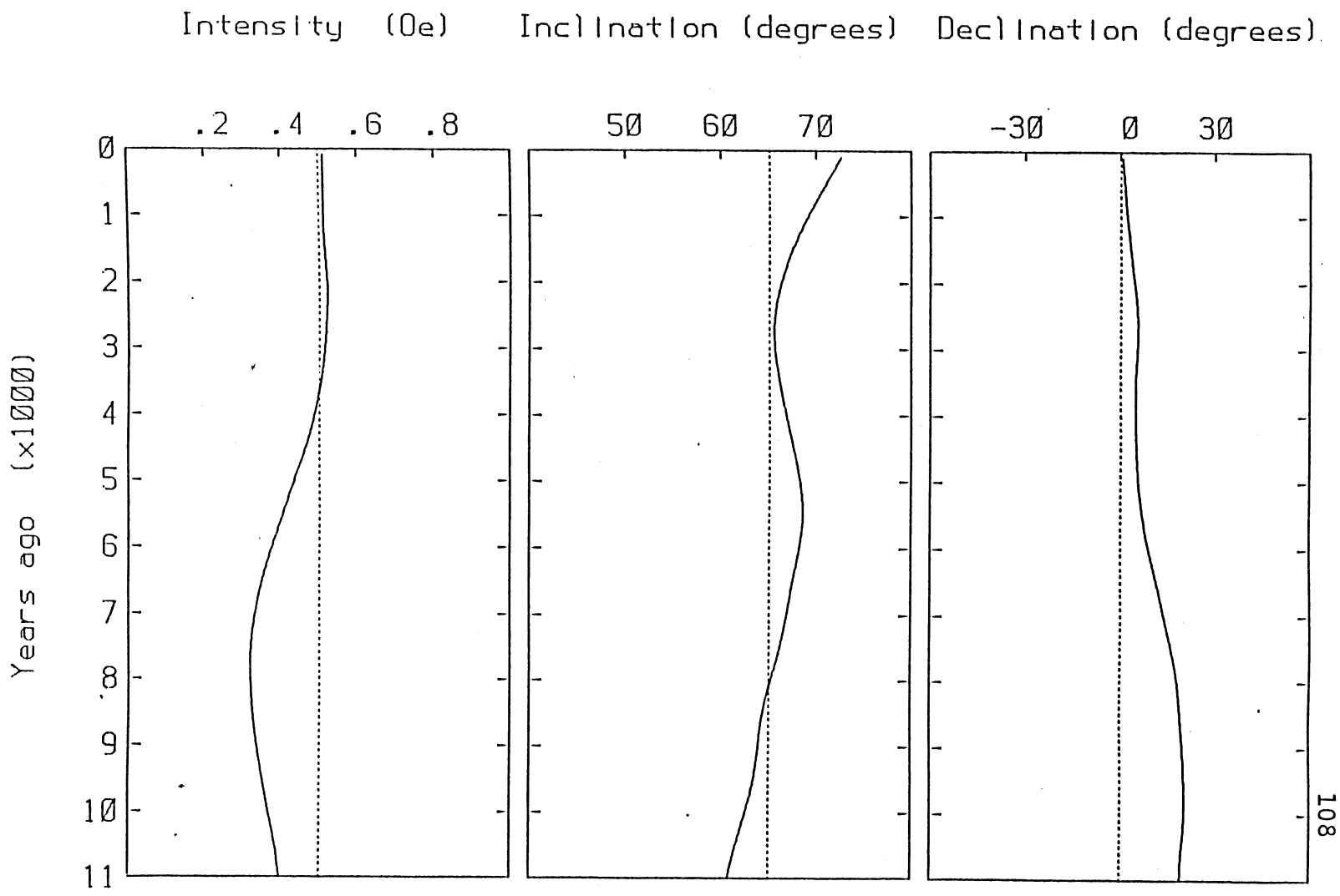
Intensity (Oe)
Inclination (degrees)
Declination (degrees)
.2
.4
.6
.8
50
60
70
-30
0
30
0
1
2
3
4
5
6
7
8
9
10
11
Years ago (x1000)

systematic errors in the Elk Lake record remains, but the record, as it stands, suggests that the field must be averaged over significantly more than 12,000 years for the axial geocentric dipole hypothesis to be valid. If this is confirmed by future work, greater care will be required in interpreting paleomagnetic results from older hard rock samples.

Additional information on the stationarity of the Elk Lake record can be obtained through periodogram or Fourier analysis. A time series of uniform sampling rate was constructed by interpolating the I and D values from Figures 57 and 58 at thirty years intervals. The thirty year sampling rate is conservative with respect to the average subsampling interval (Figure 10, p. 19), but is appropriate because 25% of the sampled pairs have been eliminated and the actual sampling interval for the stacked data is variable. Generally, any periodic components of the field with periods less than 30 years are better studied using historical rather than paleomagnetic records. Fast Fourier transform (FFT) methods were used to describe the uniform sampling rate time series as a sum of sinusoidal components of various periods and amplitudes. The squares of the Fourier transform components are proportional to the spectral power density, revealing which periodic components contribute most to the variation in the magnetic signal.

Figure 61 plots the power density spectrum or periodogram for the raw inclination time series. The range of frequencies runs from zero at the left margin to 100 picohertz at the right margin, or in terms of period, ∞ at the left to 300 years at the right. Because it is taken from the raw inclination data, this periodogram is of limited validity and usefulness, but it demonstrates that an overwhelming percentage of the spectral power is contained in the very lowest frequencies ($a=\infty$, b=15,360 yr, c=7680 yr, d=5120 yr), confirming that the Elk Lake time series is not stationary within the 12,000 year span of the record. The declination periodogram is very similar to that for inclination. More useful versions of the periodograms (filtered and detrended) will be used in the next section.

D. Core fluid motions and the origin of the secular variation.

A great deal of effort has been made over the last few decades to describe the fluid motions in the core which give rise to the magnetic field and its secular variation. Relatively little progress has been made because of the difficulty of the subject and because of the non-uniqueness of the solutions. A first step would be to constrain the number of possible fluid motion types by using what we know about the magnetic field and its history. This is not an easy problem either, but some progress has been made lately. Several workers (see Gubbins, 1982 for a review) have made progress by making the simplifying

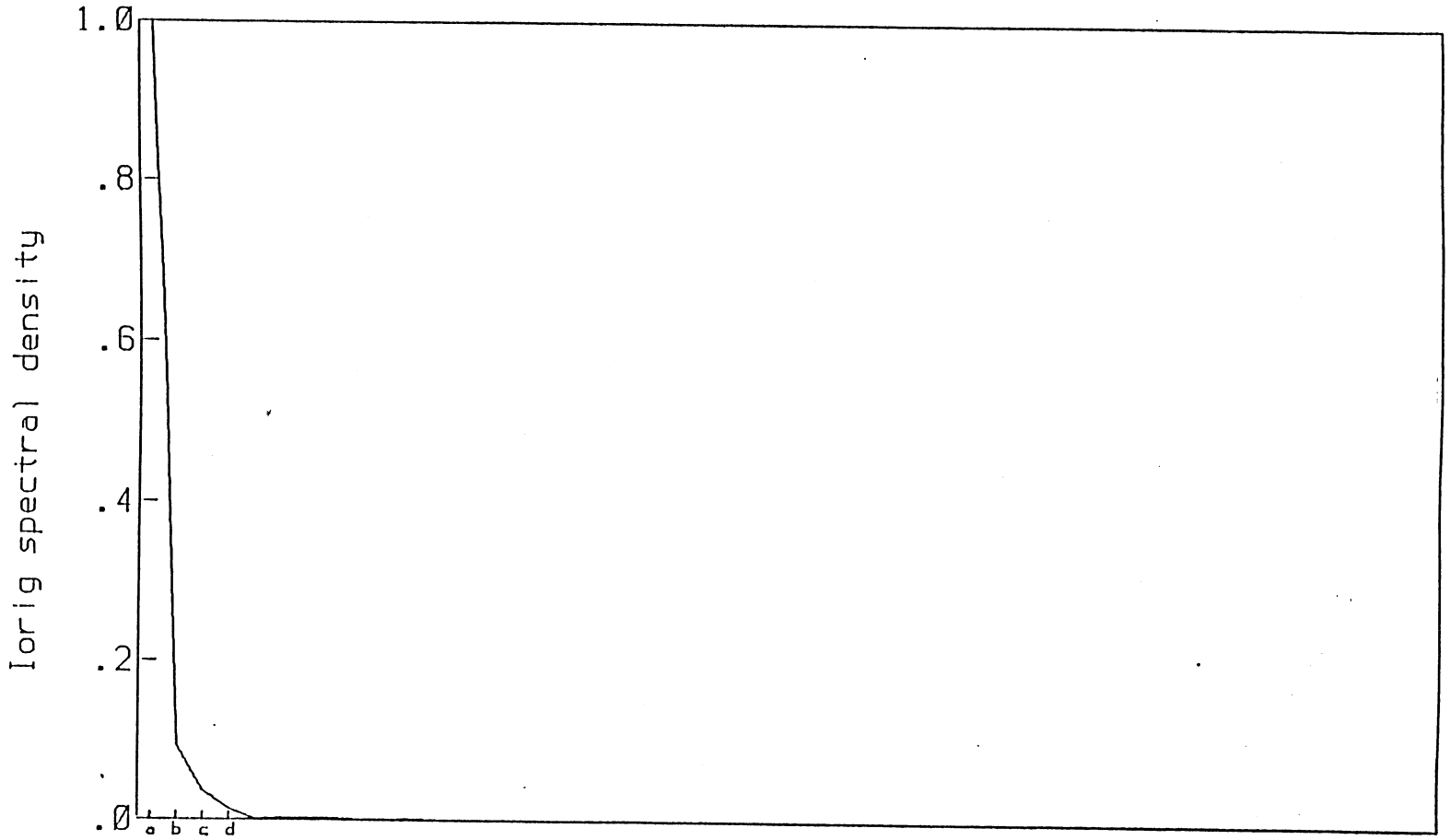

Figure 61 - Power density spectrum for unfiltered inclination (I original). The horizontal axis runs from zero Hz (∞ period) at the left margin to 100 picoHz (300 years period) at the right margin. The low frequency components of interest are labeled from a to d and represent the following periods: a) , b) 15360 yrs, c) 7680 yrs, d) 5120 yrs.

assumption that the core of the earth is infinitely conducting. For periods of time for which this is a valid approximation, the magnetic field lines are 'frozen' into the core fluid. Thus, any changes in the field at the surface must reflect fluid motions in the core. Since only the outermost portion of an infinitely conducting fluid can affect the external field, the proposed source of secular variation is eddie currents drifting along at the core-mantle boundary. The presence of eddies implies topographic irregularities on the core-mantle boundary, or some other mechanical source for the eddies. There are a number of variants on this basic theme which make up a family of possible core motion models which can be evaluated using magnetic observations.

An alternate proposal, quite different from the first, has been put forward by Olson (1985 and personal communication). Following Parker's (1967) work on the solar dynamo, Olson has proposed that secular variation in the magnetic field may be due to dynamo waves. The dynamo waves are propagating magnetic disturbances which can arise given the combination of small-scale turbulence (convection) and large-scale shear flow. The dynamo wave model differs from the frozen flux model in that the magnetic disturbances are not intimately associated with core fluid motions. The shear and turbulence provide a necessary environment for the dynamo waves, but there is no direct mapping of the secular variation to fluid motions. Additionally, the dynamo wave model does not require a physical or topographic source at the core mantle boundary.

Choosing between these models on the basis of magnetic records is not yet possible, but a beginning can be made by examining the power spectra of the Elk Lake record. It is expected that eddies produced by turbulence at the core-mantle boundary would be of random and varying size, giving rise to a continuous power spectrum. Dynamo waves, on the other hand, could well have charateristic rates of propagation, giving rise to a discrete (line) frequency spectrum.

The lowest frequencies were filtered out of the Elk Lake time series by subtracting the I and D means and the long term trends of Figure 59, leaving only the components which can be resolved within the record. The ends of the detrended time series were 10% cosine tapered to make the time series smoothly varying at the ends. The periodogram for the resultant time series in inclination is plotted in Figure 62. With the low frequency components removed, the features in the rest of the record become visible. The horizontal axis runs from a period of ∞ at the left hand side to 100 years at the right. The prominent peaks in the periodogram are labeled a through k. The periods associated with these peaks are listed in the figure caption. Figure 63 shows the declination power

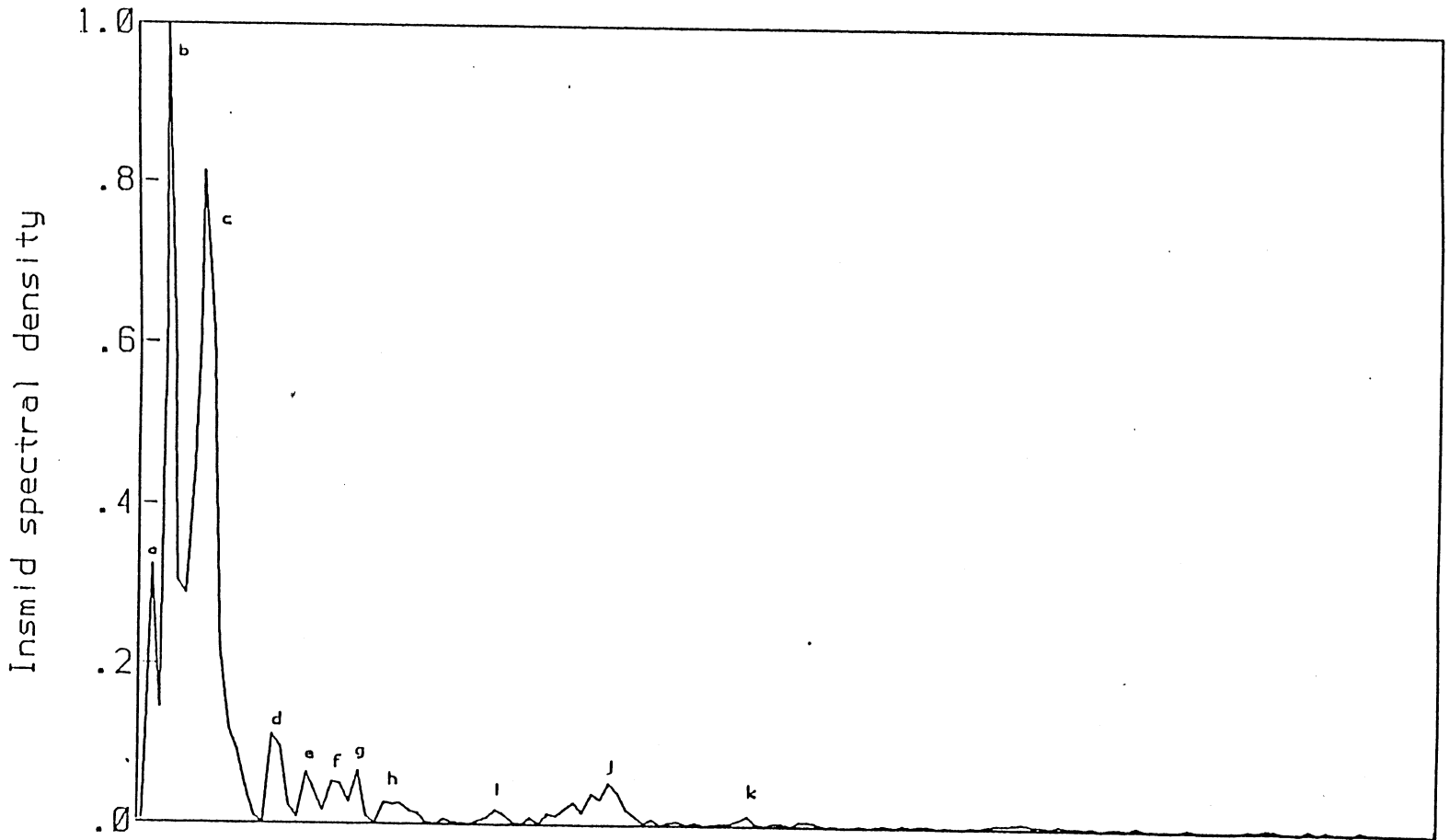

Figure 62 - Inclination periodogram. The power spectrum is plotted for the Elk Lake inclination record. The horizontal axis runs from zero Hz (∞ period) at the left to 300 picoHz (100 yrs) at the right. The prominant spectral peaks, labeled a through k, have the following associated periods: a) 15360 yrs, b) 5120 yrs, c) 2194 yrs, d) 1024 yrs, e) 808 yrs, f) 698 yrs, g) 614, h) 530 yrs, i) 375 yrs, j) 284 yrs, k) 219 yrs.

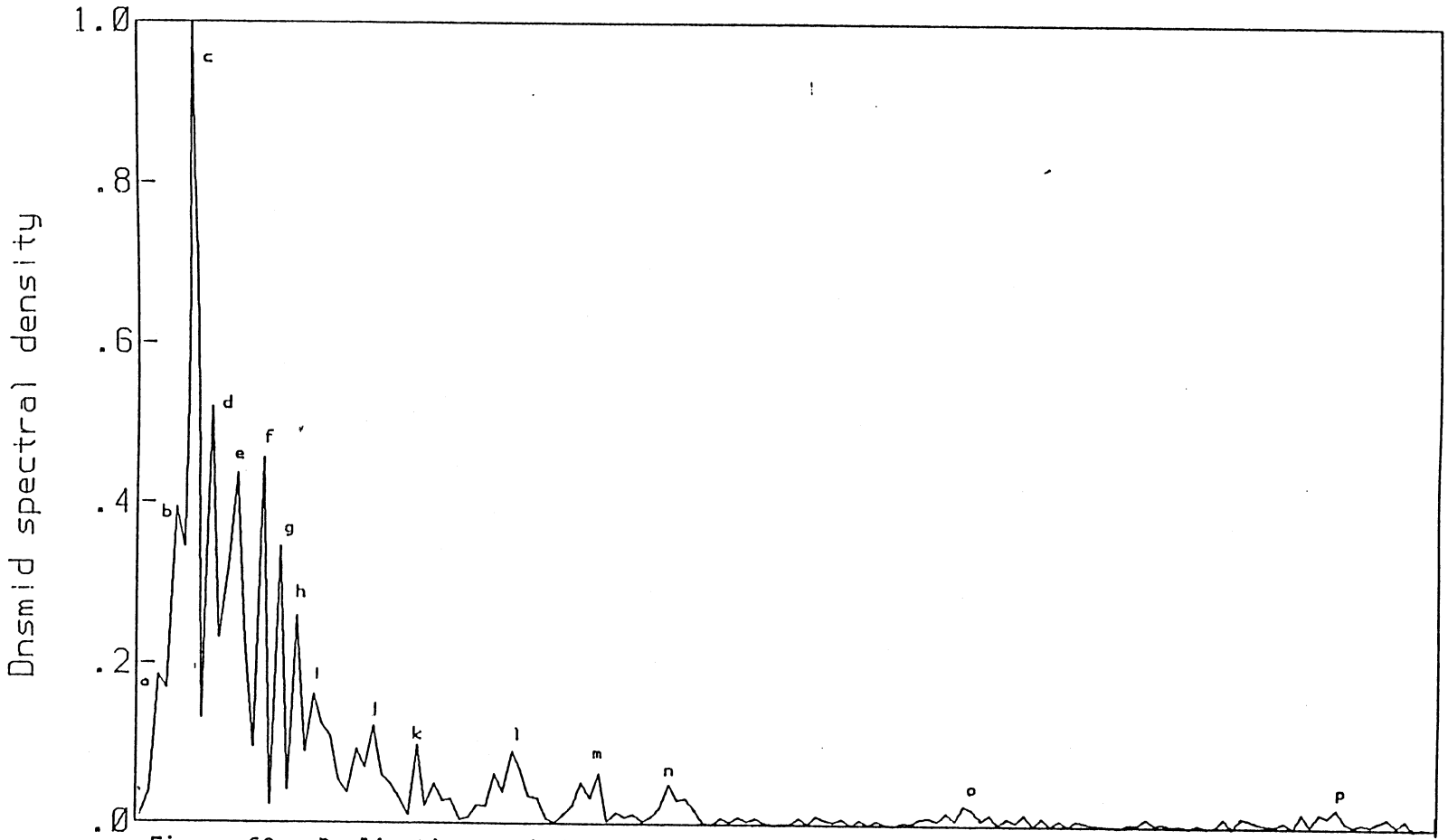

Figure 63 - Declination periodogram. The power spectrum is plotted for the declination record. The horizontal axis runs from zero Hz (∞ period) at the left, to 300 picoHz (100 yrs) at the right. The prominant spectral peaks, labeled a through p, have the following associated periods: a) 7680 yrs, b) 3840 yrs, c) 2560 yrs, d) 1920 yrs, e) 1396 yrs, f) 1097 yrs, g) 960, h) 853 yrs, i) 768 yrs, j) 569 yrs, k) 480 yrs, l) 357 yrs, m) 290 yrs, n) 252 yrs, o) 162 yrs, p) 111 yrs.

spectrum, derived in the same way.

The inclination and declination power spectra are similar in several respects. As seen for the raw periodogram, most of the spectral power is contained in the lower frequencies. While the power is spread between a wide range of periods, there is evidence for distinct periodic components in both I and D. Some of the periods may be multiples of others (several distinct features with the same period, or a single feature recorded more than once as it travels around the globe), but not all of the periods can be accounted for in this way, especially in declination. Thus, while the spectra are not fully continuous as would be expected from the frozen flux model, neither are they made up of a few eigenfrequencies which would strongly indicate magnetic wave propagation. Lund and Banerjee's (1985) analysis of the Lake St. Croix spectra is much more suggestive of discrete frequencies. Similar analysis of other records may lead to stronger support for either the frozen flux or the dynamo wave model.

E. Westward drift.

The magnetic field of the earth can conveniently be divided into a large centered dipole and several smaller positive and negative features collectively called the non-dipole field. The non-dipole field can easily be modeled using radial or eccentric dipoles (Alldredge and Stearns, 1969). Yukutake (1962) and Yukutake and Tachinaka (1968,1969) have analyzed the historical magnetic field in terms of non-dipole features which appear to stand still and others which appear to drift westward at a few tenths of a degree per year. While the division of the earth's field into dipole and non-dipole components may not have true physical significance, westward drift of various portions of the field is often sited as a fundamental property of the earth's field. An important question is whether westward drift is truly characteristic of the field over long periods of time, or whether it is a passing phenomenon. If westward drift is shown to be much more prominent than eastward (or north or south) drift, important constraints will be placed on the nature of the field and possibly on the core fluid motions that produce the secular variation.

Runcorn (1959) observed that westward drifting non-dipole features should produce a clockwise rotation in the position of the VGP (virtual geomagnetic pole, the pole position on the earth's surface for which a centered dipole would produce the observed I and D). Eastward drift on the other hand, should produce counterclockwise rotation of the VGP. Dodson (1979) details exceptions to the rule, but in general, it is valid. Figure 64

shows the observed rotation of the VGP for the Elk Lake record, along with that from Lake St. Croix (Lund and Banerjee, 1985). The two lakes show similar rotation in the upper 5000 years but disagree below 5000 years where the declination records diverge. Karlin and Levi (1985b) report counterclockwise rotation in Oregon sediment records from 300 to 1000 years ago and from 2600 to 3100 years ago Turner and Thompson (1979) report counterclockwise rotations from 600 to 1100 years ago in British sediments. The Elk Lake record shows little preference for clockwise rotation over counterclockwise, and counterclockwise rotation is clearly common during the past 1000 years or so. This implies significant eastward drift, which is unexpected given the evidence for westward drift in the historical field. Further work in computer modeling of secular variation is warrented to determine just what sort of VGP rotations are produced by possible secular variation models.

A more direct method for testing for westward drift is to compare the Elk Lake record with other records widely separated from it at about the same latitude. Records of high enough quality at the right latitude are not common, but there are a few. Figure 65 shows the archeomagnetic data from Bulgaria compiled by Kovacheva (1983). In Figure 66, the Bulgarian data is plotted along with the Elk Lake curves, with the Bulgarian data shifted up by 620 years. The correlation is very good between the declination curves and remarkable between the Bulgarian absolute paleointensity curve and the Elk Lake relative paleointensity approximation. This lends encouraging support for the relative paleointensity method developed in chapter 6. The correlation is not so convincing between the inclination records, especially at 5000 years where the curves diverge, but taken together is quite good considering the sites are separated by 115° of longitude. The phase shift of 620 years implies a western drift rate of 0.19 °/yr.

Figure 67 plots the archeomagnetic record from Paris, France as compiled by Thellier (1981). In Figure 68, Thellier's data is plotted against the Elk Lake curves, with the Paris data shifted up 475 years. The implied westward drift is about 0.2 °/yr which is very similar to that seen in the Bulgarian data. It must be noted, however, that an equally good correlation can be made by shifting the Paris data **down** 380 years implying an eastward drift of 0.25 °/yr. Such a drift seems very unlikely given the Bulgarian data, but it points out the danger of comparing records of short (< 5000 years) duration with one another.

The Bulgarian data, together with the most reasonable interpretation of the Paris data, indicate that a number of prominent features of the magnetic field have been drifting westward at a rate of about 0.2 °/yr for at least the last 8000 years. 0.2 °/yr translates into a

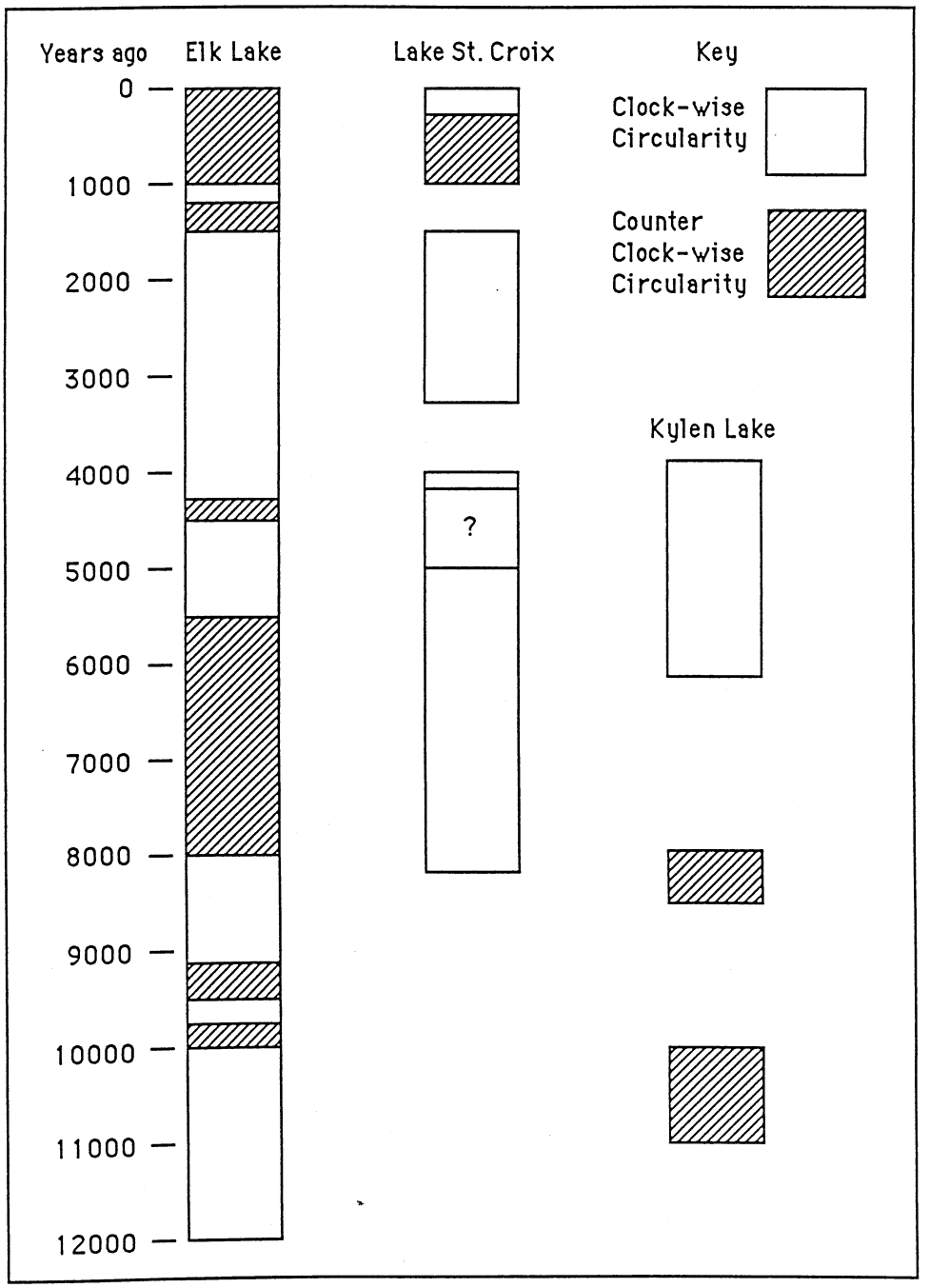

Figure 64 - VGP Circularity. The direction of looping of the VGP is plotted for the Elk Lake record and for the record from Lake St. Croix. Clockwise rotation is shown in white, while counterclockwise rotation is lined. The VGP rotations agree where the magnetic records agree and give evidence for eastward drift.

Figure 65 (p. 118) - Bulgarian archeomagnetic data. The archeomagnetic data from Bulgaria, compiled by Kovacheva (1983) are plotted along with smooth curves derived using a triangular window of 400 yr bandwidth.

Figure 66 (p. 119) - Bulgarian archeomagnetic data with Elk Lake data. The Bulgarian data from Figure 65 (circles and dotted line) are plotted along with the Elk Lake data (solid lines). The Bulgarian data are phase shifted up (younger) 620 years to account for westward drift of the magnetic record between the sites. The Bulgarian mean inclination is lower because of the difference in latitude between the sites.

Figure 67 (p. 120) - Paris archeomagnetic data. The smoothed archeomagnetic data from Paris (Thellier, 1981) are plotted against age.

Figure 68 (p. 121) - Paris archeomagnetic data with Elk Lake data. The Paris archeomagnetic data from Figure 67 (dashed curves) are plotted along with the Elk Lake data (solid lines). The Paris curves are phase shifted up (younger) 475 years to account for westward drift of the magnetic field between the sites.

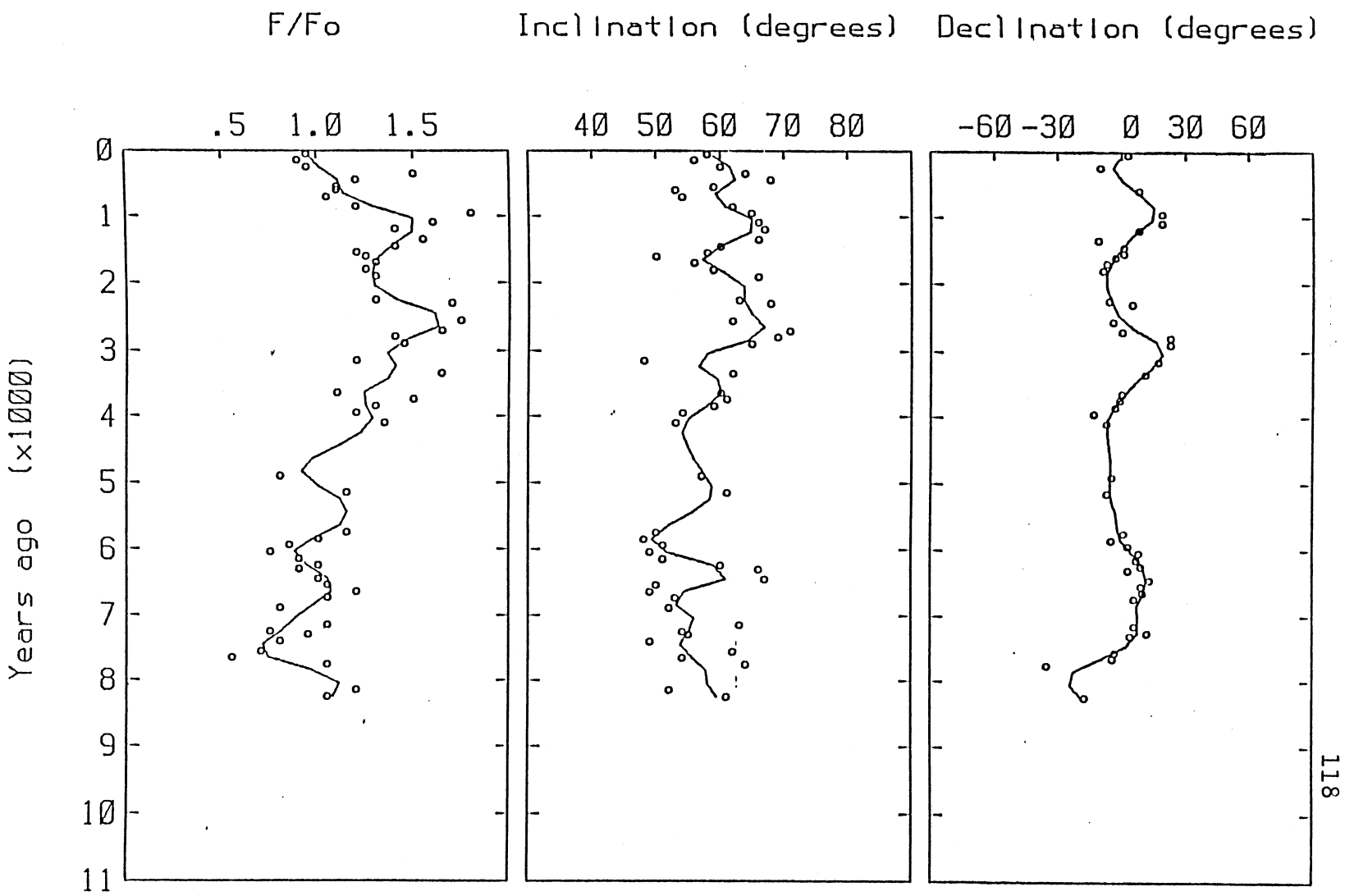
F/Fo
Inclination (degrees)
Declination (degrees)
.5 1.0 1.5
40 50 60 70 80
-60 -30 0 30 60
0
1
2
3
4
5
6
7
8
9
10
11
Years ago (x1000)

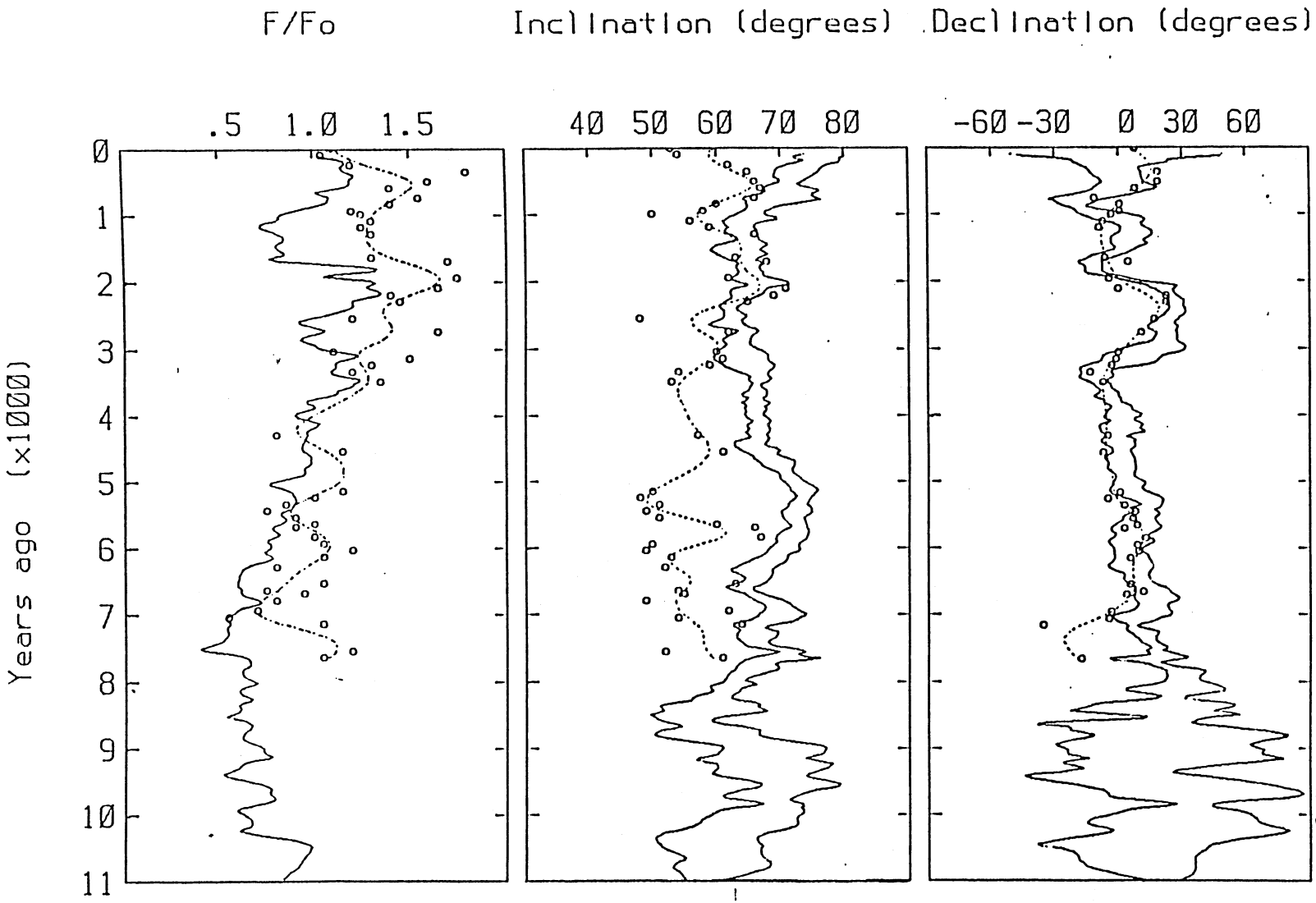
F/Fo
.5 1.0 1.5
Inclination (degrees)
40 50 60 70 80
Declination (degrees)
-60 -30 0 30 60
Years ago (x1000)
0
1
2
3
4
5
6
7
8
9
10
11

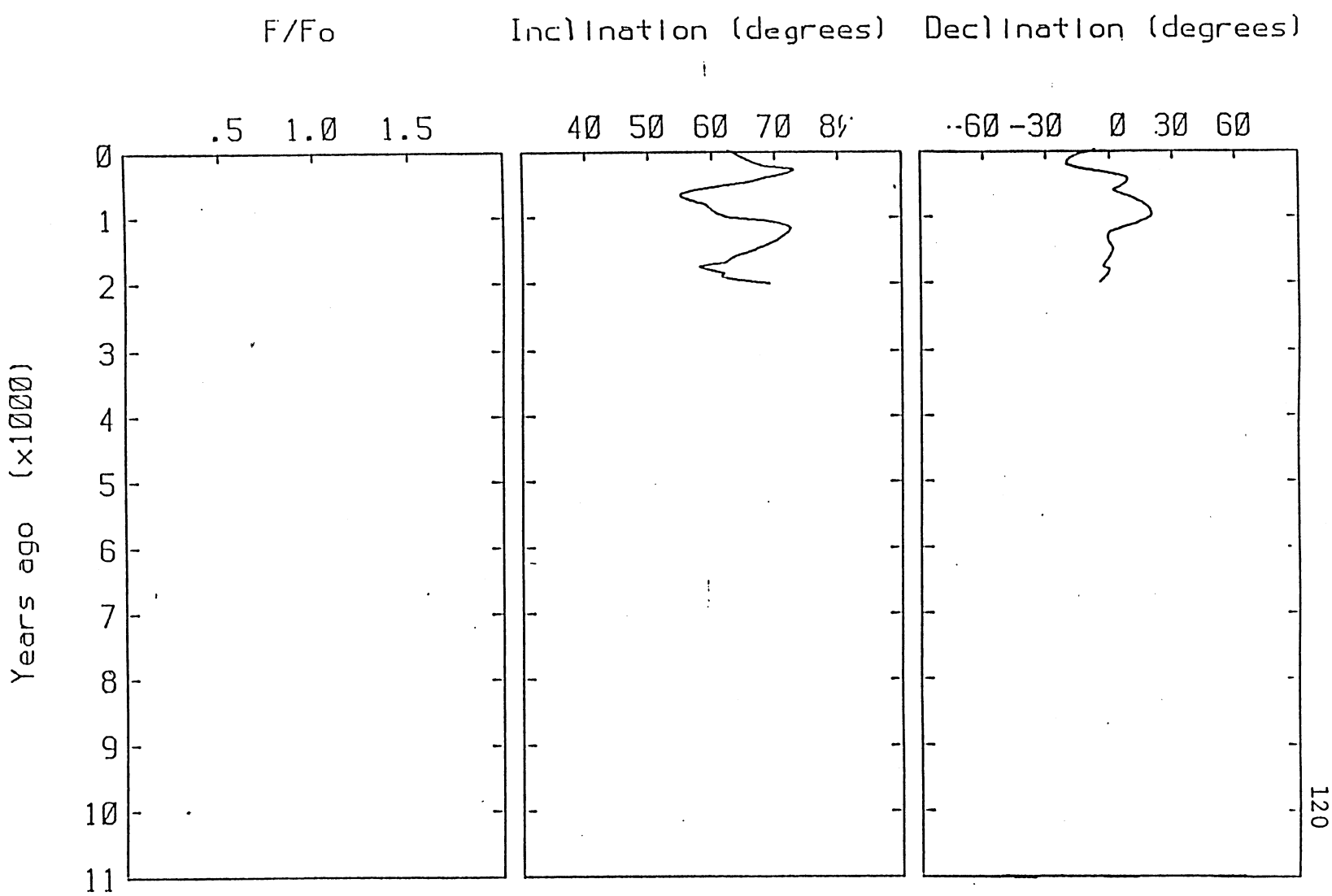
F/Fo
Inclination (degrees)
Declination (degrees)
.5
1.0
1.5
40
50
60
70
80
-60
-30
0
30
60
Years ago (x1000)
0
1
2
3
4
5
6
7
8
9
10
11
120

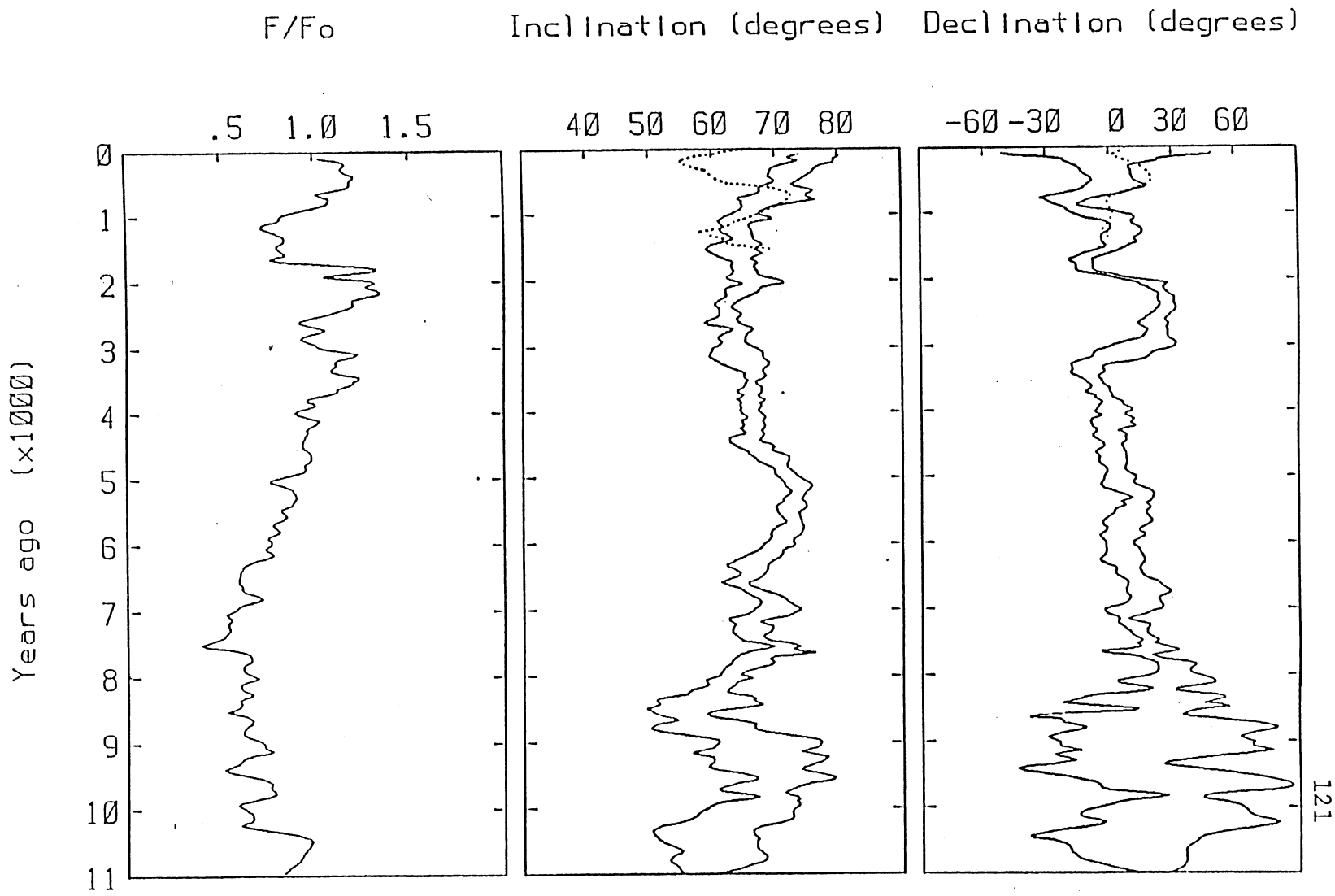
F/Fo
Inclination (degrees)
Declination (degrees)
.5 1.0 1.5
40 50 60 70 80
-60 -30 0 30 60
0
1
2
3
4
5
6
7
8
9
10
11
Years ago (x1000)

period of 1800 years for a complete trip around the globe. Periods of 1920 years and 2194 years are prominent in the power spectra of Elk Lake declination and inclination respectively. The records do not exactly repeat themselves every 1800 years, indicating that important changes occur in the drifting portion of the field within one revolution around the globe. However, the ability to match records as much as 115° apart, indicates a stability of drifting features over time spans of more than 600 years. The meaning of the counterclockwise rotation of the VGP seen in the Elk Lake and Lake St. Croix data is not certain, since the directional record appears to be accounted for by simple westward drift.

CHAPTER 8 : CONCLUSION

A. Summary.

The Elk Lake paleomagnetic record has been developed through careful field work, measurements, and data proccessing. Excellent stratigraphic control is provided by fine scale variations in magnetic susceptibility with depth. Annual laminations in the sediment, although not always perfectly preserved or easily counted, provide superior time control for the magnetic record. The varves also provide reliable limits of confidence on the age scale, something which is generally lacking in radiocarbon dated sediment records. Radiocarbon dates are available from Elk Lake and they serve to confirm the varve counts. The varve and radiocarbon dates have been used to evaluate the radiocarbon calibration curve. The Elk Lake data appear to support the results of Stuiver from Lake of the Clouds, but the resolution is not sufficient to allow firm conclusions to be drawn.

A total of seven cores, four major and three minor, were combined to produce the 12,000 year magnetic record. The multiple cores allowed limits of confidence to be constructed for both relative and absolute inclination and declination. A doubly recorded sharp change in inclination at 33.3 m depth indicates that the sediment of Elk Lake very faithfully records the ambient magnetic field with an integration time of less than 25 years.

Efforts to derive relative paleointensity from the sediments were hampered by a large change in average magnetite grain size due to magnetite dissolution. The NRM/ARM paleointensity method was modified by normalization by MDF/MDFo, producing a paleointensity estimate consistent with absolute data from the western United States and from Bulgaria.

The Elk Lake paleomagnetic record contributes significantly to our understanding of the recent history of the magnetic field in central North America. More accurate dates are provided for several prominent features in the field, while other features seen in previous records are modified or brought into question. Several lines of evidence indicate that the Elk Lake paleomagnetic record is not stationary in time through its 12,000 year span. This implies that the axial geocentric dipole hypothesis is not valid for field integration times as short as 12,000 years. Spectral analysis of the Elk Lake time series reveals a number of distinct periodicities in the record, but does not lend obvious support to the dynamo wave model as opposed to the frozen flux model for secular variation generation. While a number of periodic components are indicated by spectral analysis, comparison of the Elk Lake record with archeomagnetic records from Bulgaria and France

indicate that a large portion of the variation in the local magnetic field can be simply accounted for by westward drift of the magnetic field at a rate of about 0.2 °/yr. This appears to be at odds with the VGP circularity data which suggests a combination of westward and eastward drift in the Elk Lake record.

B. Looking ahead.

While this thesis outlines a large body of work associated with deriving the Elk Lake paleomagnetic record and a number of its implications, it has also raised a number of questions which deserve further study. The doubly recorded shift in inclination at 33.3 m in Elk Lake (Figure 36, p. 61) is a fortuitous but important discovery. Studies dating back as much as three decades have called into question the mechanism of DRM acquisition and in particular, how long it takes for the remanent signal to become stable. Various studies have yielded different results depending on the particular nature of the sediments and experiments used. Until now, evidence for rapid acquisition of a stable remanent signal was largely circumstantial. The inclination shift in Elk Lake is strong evidence that, at least in organic sediments of this sort, the magnetic signal can be very rapidly acquired (< 4 cm, < 25 years). If most organic sediments are like those of Elk Lake in this respect, then an obvious next step is to look for the same inclination shift in the records from other sites, close to Elk Lake, as further confirmation. There is evidence for just such a shift in the Lake St. Croix record, but this needs to be investigated more carefully.

The derivation of relative paleointensity from sediments remains very hopeful, but a great deal of work remains to be done. The Elk Lake sediment is in principle a poor choice for paleointensity studies because of the large change in grain size with depth (thus failing King et al's criteria) apparently due to dissolution of magnetite (for which Karlin and Levi have discounted paleointensity all together). Yet, modifying the NRM/ARM method by normalization with MDF/MDFo appears to compensate for the affects of grain size change on NRM and ARM, producing a curve which is remarkably similar to the available absolute paleointensity records. Clearly, paleointensities can be derived even from unlikely sediments, so continued effort is warranted. A better theoretical foundation for paleointensity derivation is needed, especially with regard to unusual normalization parameters, like MDF/MDFo. The stirring method of Tucker, disappointing here, is still promising and warrants further development.

The relationship between secular variation and core fluid motions is of fundamental importance, but is still poorly understood. As the theoreticians continue to develop

possible explanations for field generation in the core, observations are needed in the context of defining the nature of the field. Does it always drift west? How long do field features last? Is the field periodic in a simple way? The Elk Lake record is one piece of the puzzle, but the picture hasn't taken shape very well yet.

Finally, there is the question of VGP circularity and westward drift. How can a field which seems so neatly described in terms of simple westward drift show signs of significant eastward drift such as counterclockwise VGP circularity? Do some field features drift west while others drift east? Or can an odd set of westward drifting features produce an eastward-like VGP signature?

The goal of understanding the core of the earth using the magnetic field is still in the distance. In fact, we have a long way to go just to understand the field itself. But the task is a worthy and exciting one, and steady progress is being made. It is hoped that the paleomagnetic record from Elk Lake, Minnesota will continue to be useful toward these goals.

BIBLIOGRAPHY

Aaseng, N. E. (1976). The History, Nature, and Extent of the Major Logging Operations in Itasca State Park (1901-1919). Master's Thesis, University of Minnesota, St. Paul, Minnesota.

Alldredge, L. R., and C. O. Stearns (1969). Dipole model of the sources of the earth's magnetic field and secular change. Journal of Geophysical Research, v. 74, p. 6583.

Anderson, R. Y. (1981). Anatomy of a goof : mystery of the missing (extra) Elk Lake core. Personal memo.

Banerjee, S. K., S.P. Lund, and S. Levi (1979). Geomagnetic record in Minnesota Lake sediments - Absence of the Gothenberg and Erieau excursions. Geology, v. 7, pp. 588-591.

Barton, C.E., and M. W. McElhinny (1979). Detrital remanent magnetization in five slowly redeposited long cores of sediment. Geophysical Research Letters, v. 6, pp. 229-232.

Barton C.E., M. W. McElhinny, and D. J. Edwards (1980). Laboratory studies of depositional DRM. Geophysical Journal of the Royal Astronomical Society, v. 61, pp. 355-377.

Brower, J. V. (1904). Itasca State Park, an illustrated history. Minnesota Historical Society Collection, Volume XI. The Minnesota Historical Society, St. Paul, Minnesota, 285 p.

Bucha, V., R.E. Taylor, R. Berger, and E.W. Haury (1970). Geomagnetic intensity: changes during the past 3000 years in the western hemisphere. Science, v. 168, pp. 111-114.

Champion, D. (1980). Magnetic Field Secular Variation from Holocene Radiocarbon Dated Lave Flows. Ph.D. Thesis, Stanford University, Palo Alto, California.

Clark, R. M. and R. Thompson (1978). An objective method for smoothing paleomagnetic data. Geophysical Journal of the Royal Astronomical Society, v. 52, pp. 205-213.

Creer, K.M. and P. Tucholka (1982). Construction of type curves of geomagnetic secular variation for dating lake sediments from east central North America. Canadian Journal of Earth Sciences, v. 19, pp. 1106-1115.

Creer, K.M., D.A. Valencio, A.M. Sinito, P. Tucholka, and J.F.A. Vilas (1983). Geomagnetic secular variations 0-14,000 yr B.P. as recorded by lake sediments from Argentina. Geophysical Journal of the Royal Astronomical Society, v. 74, pp. 199-221.

Day, R., M. Fuller, and V. A. Schmidt (1977). Hysteresis properties of titanomagnetites: grain-size and compositional dependence. Physics of the Earth and Planetary Interiors, v. 13, pp. 260-267.

Dean, W.E., J.P. Bradbury, R.Y. Anderson, and C.W. Barnosky (1984). The variability of Holocene climate change: evidence from varved lake sediments. Science, v. 226, pp. 1191-1194.

Dobie, J. (1959). The Itasca Story. Ross and Haines, Inc. Minneapolis, 202 p.

Dodson, R. E. (1979). Counterclockwise precession of the geomagnetic field vector and westward drift of the non-dipole field. Journal of Geophysical Research, v. 84, pp. 637-644.

Dodson, R.E., M.D. Fuller, and W.F. Kean (1977). Paleomagnetic records of secular variation from Lake Michigan sediment cores. Earth and Planetary Science Letters, v. 34, pp. 387-395.

Foster, D. C. (1976). Lower Lasalle Lake, Minnesota : Sedimentation and Recent Fire and Vegitation History. Master's Thesis, University of Minnesota, Minneapolis, Minnesota.

Graham, S. (1974). Remanent magnetization of modern tidal flat sediments from San Francisco Bay, Califonia. Geology, v. 2, pp. 223-226.

Gubbins, D. (1982). Finding core motions from magnetic observations. Philosophical Transactions of the Royal Society of London, v. A306, pp. 247-254.

Harrison, C.G.A. (1966). The paleomagnetism of deep-sea sediments. Journal of Geophyscial Research, v.71, p. 3033.

Johnson, E.A., T. Murphy, and O.W. Torreson (1948). Pre-history of the earth's magnetic field. Terr. Mag. Atmos. Elec., v. 53, pp. 349-372.

Johnson, H.P., H. Kinoshita, and R. T. Merrill (1975). Rock magnetism and paleomagnetism of some North Pacific deep-sea sediments. Geological Society of America Bulletin, v. 86, p. 412.

Karlin, R. and S. Levi (1983). Diagenesis of magnetic minerals in recent hemipelagic sediments. Nature, v. 303, pp. 327-330.

Karlin, R. and S. Levi (1985a). Geochemical and sedimentological control on the magnetic properties of hemipelagic sediments. In press at Journal of Geophysical Research.

Karlin, R. and S. Levi (1985b). Geomagnetic secular variation recorded in Oregon hemipelagic sediments. Submitted to Geophysical Journal of the Royal Astronomical Society.

Kent, D. V. (1973). Post depositional remanent magnetization in deep sea sediments. Nature, v. 246, pp. 32-34.

King, J. W. (1983). Geomagnetic Secular Variation Curves for Northeastern North America for the Last 9,000 Years B.P. PhD Thesis, University of Minnesota, Minneapolis, Minnesota.

King, J.W., S.K. Banerjee, J. Marvin, and Ö. Özdemir (1982). A comparison of different magnetic methods for determining the relative grain size of magnetite in natural materials: some results from lake sediments. Earth and Planetary Science Letters, v. 59, pp. 404-419.

King, J.W., S.K. Banerjee, J. Marvin (1983a). A new rock magnetic approach to selecting sediments for geomagnetic paleointensity studies: application to paleointensity for the last 4000 years. Journal of Geophysical Research, v. 88, pp. 5911-5921.

King, J.W., S.K. Banerjee, J. Marvin, and S.P. Lund (1983b). Use of small amplitude paleomagnetic fluctuations for correlation and dating of continental climate changes. Palaeogeography, Palaeoclimatology, Palaeoecology, v. 42, pp. 167-183.

King, R. F. (1955). The remanent magnetism of artificially deposited sediments. Monthly Notes of the Royal Astronomical Society, Geophysical Suppliment, v. 7, pp. 115-134.

Kirshvink, J.L., and J.L. Gould (1981). Biogenic magnetite as a basis for magnetic field sensitivity in animals. Biosystems, v. 13, pp. 181-201.

Kirshvink, J. L., and H. A. Lowenstam (1979). Mineralization and magnetization of chiton teeth: palaeomagnetic, sedimentologic and biologic implications of organic magnetite. Earth and Planetary Science Letters, v. 44, pp. 193-204.

Klein, J., J.C. Lerman, P.E. Damon, and E.K. Ralph (1982). Calibration of radiocarbon dates: tables based on the consensus of the Workshop on Calibrating the Radiocarbon Time Scale. Radiocarbon, v. 24, pp. 103-150.

Kovacheva, M. (1983). Archeomagnetic data from Bulgaria and south eastern Yugoslavia. In Geomagnetism of Baked Clays and Recent Sediments, K.M. Creer, P. Tucholka, and C. Barton, eds., Elsevier, Amsterdam, 324 pp.

Larson, R. J., and M. L. Marx (1981). An Introduction to Mathematical Statistics and its Applications. Prentice-Hall, Englewood Cliffs, New Jersey.

Levi, S., and S. K. Banerjee (1976). On the possibility of obtaining relative paleointensities from lake sediments. Earth and Planetary Science Letters, v. 29, pp. 219-226.

Liddicoat, J.C., and S.P. Lund (1983). A high resolution record of secular variation from Quaternary sediments from Mono Lake, California. EOS, Transactions of the American Geophysical Union, v. 64, p. 685.

Lund, S. P. (1981). Late Quarternaty Secular Variation of the Earth's Magnetic Field as Recorded in the Wet Lake Sediments of Three North American Lakes. PhD Thesis, University of Minnesota, Minneapolis, Minnesota.

Lund, S.P. and S.K. Banerjee (1985). Late Quaternary paleomagnetic field variation from two Minnesota lakes. Journal of Geophysical Research, v. 90, pp. 803-825.

Mackereth, F.J.H. (1971). On the variation in direction of the horizontal component of remanent magnetizationin lake sediments. Earth and Planetary Science Letters, v. 12, pp. 332-338.

McElhinny, M.W. (1973). Paleomagnetism and Plate Tectonics. Cambridge University Press, Cambridge, 358 p.

Mothersill, J. (1983). Results from the Great Lakes. In Geomagnetism of Baked Clays and Recent Sediments, K.M. Creer, P. Tucholka, and C.E. Barton, eds., Elsevier, Amsterdam, 324 pp.

Nakajima, T., and N. Kawai (1973). Secular variation in the recent 60,000 years found in the Lake Biwa sediments. In Rock Magnetism and Paleogeophysics. Published by the Rock Magnetism and Paleogeophysics Research Group, Japan.

Olson, P. (1981). A simple physical model for the terrestrial dynamo. Journal of Geophysical Research, v. 86, pp. 10875-10882.

O'Sullivan, P.E. (1983). Annually-laminated lake sediments and the study of Quaternary environment changes - a review. Quaternary Science Reviews, v. 1, pp. 245-313.

Parker, E.N. (1979). Cosmical Magnetic Fields, Clarendon Press, Oxford.

Patterson, W. A., III (1978). The Effects of Past and Current Land Disturbances on Squaw Lake, Minnesota and its Watershed. PhD Thesis, University of Minnesota, St. Paul, Minnesota.

Runcorn, K. (1959). On the theory of the geomagnetic secular variation. Ann. de Geophys., v. 15, pp. 87-92.

Shuey, R.T., R.O. Ugland, and C.R. Schmit (1977). Magnetic properties and secular variation in cores from Yellowstone and Jackson lakes, Wyoming. Journal of Geophysical Research, v. 82, pp. 3739-3746.

Stacey, F. D. (1972). On the role of Brownian motion in the control of detrital remanent magnetization in sediments. Pure and Applied Geophysics, v. 98, pp. 139-145.

Stacey, F. D. and S. K. Banerjee (1975). The Physical Properties of Rock Magnetism, Elsevier Scientific Publishing Co., Holland.

Stark, D. M. I. (1971). A Paleolimnological Study of Elk Lake in Itasca State Park, Clearwater County, Minnesota. PhD Thesis, University of Minnesota, Minneapolis, Minnesota.

Stark, D. M. (1976). Paleolimnology of Elk Lake, Itasca State Park, Northwestern Minnesota. Archiv f. Hydrobiologie, Suppl. 50, pp. 208-274.

Stuiver, M. (1970). Tree ring, varve and carbon-14 chronologies. Nature, v. 228, pp. 454-455.

Tauber, H. (1970). The Scandinavian varve chronology and C-14 dating. In Olsson, I. U., ed., Radiocarbon variations and absolute chronology. Nobel symposium, 12th Proc. New York, John Wiley and Sons, pp. 173-196.

Thellier, E. (1981). Sur la direction du champ magnetique terrestre en France durant les deux derniers millenaires. Physics of the Earth and Planetary Interiors, v. 24, pp. 89-132.

Towe, K. M. and T. T. Moench (1981). Electron-optical characteristics of bacterial magnetite. Earth and Planetary Science Letters, v. 52, pp. 213-220.

Tucker, P. (1980). Stirred remanent magnetization. Journal of Geophysics, v. 48, pp. 153-157.

Tucker, P. (1981). Palaeointensities from sediments: normalization by laboratory redepositions. Earth and Planetary Science Letters, v. 56, pp. 398-404.

Turner, G. M. and R. Thompson (1979). Behavior of the earth's magnetic field as recorded in the sediment of Loch Lomond. Earth and Planetary Science Letters, v. 42, pp. 412-426.

Turner, G.M. and R. Thompson (1981). Lake sediment record of the geomagnetic secular variations in Britain during Holocene times. Geophysical Journal of the Royal Astronomical Society, v. 65, pp. 703-725.

Verosub, K. L. (1977). Depositional and postdepositional processes in the magnetization of sediments. Reviews of Geophysics and Space Physics, v. 15, pp. 129-143.

Vitorello, I. and R. Van der Voo (1977). Magnetic stratigraphy of Lake Michigan sediments obtained from cores of lucustrine clay. Quarternary Research, v. 7, pp. 398-412.

Vogel, J.C. (1980). Accuracy of the radiocarbon time scale beyond 15,000 BP. Radiocarbon, v. 22, pp. 210-218.

Wright, H. E. (1972). Quaternary history of Minnesota. In Sims, P. K. and G. B. Morey, eds., Geology of Minnesota: a Centnnial Volume. Minnesota Geological Survey.

Yukutake, T. (1962). The westward drift of the magnetic field of the earth. Bulletin of the Earthquake Research Institute of Tokyo, v. 40, pp. 1-65.

Yukutake, T. and H. Tachinaka (1968). The westward drift of the geomagnetic secular variation. Bulletin of the Earthquake Research Institute of Tokyo, v. 46, p. 1027.

Yukutake, T. and H. Tachinaka (1969). Separation of the Earth's magnetic field into drifting and standing parts. Bulletin of the Earthquake Research Institute of Tokyo, v. 47, pp. 65-97.

Appendix 1 : Record of varve counts

This appendix details the varve counts from which the varve chronology was developed. Table A1.1 describes the marker horizons between which the varves were counted, and lists the adjusted depth of each. Table A1.2 assigns a code letter to each core half used in the counts. This enables the counts to be cataloged in Table A1.3.

Table A1.1 : Description of marker horizons.

Horizon code	Adjusted depth	Horizon description
Ambr	2888 cm.	Ambrosia rise, beginning of varve record
A	2898	double white
B	2941	double white
C	2968	double white
D	2985	diatom bloom
E	3018	big white clay(?) layer
F	3032	double white
G	3040	double white
H	3074	diatom bloom
I	3083	diatom bloom
J	3094	double white
K	3103	double white
L	3122	single white, bottom of 83b1,30-31
M	3151	single white, top of 82b3
N	3239	double white
O	3255	diatom bloom
P	3283	double white
Q	3308	diatom bloom, bottom of 83b2, 32-33
R	3330	single white, top of 83b3,33-34
S	3383	thick black, middle of 83b3,33-34
T	3417	single white, bottom of 83b3,33-34
U	3429	single white, top of 83b3,34-35
V	3467	single white, middle of 83b3,34-35
W	3508	single black, bottom of 83b3,34-35
X	3554	single white, top of 83b4,35-36
Y	3600	single white, middle of 83b4,35-36
Z	3620	thick black, bottom of 83b4,35-36
AA	3641	thick black, top of 83b4,36-37
BB	3696	thick black, middle of 83b4,36-37
CC	3723	single white, bottom of 83b4,36-37
DD	3734	single black, top of 83b5, 37-38
EE	3766	thick white, middle of 83b5, 37-38
FF	3790	thick white, bottom of 83b5, 37-38
GG	3809	diatom bloom, top of 83b5, 38-39
HH	3842	thick black, middle of 83b5, 38-39
II	3877	single white, bottom of 83b5, 38-39
JJ	3885	thick black, top of 83b6, 39-40
KK	3918	single white, middle of 83b6, 39-40
LL	3966	thick white, bottom of 83b6, 39-40
MM	3970	single white, top of 83b6, 40-41
NN	4012	single white, middle of 83b6, 40-41
OO	4097	single white, top of 83b8

Table A1.1 (cont)

Horizon code	Adjusted depth	Horizon description
PP	4136	single white, bottom of 83b8
QQ	4178	single white, top of 83b9
RR	4214	single white, middle of 83b9
SS	4253	single white, bottom of 83b9
TT	4306	single white, middle of 83b10
UU	4363	single white, bottom of 83b10
VV	4380	thick white, top of 83b11
WW	4415	single white, middle of 83b11
XX	4456	single white, bottom of 83b11
YY	4471	single white, top of 83b12
ZZ	4513	thick white, middle of 83b12
AAA	4545	single white, bottom of 83b12
BBB	4564	single white, top of 83b13
CCC	4574	single white
DDD	4582	single white
EEE	4610	thick white
FFF	4627	single white, bottom of 83b13
GGG	4661	single white, top of 83b14
HHH	4668	transition to non-varved, late-glacial sediments

Table A1.2 : Code designations for individual core segments.

Code	Core segment	Code	Core segment	Code	Core segment	Code	Core segment
a	82b1(surf)	r	83a6	jj	83b3b33-34	bbb	83b10a
b	84aa	s	83a7	kk	83b3a34-35	ccc	83b10b
c	84ab	t	83a8a	ll	83b3b34-35	ddd	83b11a
d	84ba	u	83a9a	mm	83b4a35-36	eee	83b11b
e	84bb	v	83a11a	nn	83b4b35-36	fff	83b12a
f	84ca	w	82c1	oo	83b4a36-37	ggg	83b12b
g	84cb	x	82c3	pp	83b4b36-37	hhh	83b13a
h	82e1a30-30	y	82c4	qq	83b5a37-38	iii	83b13b
i	82e1b30-30	z	82e5a	rr	83b5b37-38	jjj	83b14a
j	82a2a29-31	aa	78ki	ss	83b5a38-39	kkk	83b14b
k	82b2a29-31	bb	78kk	tt	83b5b38-39	lll	83a1b
l	82b3a31-33	cc	78kl	uu	83b6a39-40	mmm	83a2b
m	83a1a	dd	83b1b29-30	vv	83b6b39-40	nnn	83a3b
n	83a2a	ee	83b1a30-31	ww	83b6a40-41	ooo	83a4b
o	83a3a	ff	83b1b30-31	xx	83b6b40-41	ppp	83a8b
p	83a4a	gg	83b2a32-33	yy	83b8a	qqq	83a9b
q	83a5	hh	83b2b32-33	zz	83b9a	rrr	8311b
		ii	83b3a33-34	aaa	83b9b	sss	82e5b

The following is a key for Table A1.3. Each horizon (Table A1.1) is given a line in the table. Counts given are from the previous horizon to the listed horizon. If more than four counts are available for a particular horizon, more than one line is printed for that horizon. The horizon code letter is followed by a varve quality index: v for very good, g for good, f for fair, and p for poor. Following a particular count, the core segment code (Table A1.2) from which the count was made is given. Additionally, one or more of the following symbols may be applied to a particular count.

? - indicates uncertainty in the horizon location in this core.

* - indicates that this particular count was used for the varve chronology.

@ - indicates that full coverage of the interval is not available, count is an estimate.

- indicates that this count was not figured into the statistics.

ave - indicates an average of several imprecise counts.

The final column gives the average count, standard deviation, and percent standard deviation used to calculate the numerical error estimates of Chapter 4 (Table 1).

Table A1.3 : Record of varve counts.

Horizon	Count 1	Count 2	Count 3	Count 4	Count 5	Statistics
A - v	33 a ?#	32 b ?#	56 d *	54 e	53 f	53.5, 1.8, 3.4%
A	51 g					
B - v	154 a ?#	220 b	215 c	215 d *	212 e	213.2, 4.5, 2.1
B	205 f	212 g				
C - v	148 b	149 c	151 d	148 e	151 f	148.9, 2.3, 1.5
C	148 g	147 j	153 k *	145 dd		
D - v	104 d	103 e	106 f	115 g *	104 j	105.4, 7.1, 6.8
D	114 k	92 dd				
E - v	179 h	176 i	181 j	197 k *	172 dd	181.0, 8.6, 4.7
F - v	74 h	77 i *	71 j	75 k		74.3, 2.2, 2.9
G - v	50 j	57 k *				53.5, 3.5, 6.5
H - v	166 j	191 k	201 ee *	196 ff		188.5, 13.5, 7.1
I - v	58 j	65 k	67 ee	72 ff *		65.5, 5.0, 7.7
J - v	59 k	77 ee *	74 ff			70.0, 7.9, 11.2
K - v	68 ee *	66 ff				67.0, 1.0, 1.5
L - v	125 ee *	125 ff				125.0, 0.0, 0.0
M - v	143 m	157 lll *				150.0, 7.0, 4.7
N - v	483 l *#					-
O - v	97 l	104 gg	113 hh *			104.7, 6.5, 6.3
P - v	161 l	189 gg *	183 hh			177.7, 12.0, 6.8
Q - v	150 l	161 gg *	147 hh			152.7, 6.0, 3.9
R - v	127 n *	119 mmm				123.0, 4.0, 3.3
S - v	373 ii *	372 jj				372.5, 0.5, 0.1
T - v	240 ii	241 jj *				240.5, 0.5, 0.2
U - v	68 w *					-
V - p	195 kk	198 ll *				196.5, 1.5, 0.8
W - p	161 kk	192 ll *				176.5, 15.5, 8.8
X - p	191 o	210 nnn *				200.5, 9.5, 4.7
Y - p	215 mm	218 nn *				216.5, 1.5, 0.7
Z - p	95 mm *	93 nn				94.0, 1.0, 1.1
AA - p	89 p @*	80 ooo @	59 z	53 sss		70.3, 14.7, 21.0
BB - f	286 oo	294 pp *				290.0, 4.0, 1.4
CC - v	215 oo *	213 pp				214.0, 1.0, 0.5
DD - v	83 p	85 ooo *				84.0, 1.0, 1.2
EE - g	231 qq	251 rr *				241.0, 10.0, 4.1
FF - f	127 qq	163 rr *				145.0, 18.0, 12.4
GG - p	72 x *					-
HH - g	164 ss	204 tt *				184.0, 20.0, 10.9
II - g	191 ss	214 tt *				202.5, 11.5, 5.7
JJ - g	57 q *	50 y	51 y			52.7, 3.1, 5.9
KK - f	227 uu	229 vv *				228.0, 1.0, 0.4

Table A1.3 (cont)

Horizon	Count 1	Count 2	Count 3	Count 4	Count 5	Statistics
LL - g	425 uu *	416 vv				420.5, 4.5, 1.1
MM - g	16 r @#	28 r @#	22 ave *#			-
NN - v	340 ww *	319 xx				329.5, 10.5, 3.2
OO - p	557 r,s @#	446 r,s @#	502 ave *#			-
PP - f	180 yy *					-
QQ - p	182 t	187 ppp *				184.5, 2.5, 1.4
RR - p	204 zz *	171 aaa				187.5, 16.5, 8.8
SS - p	228 zz	238 aaa *				233.0, 5.0, 2.1
TT - p	260 u *	247 qqq				253.5, 6.5, 2.6
UU - f	289 bbb	297 ccc *				293.0, 4.0, 1.4
VV - p	116 aa @*					-
WW - p	209 ddd *					-
XX - f	259 ddd	284 eee *				271.5, 12.5, 4.6
YY - p	136 v @#	159 rrr @#	148 ave *#			-
ZZ - p	259 fff *	230 ggg				244.5, 14.5, 5.9
AAA - f	284 fff *	276 ggg				280.0, 4.0, 1.4
BBB - f	145 bb *					-
CCC - f	127 hhh	137 iii *				132.0, 5.0, 3.8
DDD - f	64 hhh	73 iii *				68.5, 4.5, 6.6
EEE - f	268 hhh	299 iii *				283.5, 15.5, 5.5
FFF - g	250 hhh	256 iii *				253.0, 3.0, 1.2
GGG - p	639 cc @#					-
HHH - p	60 jjj	79 kkk *				69.5, 9.5, 13.7

Appendix 2 : Anatomy of a goof revisited

In November of 1981, Roger Anderson wrote 'Anatomy of a goof,' a description of his efforts to decipher an error in the 1978 field work. He confirmed the preliminary evidence of a repeated section and recommended corrections to the stratigraphy and data set. But having only the 1978 cores to work with, he was unable to uniquely determine how much sediment was actually missing. With the results from four additional cores, I can now readdress the question of missing material in the 1978 cores.

The present reconstruction is based on several lines of evidence. The primary evidence is magnetic susceptibility plotted against the adjusted depth scale in Figure 7 (p. 13). The same data are plotted against the original depth scales in Figure 6 Figure 7 was derived from Figure 6 (p. 12) in the following way. Susceptibility (X) features and prominent strtigraphic features were used to correlate the various drives from cores 83a and 83b. Generally, this allowed the gaps between drives to be uniquely determined, except near the bottom, where the field notes had to be trusted. Correction of the gaps shrank the total 1983 section by about 0.5 m. The 1978 and 1982 curves were then linearly stretched to match the 1983 master curves.

Two possible sources of error in the curve matching should be noted. First, none of the measurements shown in Figure 7 are corrected for sample mass. Since the variations in X mainly reflect sample density, comparing the curves assumes that the same volume of material was put into each sample box. More critically, the 1978 and 1980's measurements were made on different instruments. The 1978 data are direct field measurements, while the 1980's data are alternating field measurements. The two are not always equivalent, eg., in Figures 6 and 7, the 1978 data are plotted at half amplitude.

Even so, the correlation of X features from year to year is remarkable. The features between 36 and 39 m (adjusted) are unmistakable and provide a known region from which to work out. Below 39 m, correlation of the 78 data with the 83 data solely on the basis of X is somewhat ambiguous, but we have three additional tie points. First is the unmistakable feature in X at 46 m. Second is the rise in X and cessation of varving at 47 m, signaling the transition to late glacial type sediments. Third is an unmistakable visual correlation between 78km-29 and 83b14-4736. So 78k is pretty well accounted for.

But the coring error is in 78j, and here X is not as useful. Fortunately, we have two more tie points. At adjusted depth 3100 there is a sharp transition in magnetic grainsize which shows up best in the plot of anhysteretic remanent magnetization (ARM) (Figure

A2.1). The double record of this feature in 78j provides confirmation of Anderson's visual overlap of drives 2 and 3. The final tie point is the predominant clay (?) layer at depth 3089 in 78j and depth 3018 in 83a.

Thus, the final adjustments to 78j are as follows.

Drive 1 : OK
Drive 2 : OK
Drive 3 : Repeats drive 2
Gap : 339 cm
Drive 4 : OK

While the correlation in Figure 7 is very convincing, it is curious that the 78 cores must be shrunk so much to fit. A difference in water level can partly, but not entirely, account for the difference. Apparently, the cores were taken from locations with sedimentation rates differing by as much as 50%, with an overall difference of about 10%. When the 78 depths are adjusted to match the 83 cores, the 339 cm gap in 78j becomes 128 cm. The gap covers the varve years 3050 to 3850 and can be covered by 150 cm worth of material from 82c, namely, batch sample numbers 41 through 61. Also of note is the adjusted overlap of 78j with 78k, with drive j4 moved up about a meter.

A separate question regards the varve counts. I have counted the varves from unfrozen cores, which should be more reliable than frozen ones. I also have the benefit of counting multiple sections, although the majority of the dating was done on 83b, for which I have the best photographic record. Figures 10 through 13 show the varve count results in various forms. Figure 12, varve thickness vs. varve years, compares pretty well with Anderson's curve except in the 5500 to 7000 varve year range, where I find thinner varves. I have rechecked this section, without any change.

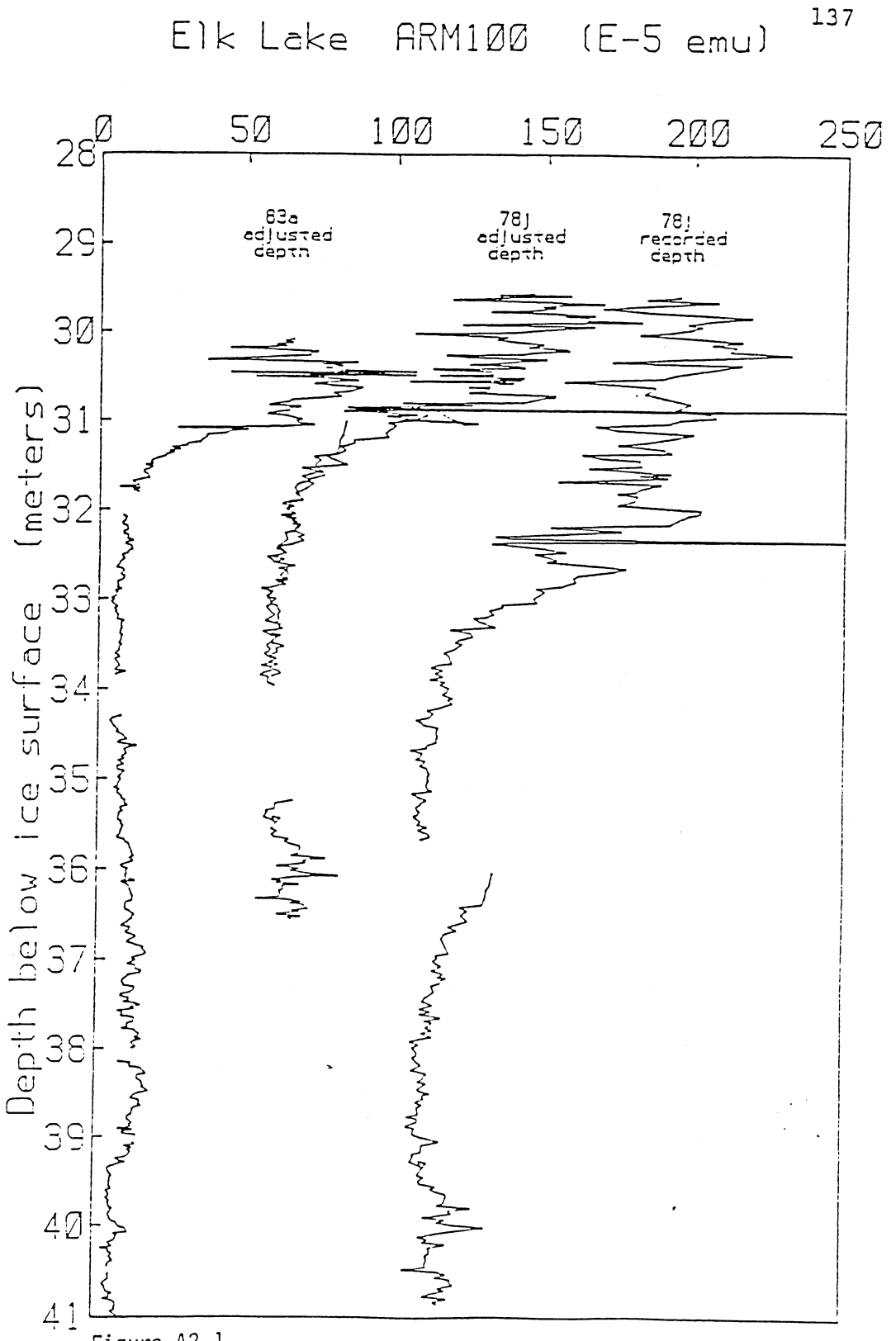
Elk Lake ARM100 (E-5 emu)
0
50
100
150
200
250
28
29
30
31
32
33
34
35
36
37
38
39
40
41
Depth below ice surface (meters)
83a adjusted depth
78J adjusted depth
78J recorded depth

Figure A2.1.

Appendix 3 : Record of outlier trimmings.

This appendix contains the record of outlier trimmings for the seven cores, as described in Chapter 5. For each core, there are two tables, one for inclination trimmings and one for declination. Each table has two portions, the upper portion describing the trimming results with regard to the differences between the two measurements of a given pair (1st trimming), the lower portion describing the trimming results for the differences between the means of adjacent pairs (2nd trimming). The order of operations is as follows. The upper portion of the 'raw data' column lists the original number of data pairs, their mean and std. dev., and the minimum and maximum difference values among the original pairs. The upper portion of the 'center hist' column lists the new mean and std. dev. derived for the central portion of the histogram. The cutoff values are 2.6 std. dev. below and above the new mean, beyond which, values are considered outliers. When these parameters are defined for both I and D, the first trimming is made, after which the values of the '1st trimming' column are calculated. Then the differences in means between adjacent pairs are examined, yielding the values in the 'raw data' column of the lower portion of the tables (note that these values are calculated using the trimmed data). A new mean and std. dev. are calculated for these values, along with the appropriate cutoff values, given in the lower portion of the 'center hist' column. After this second trimming is made, the values for the differences within pairs are recalculated, given in the '2nd trimming' column. The parameter of greatest interest in this column is the final number of data pairs remaining.

82c inc.	raw data	center hist.	1st trimming	2nd trimming
# of pairs	399		357	336
mean	-1.408	-0.3366	-0.3207	-0.2926
std. dev.	7.146	1.231	1.196	1.190
min dif.	-74.8		-3.4	-3.3
max dif.	6.9		2.8	2.8
cutoff values		-3.54, 2.86		
# of pairs	319			
mean	0.0382	0.0500		
std. dev.	1.226	0.9927		
min dif.	-5.35			
max dif	7.75			
cutoff values		-2.53, 2.63		

82c dec.	raw data	center hist.	1st trimming	2nd trimming
# of pairs	399		357	338
mean	2.116	-0.1043	-0.1929	-0.2917
std. dev.	18.2	5.182	4.816	4.793
min dif.	-34.5		-12.0	-12.0
max dif.	182.1		12.3	12.3
cutoff values		-13.58, 13.37		
# of pairs	319			
mean	0.0688	-0.4514		
std. dev.	5.002	3.483		
min dif.	-12.85			
max dif	61.2			
cutoff values		-9.507, 8.604		

82e inc.	raw data	center hist.	1st trimming	2nd trimming
# of pairs	669		592	556
mean	-0.044	-0.215	-0.279	-0.2906
std. dev.	5.703	1.315	1.279	1.275
min dif.	-34.4		-3.6	-3.6
max dif.	52.9		3.1	3.10
cutoff values		-3.63, 3.20		
# of pairs	515			
mean	0.0207	-0.251		
std. dev.	1.281	1.091		
min dif.	-3.75			
max dif	6.7			
cutoff values		-3.09, 2.59		

82e dec.	raw data	center hist.	1st trimming	2nd trimming
# of pairs	668		592	556
mean	3.538	0.2731	0.392	0.2953
std. dev.	29.68	5.011	4.978	4.867
min dif.	-302.3		-12.6	-12.6
max dif.	229.8		13.2	13.2
cutoff values		-12.76, 13.3		
# of pairs	515			
mean	-0.213	0.0447		
std. dev.	4.764	3.632		
min dif.	-17.95			
max dif	18.15			
cutoff values		-9.40, 9.487		

83a inc.	raw data	center hist.	1st trimming	2nd trimming
# of pairs	725		562	518
mean	1.061	0.9198	0.752	0.820
std. dev.	5.651	2.405	2.349	2.303
min dif.	-17.59		-5.19	-5.19
max dif.	41.72		7.14	7.14
cutoff values		-5.33, 7.17		
# of pairs	459			
mean	-0.054	-0.095		
std. dev.	2.298	1.553		
min dif.	-13.64			
max dif	10.49			
cutoff values		-4.132, 3.941		

83a dec.	raw data	center hist.	1st trimming	2nd trimming
# of pairs	725		562	520
mean	2.551	-1.02	-0.973	-0.9208
std. dev.	32.21	5.661	5.653	5.558
min dif.	-75.8		-15.1	-15.1
max dif.	318.1		13.3	13.3
cutoff values		-15.74, 13.69		
# of pairs	459			
mean	0.0989	-0.0504		
std. dev.	5.74	3.58		
min dif.	-35.45			
max dif	33.75			
cutoff values		-9.358, 9.257		

83b inc.	raw data	center hist.	1st trimming	2nd trimming
# of pairs	704		539	511
mean	0.326	0.3865	0.369	0.3762
std. dev.	10.04	2.916	3.006	2.971
min dif.	-64.6		-6.93	-6.93
max dif.	54.29		7.96	7.78
cutoff values		-7.195, 7.968		
# of pairs	454			
mean	-0.1108	-0.1108		
std. dev.	2.584	2.092		
min dif.	-15.27			
max dif	9.445			
cutoff values		-5.55, 5.328		

83b dec.	raw data	center hist.	1st trimming	2nd trimming
# of pairs	708		542	514
mean	2.521	0.1789	-0.3734	-0.3868
std. dev.	29.28	6.549	6.44	6.264
min dif.	-102.6		-16.1	-16.1
max dif.	289.5		16.5	16.2
cutoff values		-16.85, 17.206		
# of pairs	460			
mean	0.2202	0.0461		
std. dev.	5.804	4.042		
min dif.	-31.7			
max dif	36.1			
cutoff values		-10.46, 10.56		

84a inc.	raw data	center hist.	1st trimming	2nd trimming
# of pairs	48		41	41
mean	0.1754	0.9608	0.979	0.979
std. dev.	5.134	1.418	1.612	1.612
min dif.	26.35		-2.52	-2.52
max dif.	-29.4		4.64	4.64
cutoff values		-2.726, 4.648		
# of pairs	36			
mean	-0.2572	-0.257		
std. dev.	1.393	1.117		
min dif.	-3.18			
max dif	2.705			
cutoff values		-3.161, 2.647		

84a dec.	raw data	center hist.	1st trimming	2nd trimming
# of pairs	67		41	41
mean	1.288	0.0894	2.866	2.866
std. dev.	22.19	10.87	11.1	11.1
min dif.	-101.0		-27.7	-27.7
max dif.	72.5		21.6	21.6
cutoff values		-28.17, 28.35		
# of pairs	36			
mean	0.0083	0.0545		
std. dev.	9.226	8.513		
min dif.	-18.5			
max dif	29.85			
cutoff values		-22.08, 22.188		

84b inc.	raw data	center hist.	1st trimming	2nd trimming
# of pairs	74		65	65
mean	0.5678	0.9812	1.107	1.107
std. dev.	5.368	1.985	1.97	1.97
min dif.	-27.24		-4.01	-4.01
max dif.	13.11		5.63	5.63
cutoff values		-4.18, 6.142		
# of pairs	60			
mean	0.0606	0.0606		
std. dev.	2.287	2.287		
min dif.	-5.175			
max dif	6.18			
cutoff values		-5.89, 6.007		

84b dec.	raw data	center hist.	1st trimming	2nd trimming
# of pairs	74		65	65
mean	2.665	1.496	0.4677	0.4677
std. dev.	17.19	9.693	9.696	9.696
min dif.	-38.1		-23.3	-23.3
max dif.	73.8		25.7	25.7
cutoff values		-23.71, 26.7		
# of pairs	60			
mean	0.2625	0.9067		
std. dev.	7.856	7.322		
min dif.	-16.1			
max dif	28.95			
cutoff values		-18.13, 19.94		

84c inc.	raw data	center hist.	1st trimming	2nd trimming
# of pairs	75		48	48
mean	-0.834	0.563	0.7445	0.7445
std. dev.	9.251	1.357	1.494	1.494
min dif.	-26.9		-2.93	-2.93
max dif.	49.0		3.94	3.94
cutoff values		-2.965, 4.091		
# of pairs	41			
mean	-0.2812	-0.2797		
std. dev.	1.559	1.528		
min dif.	-3.19			
max dif	4.29			
cutoff values		-4.253, 3.993		

84c dec.	raw data	center hist.	1st trimming	2nd trimming
# of pairs	75		48	48
mean	-14.77	-4.276	-2.06	-2.06
std. dev.	33.4	9.607	8.56	8.56
min dif.	-157.3		-16.4	-16.4
max dif.	25.9		16.9	16.9
cutoff values		-29.25, 20.7		
# of pairs	41			
mean	1.279	1.279		
std. dev.	8.727	5.838		
min dif.	-18.05			
max dif	39.75			
cutoff values		-13.90, 16.46		

Appendix 4 : Inclination and declination shifting.

The amount of shifting for both I and D is listed for each core segment (Chapter 5). The reference core segment for the shift and the order in which the shift was made are important since the shifts are sequential. Assumed reference cores are listed as "fixed". Both I and D were shifted at the same time, relative to the same reference core.

Core segment	depth	reference core	order of shift	shift in I (°)	shift in D (°)
83a01	3010-3180	fixed	-	0	0
02	3208-3384	82c01	13	5.5	2.7
03	3431-3613	82c02	11	-0.4	9.5
04	3612-3798	fixed	-	0	0
05	3815-3897	83b05	6	-0.8	-7.3
06	3907-4043	83b06	24	-3.5	-14.6
07	4053-4137	82e11	25	-10.0	37.2
08	4140-4228	83b08	27	-6.7	7.1
09	4240-4322	83b09	29	1.3	-42.7
10	4302-4348	83b10	31	-1.6	-38.0
11	4403-4471	83b11	32	4.2	-40.1
12	4501-4543	83b12	34	7.8	6.4
13	4565-4629	fixed	-	0	0
14	4665-4691	fixed	-	0	0
15	4765-4813	fixed	-	0	0
83b01	2938-3120	82e02	36	6.7	-64.1
02	3221-3321	83a02	15	3.8	7.6
03	3331-3515	82c01	14	-	-
04	3545-3727	83a04	4	11.2	-8.3
05	3730-3880	83a04	5	0.2	13.6
06	3882-4070	82e08	18	7.9	32.3
08	4081-4169	83a07	26	11.5	56.1
09	4168-4260	83a08	28	13.1	32.5
10	4271-4363	83a09	30	-18.8	16.6
11	4370-4458	fixed	-	0	0
12	4463-4543	fixed	-	0	0
13	4545-4629	fixed	-	0	0
14	4646-4720	fixed	-	0	0
15	4652-4722	fixed	-	0	0
84a		82e01	38	3.6	9.6
84b		82e01	39	3.3	35.9
84c		82e01	40	1.4	30.2
82c01	3322-3508	83a03	12	-1.8	-0.5
02	3519-3656	82e05	3	4.0	-4.4
03	3663-3828	83a04	1	1.2	13.3
04	3801-3898	83b05	8	2.1	31.0
05	3886-3956	83b06	19	1.4	8.0
06	3960-4040	83b06	20	4.1	18.2

Core segment	depth	reference core	order of shift	shift in I (°)	shift in D (°)
82e01	2895-3047	83b01	37	3.4	24.4
02	3056-3218	83a01	35	-2.7	5.5
03	3226-3386	83a02	17	-3.0	16.3
04	3411-3577	83a03	16	-1.7	-7.9
05	3570-3719	83a04	2	-1.2	-0.7
06	3728-3896	83b05	7	1.9	-3.6
07	3737-3820	83b05	9	-0.9	14.6
08	3816-3902	83b05	10	-1.6	15.3
09	3889-3962	83b06	21	-1.1	19.3
10	3973-4033	83b06	22	-1.9	16.1
11	4034-4099	83b06	23	-6.4	13.4